STUDIES ON RADIATION SHIELDING OF ENERGY DOUBLER MAGNETS (1)

H. Edwards, S. Mori, and A. Van Ginneken

December 27, 1978

I Introduction

Several measurements have been made to understand quench problems of superconducting magnets due to beam energy deposition in magnet coils.[1] Some preliminary analysis of quench problems of Energy Doubler magnets due to beam losses at injection, during acceleration and at extraction have already appeared.[2,3] In this report we discuss radiation problems due to beam losses during acceleration and extraction. We also discuss various proposed schemes to minimize such problems.

II. Limits of Energy Deposition

Figure 1 shows an estimate of the relation between limits of energy deposition in superconducting coils and magnet excitation current.[2] These limits appear consistent with measurements.[1] Table I summarizes the limits for extraction beam losses.

Table I. Limits of energy deposition at extraction energy.

Mode	Limits
Slow	4 $mw.g^{-1}$
Fast (1ms)	1 $mj.g^{-1}.pulse^{-1}$
Abort (20 μs)	0.5 $mj.g^{-1}.pulse^{-1}$

We assumed that $I/I_{max} \simeq 0.9$ for the following reasons. Fristly, the highest energy deposited inside the coils always appears near the horizontal median plane because of magnetic field effects on charged secondary particles and because of the curvature of the magnets. The magnetic field strength inside the coils around the horizontal median plane is about 10% lower than the maximum field which appears at the top and bottom corners of the coils. Secondly, it seems to be reasonable to operate the Energy Doubler at a slightly lower current level than the extreme quench level.

III. Extraction Beam Losses

Extraction beam losses are primarily caused by beam scattering and nuclear interactions in the electrostatic septum wires and Lambertson septum magnets.

(A) Radiation Due to Scattering From Electrostatic Septum Wires:

The program CASIM[4] was modified to calculate energy deposited in Doubler magnets.[5] The wire septum and dipole magnet string have been modelled in all revelant geometric detail including the presence of electric and magnetic fields. However, in the present study a string of four quadrupole magnets to be placed upstream of the dipole string were omitted. A schematic drawing of the arrangement is shown in Figure 2. Figure 3 shows the energy deposition in the dipole string as a function of depth for a shallow (0.59 cm thick) radial region located near the inner radius of the coils for a 1000 GeV proton beam (0.2 cm high) uniformly distributed over the lateral dimension of the wire. Curves are drawn to guide the eye. The collimator upstream of the magnet string was omitted. Two distinct peaks are seen. The first peak is due to radiation

through the upstream magnet surface and can be suppressed by placing a collimator in front of the magnet. This is shown in Figure 4. An iron collimator with a hole radius of 2 cm and a length of 2m was placed as shown in Figure 2. The first peak was suppressed by a factor of roughly 100. The second peak is most prominent near $\phi = \pi$ and is mainly due to high energy photons from neutral pions produced in the forward direction. The collimator reduced the energy density at the second peak in general, but its maximum value (near $\phi = \pi$) was not significantly lowered. This large energy deposition of 3×10^{-3} GeV.cm^{-3} (inc. proton)$^{-1}$ therefore presents a more difficult problem. Table II gives the maximum numbers of protons that can be extracted under these conditions. The extraction inefficiency was assumed to be 2.5%, i.e. 2.5% of protons strike septum wires.

Table II. Numbers of protons that can be extracted for the electrostatic septum arrangement shown in Figure 2.

Mode	Number of Protons
Slow	2.7×10^{12} protons/sec
Fast (1ms)	0.7×10^{12} protons/pulse

Those limits are unacceptably low, particularly for fast spill. T. Collins proposed a modification of a long straight section to provide a large β region in the horizontal plane[6], shown in Figure 5. If conventional magnets are used at the middle of the straight section, this will considerably reduce energy deposition in the Doubler magnets. Detailed calculations are in progress. In this arrangement good field tracking between superconducting and conventional magnets is required.

A bump as large as 4 mrad may not be needed to achieve a sufficient reduction of energy deposition density at the Doubler

magnets. Then, as shown in Figure 6, a simpler bump by conventional magnets only which does not require the same high degree of field tracking is more attractive. The direction of the bump can be outward or inward in the radial direction.

(B) Radiation Due to Scattering From Lambertson Magnets:

Protons which are scattered out of the electrostatic septum wires may strike the Lambertson magnet septum region and may cause radiation in downstream Doubler magnet coils. Figure 7 shows the schematic drawing of the arrangement used in the calculation. The energy density distribution in the Doubler magnet is shown in Figure 8. It was assumed that a 1000 GeV proton beam (0.2 cm high) was uniformly distributed over the central (narrowest) region of the septum, and struck the upstream surface of the septum perpendicularly. Nearly all incident protons underwent nuclear interactions in the septum. The large peaks at the upstream end can be suppressed by a collimator as in the electrostatic septum case. Unlike in the latter case the second peak corresponding to neutral pion production does not appear there because the Lambertson magnets have enough absorbing material at the septum region in the forward direction. The maximum energy density is about 4×10^{-4} GeV.cm^{-3} (inc. proton on Lambertson magnet).[-1] Table III gives the maximum numbers of protons that can be extracted through the Lambertson magnets. The interaction rate of protons at the Lambertson magnets was assumed to be 0.63% which is obtained if one quarter of protons which strike the electrostatic septum wires intersect the Lambertson magnets.

Table III. Numbers of protons that can be extracted through the Lambertson magnets.

Mode	Number of Protons
Slow	7.9×10^{13} protons/sec
Fast (1ms)	2.0×10^{13} protons/pulse

These limits are quite acceptable. No special arrangement seems to be required for the Lambertson magnet area. However, the assumption that the beam is uniformly distributed on the septum region (Figure 7) is perhaps questionable. Figure 9 shows the energy density distribution when the protons were incident uniformly distributed over the first 3.2 m on the side surface of the no-field region of the septum with an angle of 30 μrad. The energy density is much larger than in Figure 8. Furthermore, a second peak appear around $\phi = \pi$ as in the electrostatic septum case. If a large fraction of the protons lost at the Lambertson magnet is typified by this mode, then the limits given in Table III must be substantially lowered.

The Lambertson magnet arragnement for the beam abort system has a lower limit of energy deposition because of the single-turn extraction. However, in principle it may have less problems since the extraction can be done more cleanly. Of the order of 6×10^{10} protons are allowed to hit the septum.

IV. Beam Losses During Acceleration

Figure 10 shows the schematic drawing of the case in which protons strike the vacuum chamber of the Doubler magnet on the inside edge. The proton energy is 1000 GeV. Figures 11 and 12 show energy density distributions in the Doubler magnet coils as functions of azimuthal angle and coil radius when protons interact with the vacuum chamber at $\phi = 0$ (at the accelerator inner

radius as indicated in Figure 10). For the vacuum chamber radius of 3.68 cm, the energy density distribution has a sharp peak near the proton interaction point $\phi = 0$ and reaches about 2 GeV cm^{-3} (interacting proton)$^{-1}$, which corresponds to about 4×10^{-8} mj. g^{-1} (interacting proton)$^{-1}$. This peak density is much smaller and has a gentler dependence when the vacuum chamber is placed at 3.18 cm inner radius. The second peak which appears at the downstream outer radius ($\phi = \pi$) is again due to neutral pions produced in the forward direction. The peak values are roughly the same for the both cases.

Figures 13 and 14 show energy density distributions when protons interact with the inside edge of the vacuum chamber at $\phi = \pi$ (at the outer accelerator radius). Essentially all the characteristics of the energy density distributions are identical to those distributions shown in Figures 11 and 12 with the ϕ angles reversed except for the second peaks corresponding to neutral pions. The latter cases do not have a neutral pion peak for geometrical reasons.

The first peak can be suppressed by long scrapers ($\gtrsim$3m), for example at medium straight sections. However, the second peak of about 1×10^{-9} mj g^{-1} (interacting proton)$^{-1}$ when protons interact with the vacuum chamber inside edge at the accelerator inner radius is difficult to reduce by a simple arrangement. If long straight sections are available for beam scraping, an arrangement of a beam scraper and absorbers with a beam dump system of conventional magnets seems to be a good solution, as shown in Figure 6. If no long straight section is available for beam scraping, T. Collins proposed a special beam scraper arrangement at medium straight sections, as shown in Figures 15 and 16. This arrangement requires special dipole magnets of a larger aperture and half the length of the normal Doubler dipole magnet. Detailed studies are in progress.

V. Conclusions

A special beam bump arrangement is required at the long straight section where the electrostatic septum is installed for extraction. The Lambertson magnet areas for both the normal extraction and the beam abort system may not require any special system other than simple beam collimators.

Beam scraper systems which localize beam losses and minimize radiation to the Doubler magnet coils during acceleration may have to be installed in medium straight sections. Further detailed studies are needed.

References

1. H. Edwards, C. Rode, and J. McCarthy, IEEE Trans. on Magnetics, Vol. 1, Mag 13, 1977, p 666, and B. Cox, P.O. Mazur, and A. Van Ginneken, "Sensitivity of an Energy Doubler Dipole to Beam Induced Quenches", TM-828A, 1978.
2. H. Edwards, "Beam Abort System", Internal Report, June 3, 1977.
3. T. Collins, "Radiation on Magnet Coils from the Wire Septum", Internal Report, 1978.
4. A. Van Ginneken, "CASIM, A Program to Simulate Hadronic Cascades in Bulk Matter", FN-272, January 1975.
5. A. Van Ginneken, "Distribution of Heat Due to Beam Loss in Energy Doubler/Saver Type Superconducting Magnets", TM-685, September 13, 1976.
6. T. Collins, "High-beta Straight Sections for the Doubler", UPC No. 14, November 14, 1978.
7. T. Collins, "Charged Particle Distributions Estimate", Internal Report, 1978.

Figure Captions

Figure 1. Limits of energy deposition in Doubler superconducting magnet coils.

Figure 2. Schematic drawing of the arrangement of the electrostatic wire septum for extraction at a long straight section. The second unit is tilted by 30 μrad away from the normal orbit so that wires of the second unit do not intersect protons. The ϕ angle is measured from the inner accelerator radius in the median plane.

Figure 3. Energy density distributions in Doubler magnet coils due to scattering from the extraction electrostatic wire septum for a shallow radial region of 3.81 cm to 4.40 cm. The incident proton energy was 1000 GeV. No collimator was present.

Figure 4. Energy density distributions in Doubler magnet coils due to scattering from the extraction electrostatic wire septum for a shallow radial region of 3.81 cm to 4.40 cm. The incident proton energy was 1000 GeV. An iron collimator of a hole radius of 2 cm and a length of 2 m was placed upstream of the Doubler magnets.

Figure 5. Schematic drawing of a modified high-β long straight section by T. Collins. (See Reference 3.)

Figure 6. Schematic drawing of a bump arrangement of conventional B-2 magnets at a long straight section.

Figure 7. Schematic drawing of the Lambertson septum magnet arrangement for extraction.

Figure 8. Energy density distributions in Doubler magnet coils due to scattering from the extraction Lambertson septum magnets for a shallow radial region of 3.81 cm to 4.40 cm. It was assumed that 1000 GeV protons were distributed uniformly over the central region of the septum and struck perpendicularly the upstream surface of the septum. No collimator was present.

Figure 10. Energy density distributions in Doubler magnet coils due to scattering from the extraction Lambertson septum magnets for a shallow radial region of 3.81 cm to 4.40 cm. It was assumed that 1000 GeV protons struck the side surface of the septum from the normal beam orbit side with an angle of 30 μrad, uniformly distributed over the first 3.2 m of the septum. No collimator was present.

Figure 11. Schematic drawing of the case in which 1000 GeV protons strike the vacuum chamber of a Doubler magnet. The proton beam was assumed to have a distribution of a δ-function in the vertical direction and interact the inside edge of the vacuum chamber in the median plane. The vacuum chamber radius is from 3.18 to 3.31 cm and 3.68 to 3.81 cm. The ϕ angle is measured from the inner accelerator radius in the median plane.

Figure 12. Energy density distributions in Doubler magnet coils due to beam losses on the vacuum chamber. The proton beam of 1000 GeV struck the inside edge of the vacuum chamber at the inner accelerator

radius (ϕ= 0). The vacuum chamber radius was from 3.68 cm to 3.81 cm. The inner radius of the superconducting coils was 3.81 cm.

Figure 13. Energy density distributions in Doubler magnet coils due to beam losses on the vacuum chamber. The proton beam of 1000 GeV struck the inside edge of the vacuum chamber at the inner accelerator radius (ϕ = 0). The vacuum chamber radius was from 3.18 to 3.31 cm. The inner radius of the superconducting coils was 3.81 cm.

Figure 14. Energy density distributions in Doubler magnet coils due to beam losses on the vacuum chamber. The proton beam of 1000 GeV struck the inside edge of the vacuum chamber at the outer accelerator radius (ϕ= π). The vacuum chamber radius was from 3.68 cm to 3.81 cm. The inner radius of superconducting coils was 3.81 cm.

Figure 15. Energy density distributions in Doubler magnet coils due to beam losses on the vacuum chamber. The proton beam struck the inside edge of the vacuum chamber at the outer accelerator radius (ϕ= π). The vacuum chamber radius was from 3.18 cm to 3.31 cm. The inner radius of superconducting coils was 3.81 cm.

Figure 15. Schematic drawing of a modified medium straight section with two half-bending magnets and beam scraper arrangement proposed by T. Collins (See Reference 3.).

Figure 16 Trajectories of neutral particles scattered from edges of the beam scraper in a Collins' modified medium straight section (See Reference 3.).

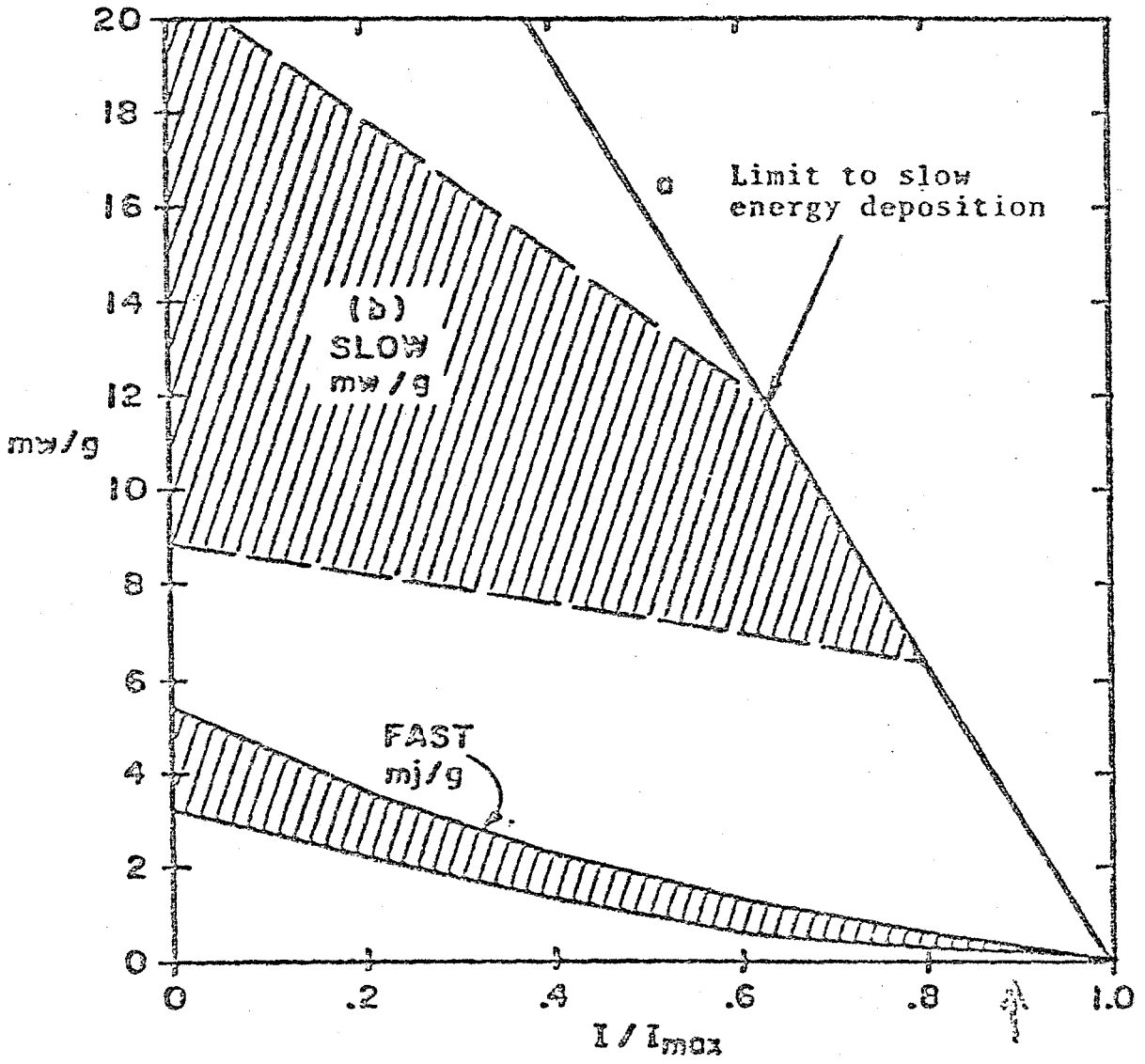

Figure 1. LIMITS OF ENERGY DEPOSITION IN DOUBLER SUPERCONDUCTING MAGNETS.

ELECTROSTATIC WIRE SEPTUM

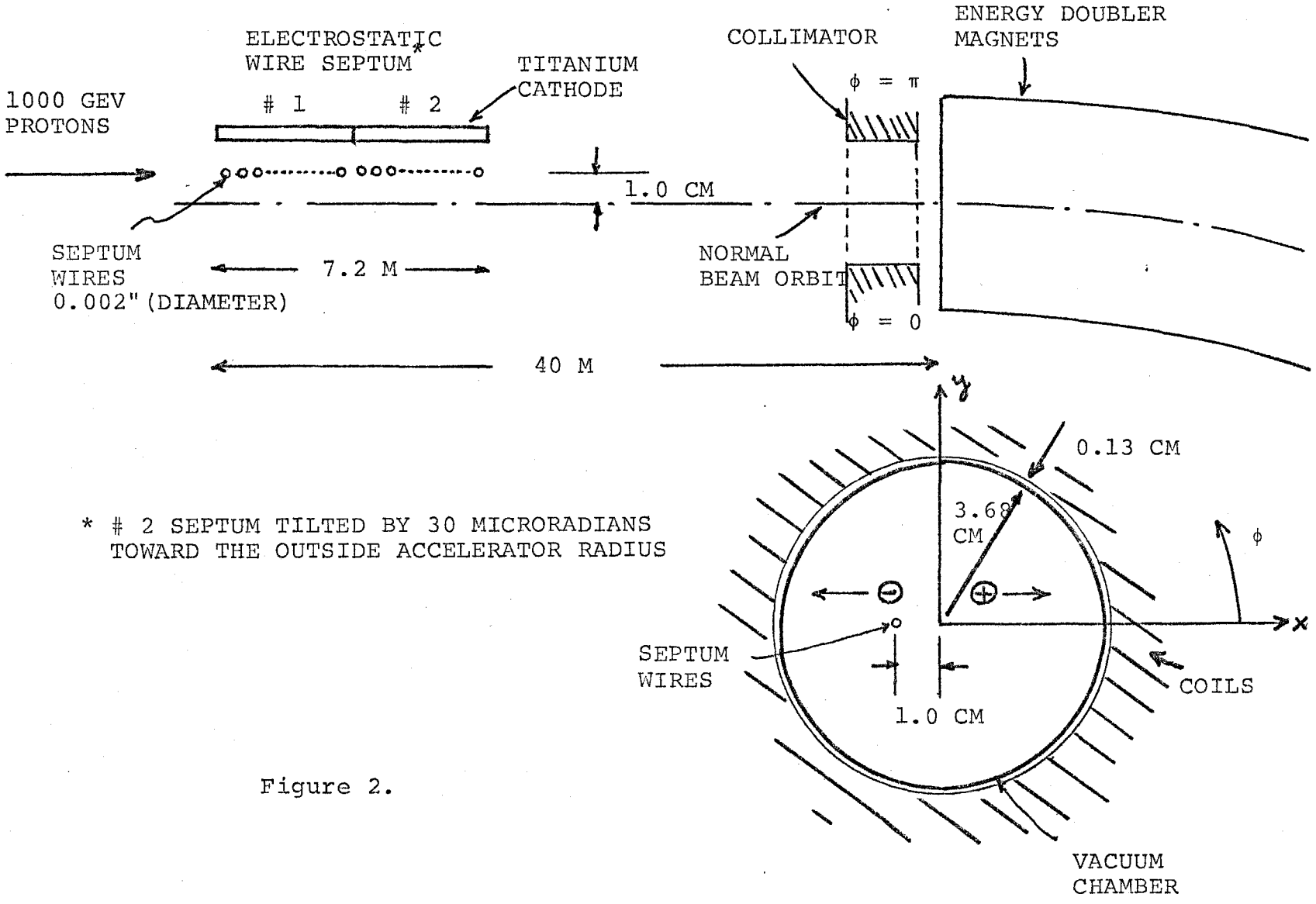

* # 2 SEPTUM TILTED BY 30 MICRORADIANS
TOWARD THE OUTSIDE ACCELERATOR RADIUS

Figure 2.

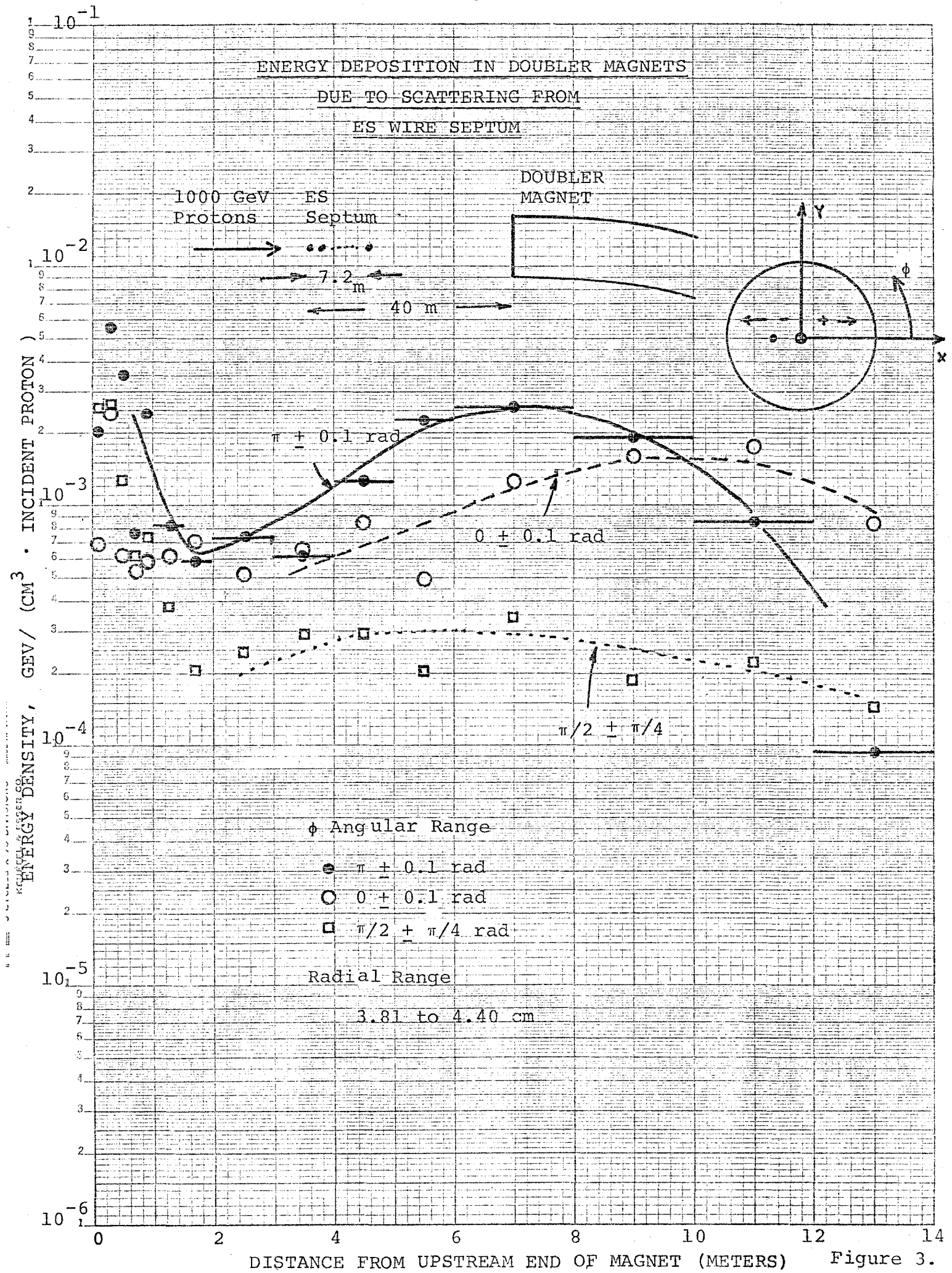
ENERGY DEPOSITION IN DOUBLER MAGNETS
DUE TO SCATTERING FROM
ES WIRE SEPTUM
1000 GeV Protons
ES Septum
DOUBLER MAGNET
7.2 m
40 m
Y
X
ϕ
π ± 0.1 rad
0 ± 0.1 rad
π/2 ± π/4
ENERGY DENSITY, GEV/ (CM3 · INCIDENT PROTON)
ϕ Angular Range
π ± 0.1 rad
0 ± 0.1 rad
π/2 ± π/4 rad
Radial Range
3.81 to 4.40 cm
DISTANCE FROM UPSTREAM END OF MAGNET (METERS)

Figure 3.

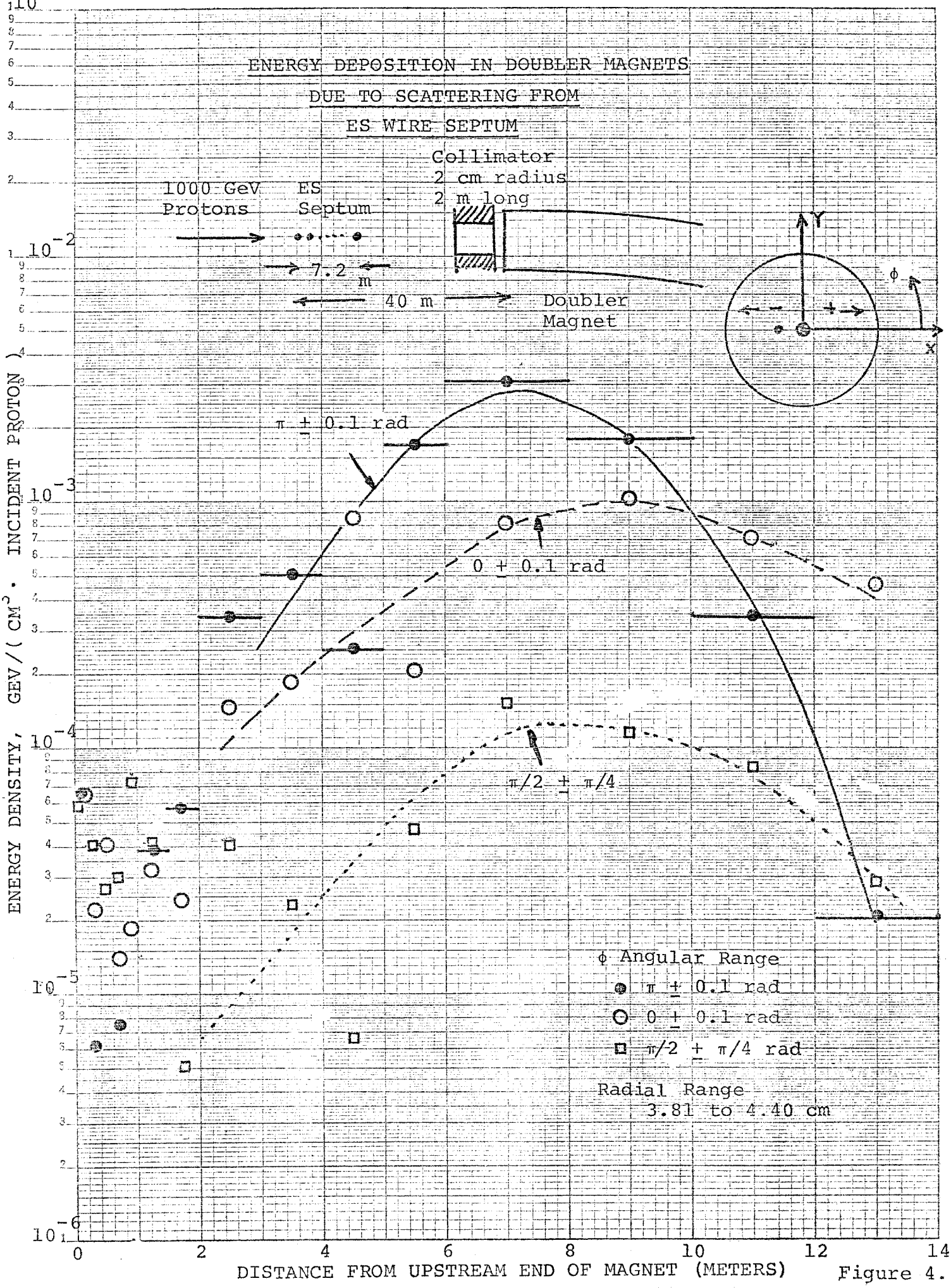
ENERGY DEPOSITION IN DOUBLER MAGNETS
DUE TO SCATTERING FROM
ES WIRE SEPTUM
1000 GeV Protons
ES Septum
Collimator
2 cm radius
2 m long
7.2 m
40 m
Doubler Magnet
Y
X
ϕ
π ± 0.1 rad
0 ± 0.1 rad
π/2 ± π/4
ϕ Angular Range
π ± 0.1 rad
0 ± 0.1 rad
π/2 ± π/4 rad
Radial Range
3.81 to 4.40 cm
ENERGY DENSITY, GEV/(CM³ · INCIDENT PROTON)
DISTANCE FROM UPSTREAM END OF MAGNET (METERS)

Figure 4.

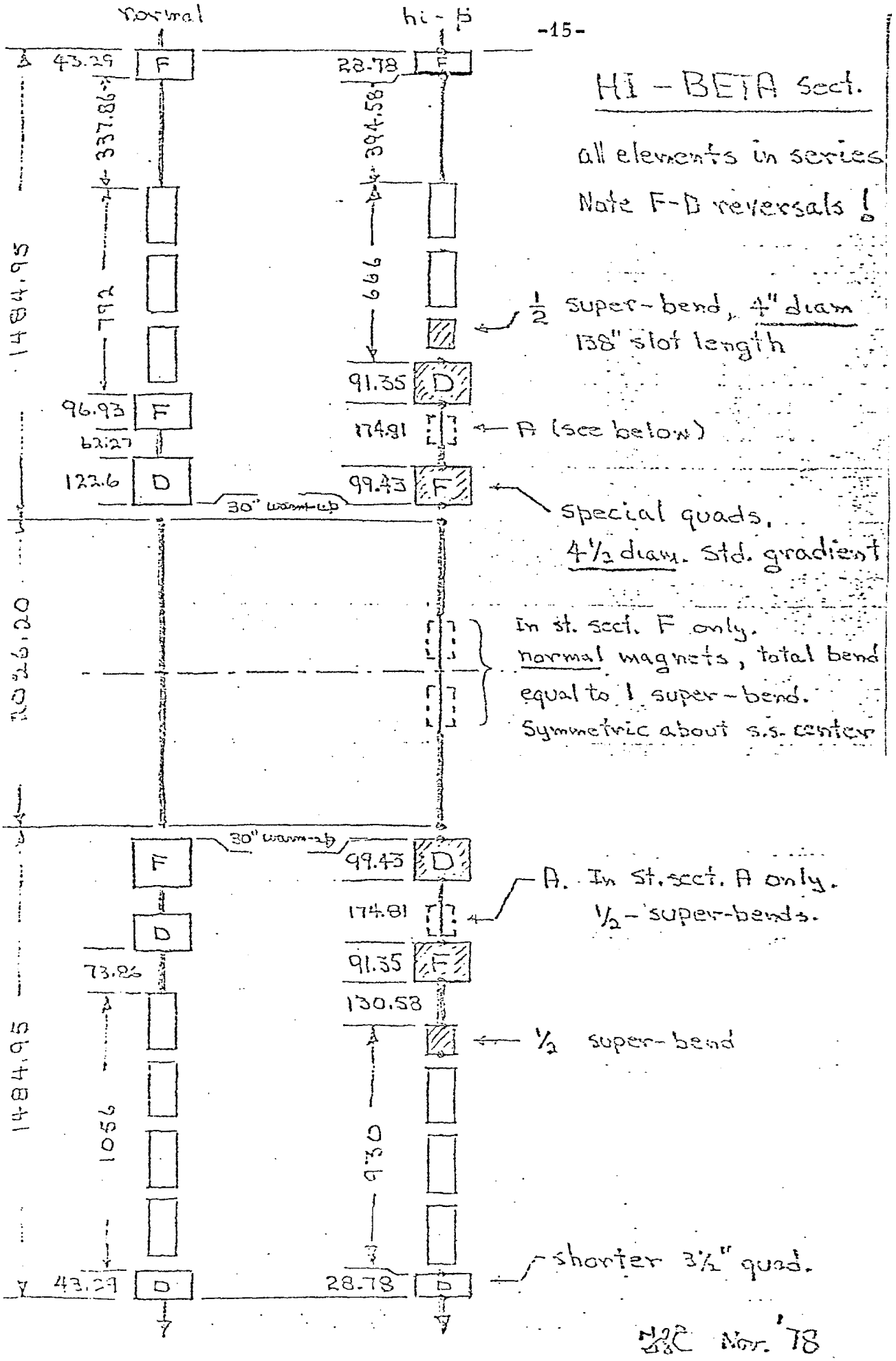
normal
hi - β
HI - BETA sect.
all elements in series
Note F-D reversals !
43.29
F
337.86
792
96.93
F
62.27
122.6
D
30" warm-up
1484.95
28.78
F
394.58
666
½ super-bend, 4" diam
138" slot length
91.35
D
174.81
A (see below)
99.43
F
Special quads,
4½ diam. Std. gradient
In st. sect. F only.
normal magnets, total bend
equal to 1 super-bend.
Symmetric about s.s. center
30" warm-up
F
D
73.86
1056
43.29
D
99.43
D
174.81
A. In st. sect. A only.
½-super-bends.
91.35
F
130.58
½ super-bend
930
28.78
D
shorter 3½" quad.
WJC Nov. '78

Figure 5.

SIMPLE BUMP BY CONVENTIONAL MAGNETS (B-2)

AT F0 LONG STRAIGHT SECTION*

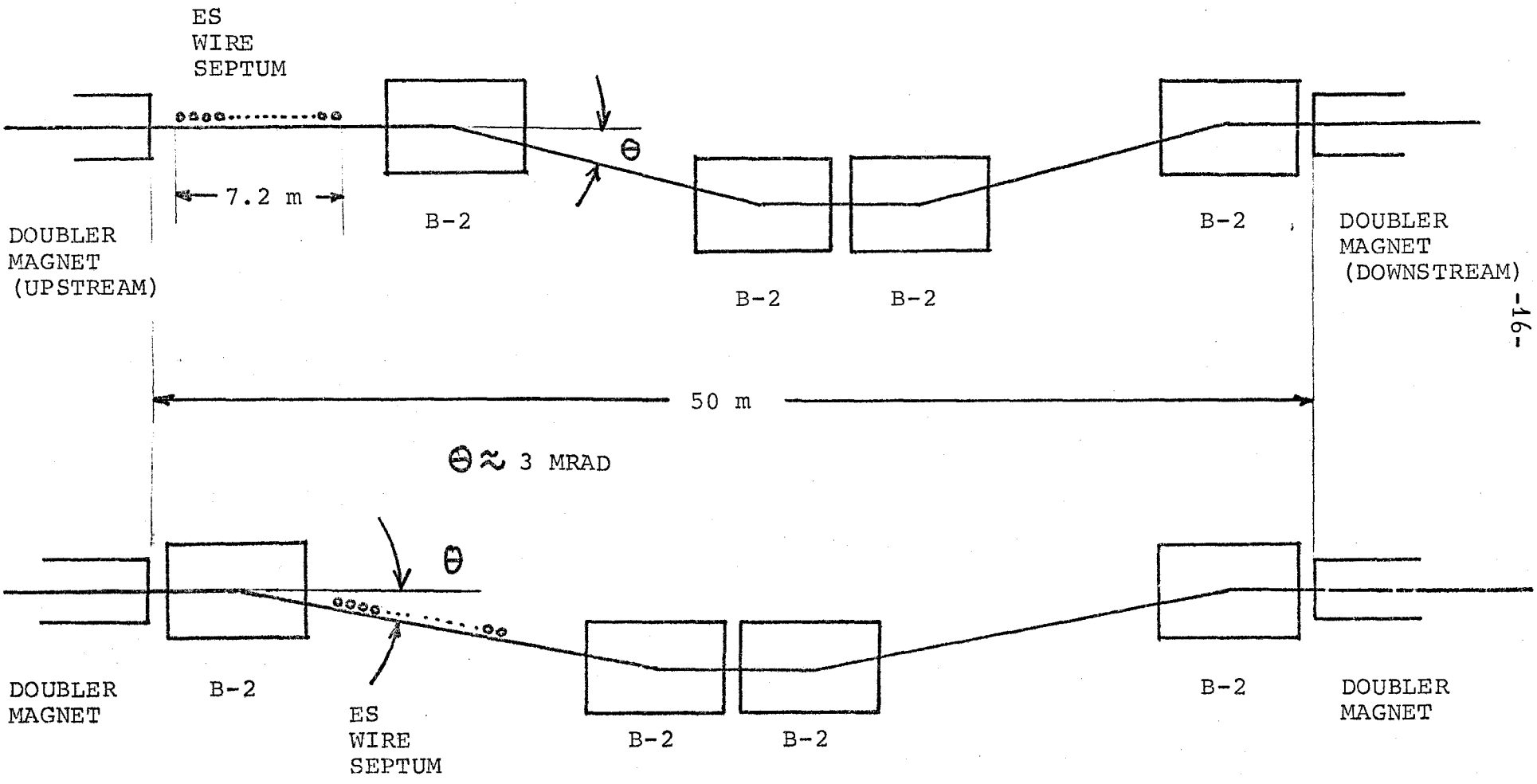

* COLLIMATORS PLACED INSIDE AND/OR IN FRONT OF B-2 MAGNETS DOWNSTREAM OF THE ES WIRE SEPTUM.

Figure 6.

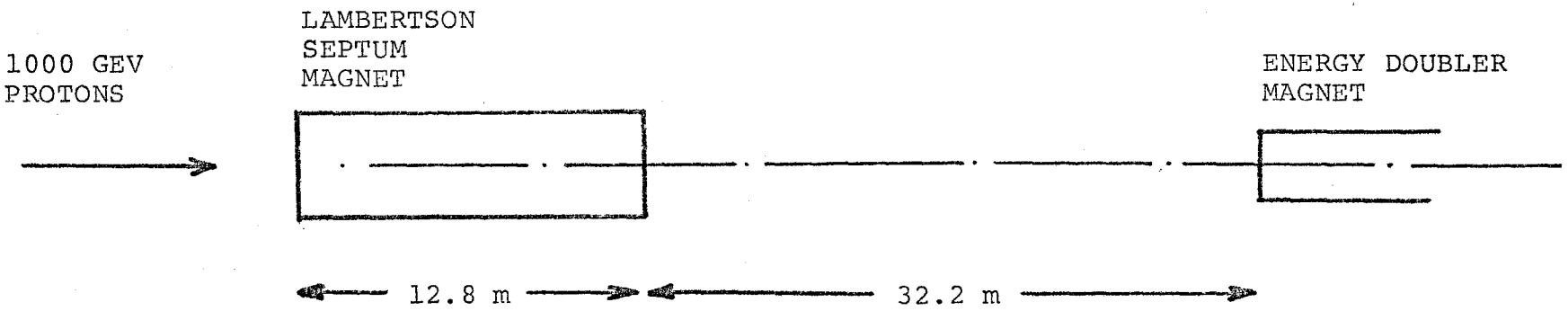
1000 GEV
PROTONS
LAMBERTSON
SEPTUM
MAGNET
ENERGY DOUBLER
MAGNET
12.8 m
32.2 m

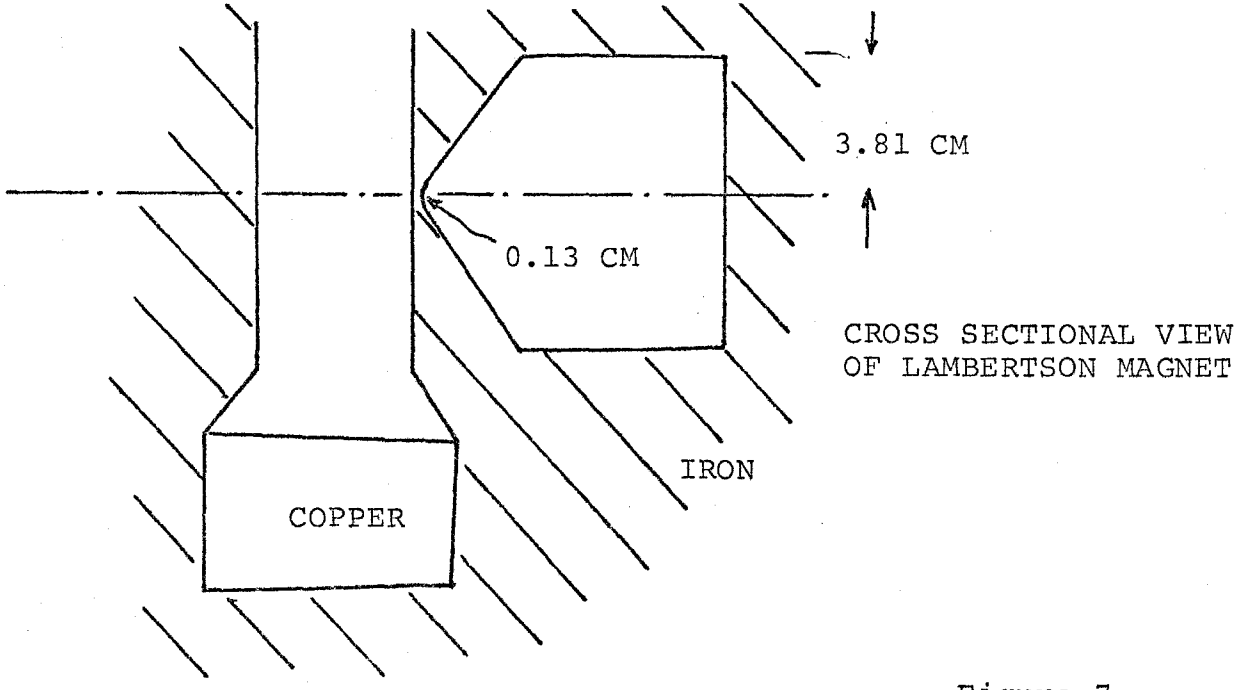
3.81 CM
0.13 CM
CROSS SECTIONAL VIEW
OF LAMBERTSON MAGNET
IRON
COPPER

Figure 7.

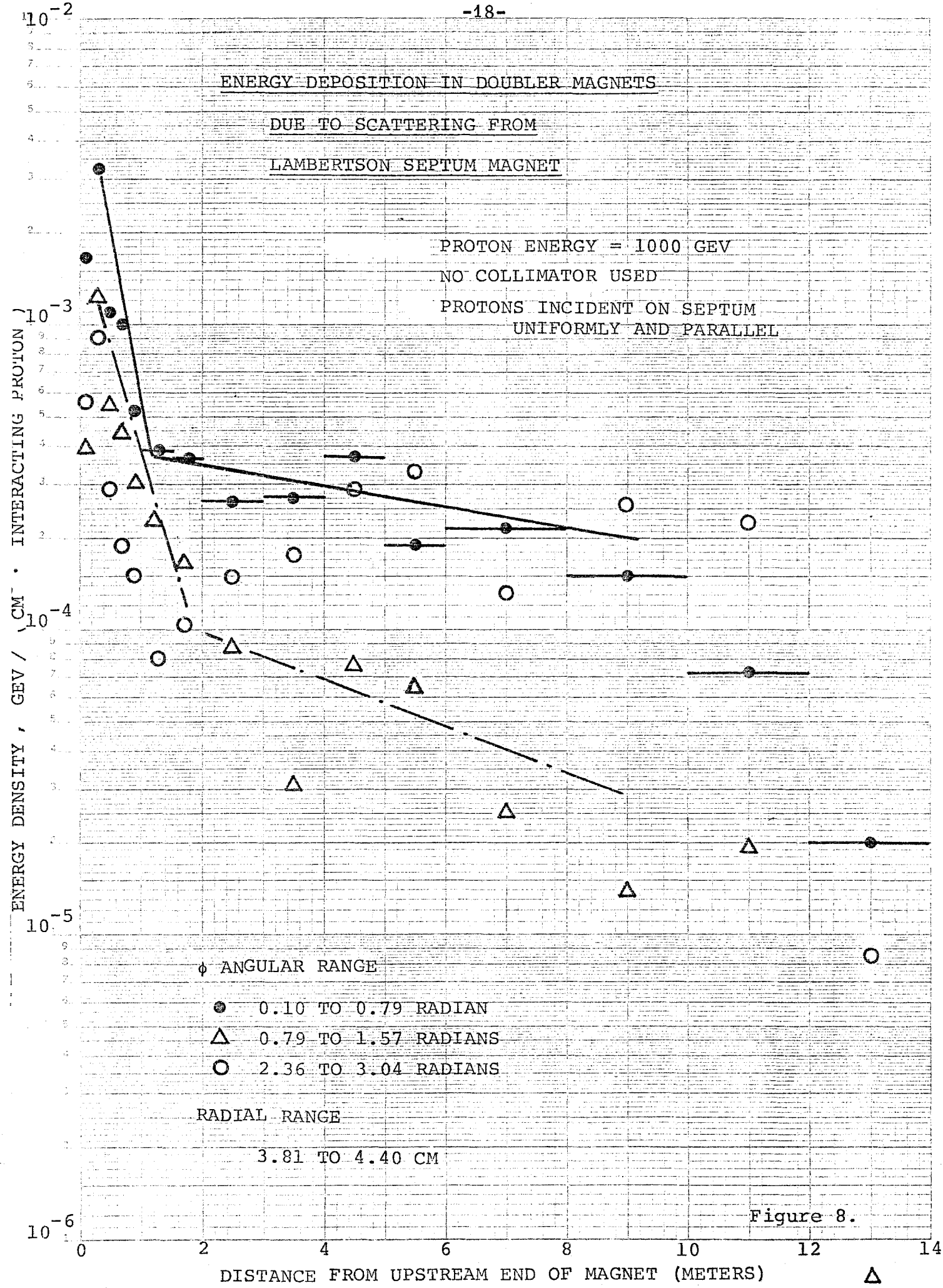
ENERGY DEPOSITION IN DOUBLER MAGNETS
DUE TO SCATTERING FROM
LAMBERTSON SEPTUM MAGNET
PROTON ENERGY = 1000 GEV
NO COLLIMATOR USED
PROTONS INCIDENT ON SEPTUM
UNIFORMLY AND PARALLEL
ENERGY DENSITY , GEV / CM³ · INTERACTING PROTON)
10⁻²
10⁻³
10⁻⁴
10⁻⁵
10⁻⁶
φ ANGULAR RANGE
0.10 TO 0.79 RADIAN
0.79 TO 1.57 RADIANS
2.36 TO 3.04 RADIANS
RADIAL RANGE
3.81 TO 4.40 CM
0
2
4
6
8
10
12
14
DISTANCE FROM UPSTREAM END OF MAGNET (METERS)

Figure 8.

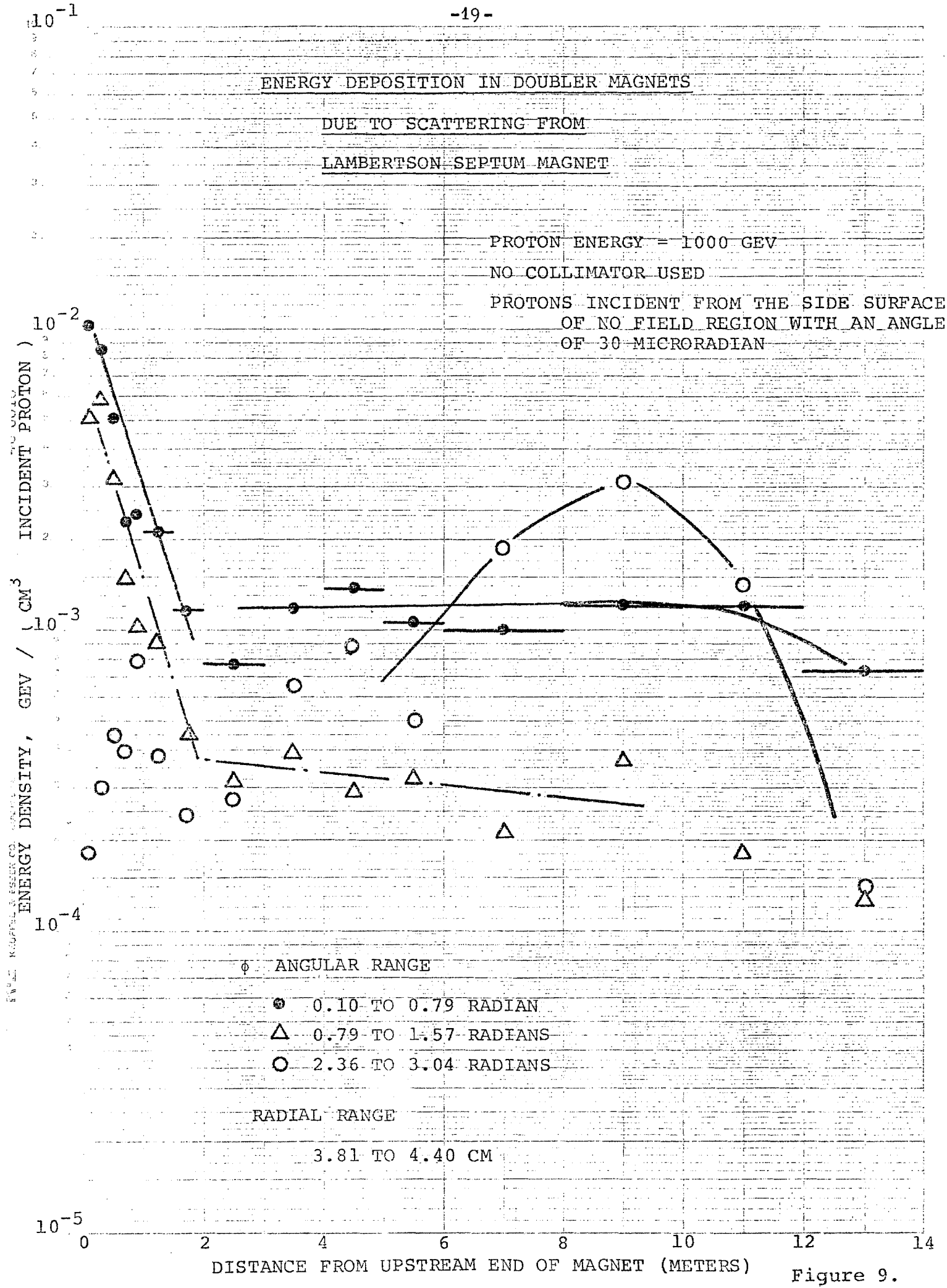
ENERGY DEPOSITION IN DOUBLER MAGNETS
DUE TO SCATTERING FROM
LAMBERTSON SEPTUM MAGNET
PROTON ENERGY = 1000 GEV
NO COLLIMATOR USED
PROTONS INCIDENT FROM THE SIDE SURFACE OF NO FIELD REGION WITH AN ANGLE OF 30 MICRORADIAN
ENERGY DENSITY, GEV / CM³ / INCIDENT PROTON
10⁻¹
10⁻²
10⁻³
10⁻⁴
10⁻⁵
φ ANGULAR RANGE
0.10 TO 0.79 RADIAN
0.79 TO 1.57 RADIANS
2.36 TO 3.04 RADIANS
RADIAL RANGE
3.81 TO 4.40 CM
0
2
4
6
8
10
12
14
DISTANCE FROM UPSTREAM END OF MAGNET (METERS)

Figure 9.

STRAIGHT HIT ON VACUUM CHAMER BY 1000 GEV PROTONS

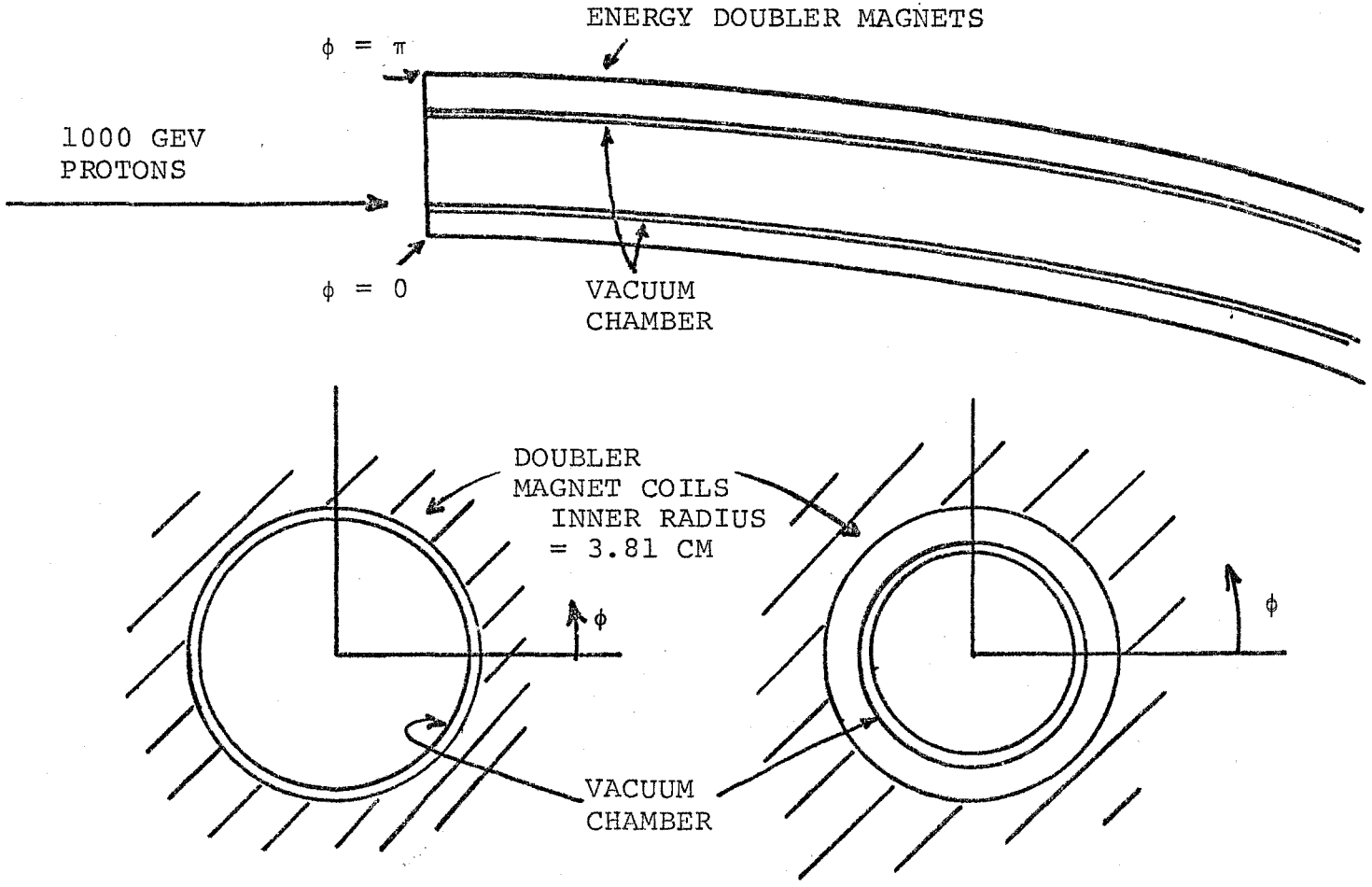

(I) VACUUM CHAMBER

INNER RADIUS = 3.68 CM
OUTER RADIUS = 3.81 CM

(II) VACUUM CHAMBER

INNER RADIUS = 3.18 CM
OUTER RADIUS = 3.31 CM

Figure 10.

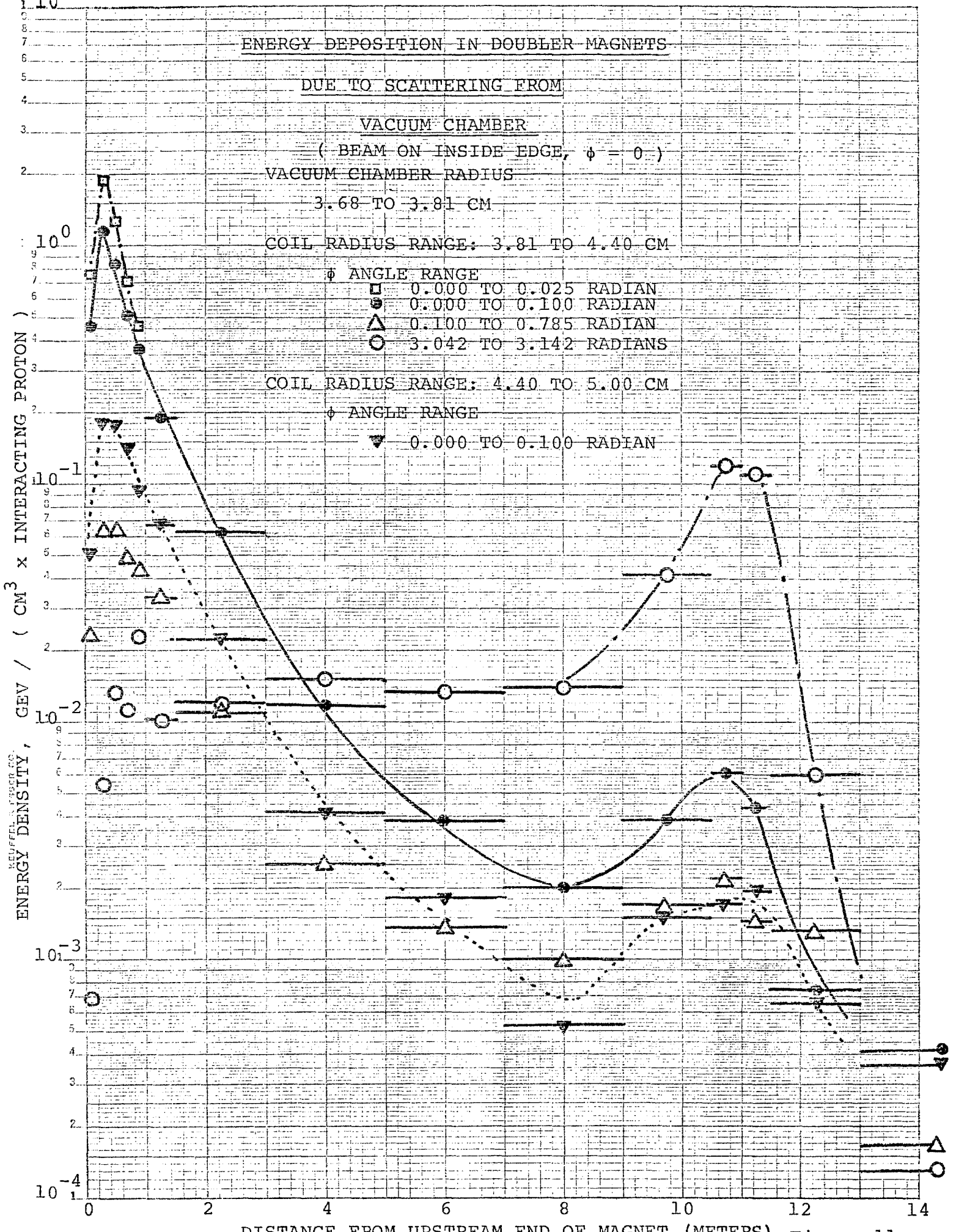
ENERGY DEPOSITION IN DOUBLER MAGNETS
DUE TO SCATTERING FROM
VACUUM CHAMBER
(BEAM ON INSIDE EDGE, φ = 0)
VACUUM CHAMBER RADIUS
3.68 TO 3.81 CM
COIL RADIUS RANGE: 3.81 TO 4.40 CM
φ ANGLE RANGE
0.000 TO 0.025 RADIAN
0.000 TO 0.100 RADIAN
0.100 TO 0.785 RADIAN
3.042 TO 3.142 RADIANS
COIL RADIUS RANGE: 4.40 TO 5.00 CM
φ ANGLE RANGE
0.000 TO 0.100 RADIAN
ENERGY DENSITY, GEV / (CM3 x INTERACTING PROTON)
DISTANCE FROM UPSTREAM END OF MAGNET (METERS)

Figure 11.

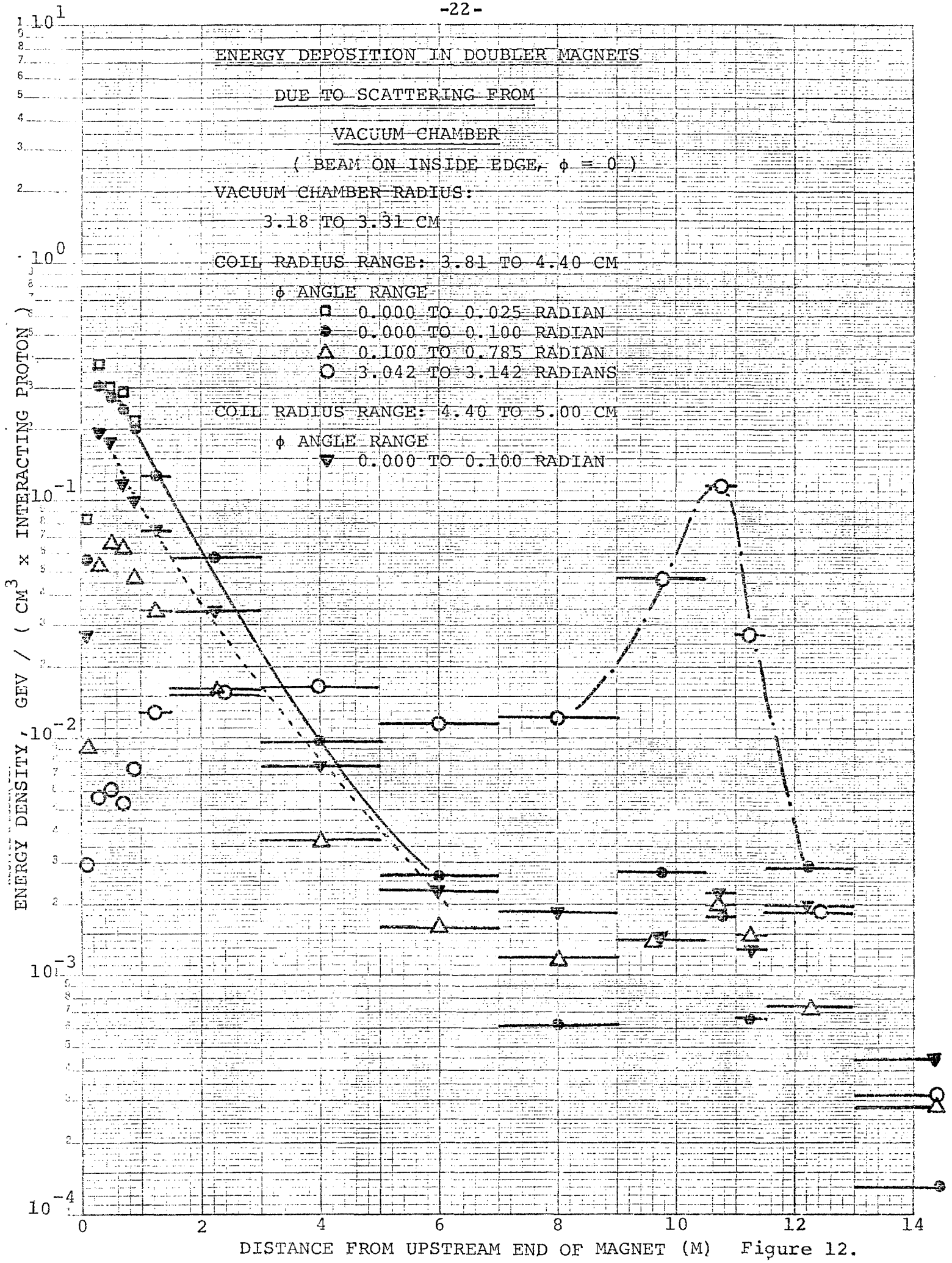
ENERGY DEPOSITION IN DOUBLER MAGNETS
DUE TO SCATTERING FROM
VACUUM CHAMBER
(BEAM ON INSIDE EDGE, φ = 0)
VACUUM CHAMBER RADIUS:
3.18 TO 3.31 CM
COIL RADIUS RANGE: 3.81 TO 4.40 CM
φ ANGLE RANGE
0.000 TO 0.025 RADIAN
0.000 TO 0.100 RADIAN
0.100 TO 0.785 RADIAN
3.042 TO 3.142 RADIANS
COIL RADIUS RANGE: 4.40 TO 5.00 CM
φ ANGLE RANGE
0.000 TO 0.100 RADIAN
ENERGY DENSITY , GEV / (CM3 x INTERACTING PROTON)
DISTANCE FROM UPSTREAM END OF MAGNET (M)

Figure 12.

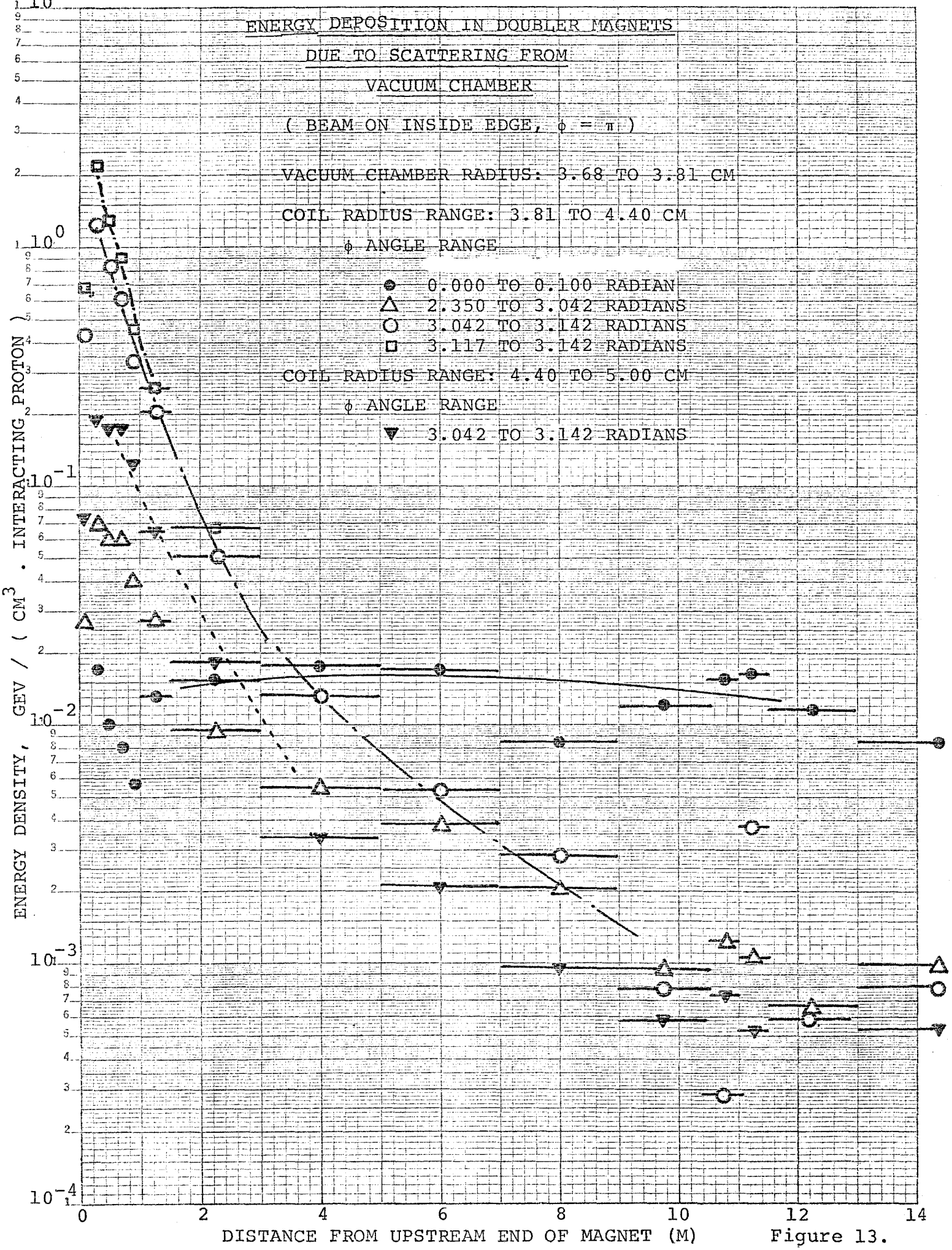
ENERGY DEPOSITION IN DOUBLER MAGNETS
DUE TO SCATTERING FROM
VACUUM CHAMBER
(BEAM ON INSIDE EDGE, φ = π)
VACUUM CHAMBER RADIUS: 3.68 TO 3.81 CM
COIL RADIUS RANGE: 3.81 TO 4.40 CM
φ ANGLE RANGE
0.000 TO 0.100 RADIAN
2.350 TO 3.042 RADIANS
3.042 TO 3.142 RADIANS
3.117 TO 3.142 RADIANS
COIL RADIUS RANGE: 4.40 TO 5.00 CM
φ ANGLE RANGE
3.042 TO 3.142 RADIANS
ENERGY DENSITY, GEV / (CM3 . INTERACTING PROTON)
DISTANCE FROM UPSTREAM END OF MAGNET (M)

Figure 13.

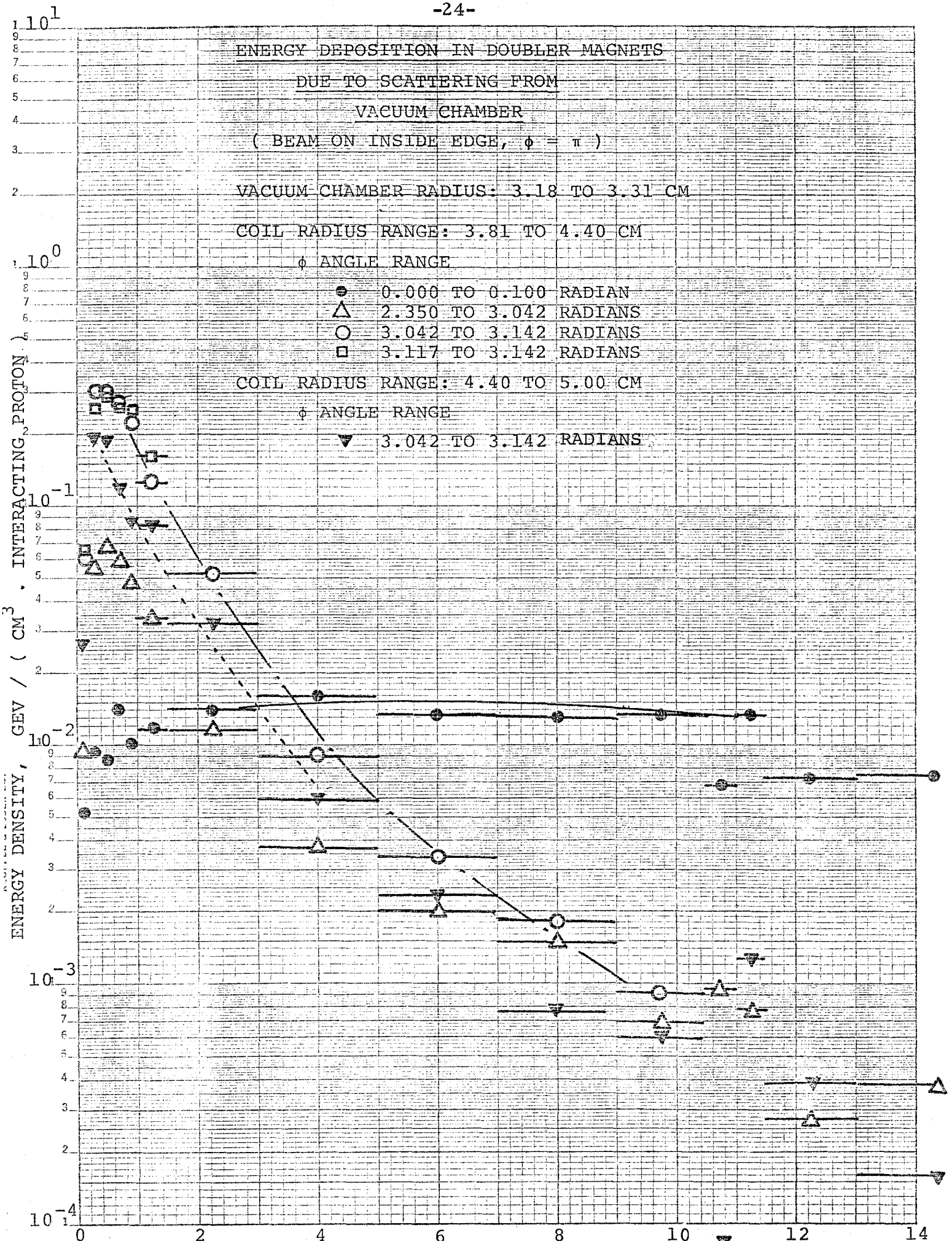
ENERGY DEPOSITION IN DOUBLER MAGNETS
DUE TO SCATTERING FROM
VACUUM CHAMBER
(BEAM ON INSIDE EDGE, φ = π)
VACUUM CHAMBER RADIUS: 3.18 TO 3.31 CM
COIL RADIUS RANGE: 3.81 TO 4.40 CM
φ ANGLE RANGE
0.000 TO 0.100 RADIAN
2.350 TO 3.042 RADIANS
3.042 TO 3.142 RADIANS
3.117 TO 3.142 RADIANS
COIL RADIUS RANGE: 4.40 TO 5.00 CM
φ ANGLE RANGE
3.042 TO 3.142 RADIANS
ENERGY DENSITY, GEV / (CM3 . INTERACTING PROTON)
DISTANCE FROM UPSTREAM END OF MAGNET (M)

Figure 14.

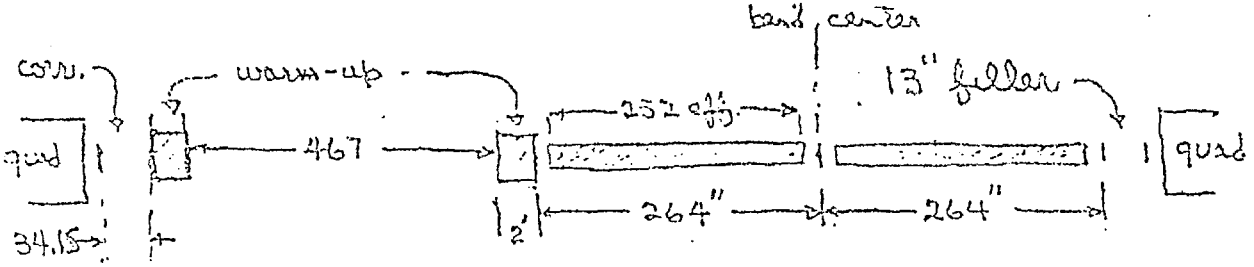

Medium straight section as designed.

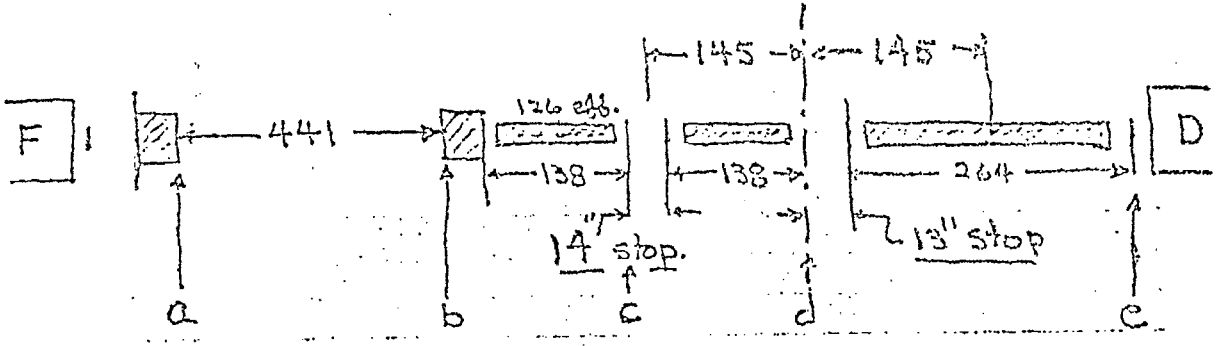

Medium straight - modified with 2 half-bends and using filler space to create spaces for absorbers.

Figure 15.

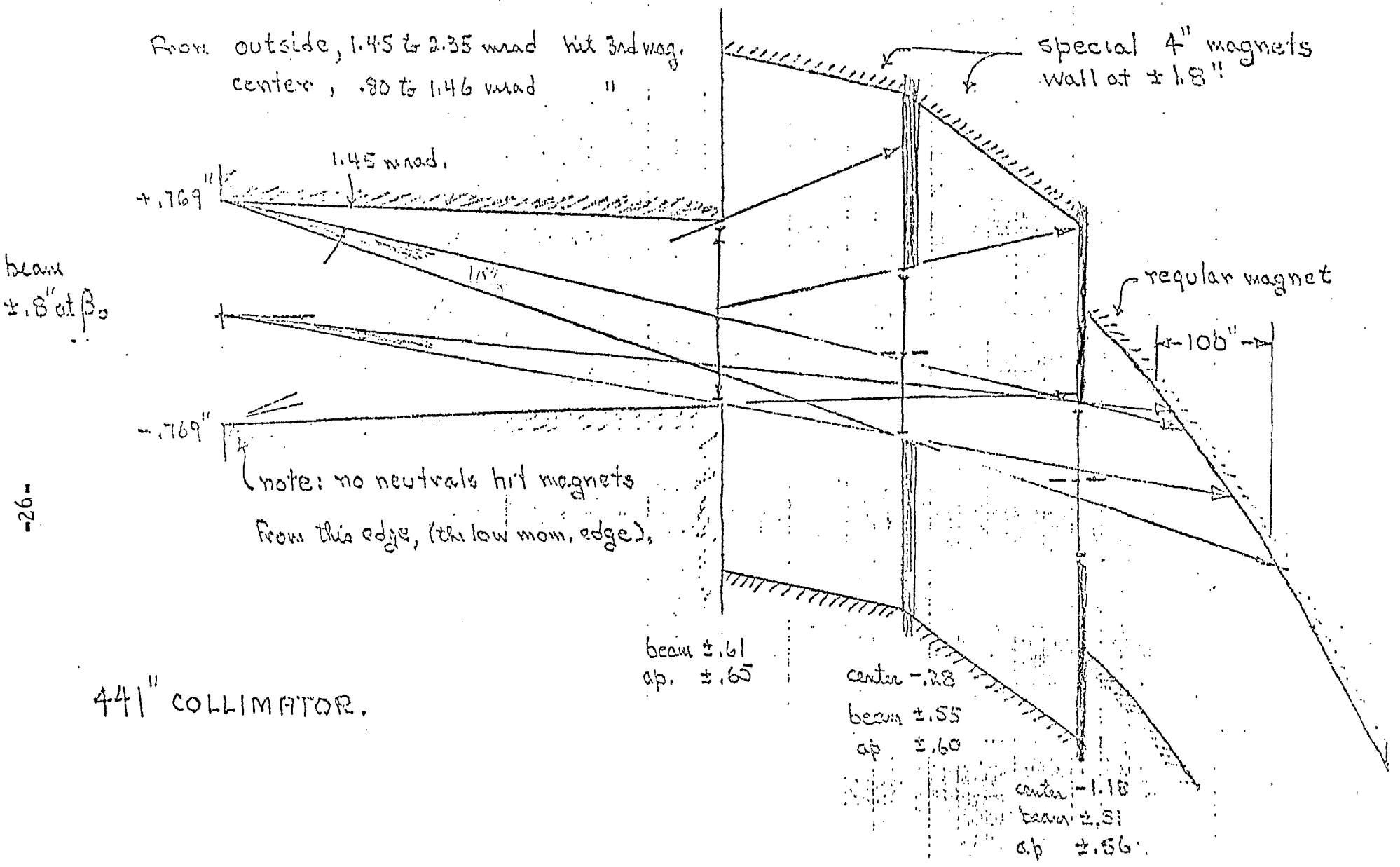
From outside, 1.45 to 2.35 mrad hit 3rd mag.
center, .80 to 1.46 mrad "
special 4" magnets
wall at ± 1.8"
1.45 mrad.
+.769"
beam
±.8" at β₀
regular magnet
100"
-.769"
note: no neutrals hit magnets
From this edge, (the low mom. edge),
beam ±.61
ap. ±.65
center -.28
beam ±.55
ap ±.60
center -1.18
beam ±.51
ap ±.56
44|" COLLIMATOR.

Figure 16.

S. Mori, H. Edwards,
and A. Van Ginneken
January 12, 1979

SUPPLEMENT TO UPC 30

We have discussed some of the typical cases in which the proton beam strikes the vacuum chamber of the Doubler magnets on the inside edge. In this supplement we report various cases in which protons strike different parts of the vacuum chamber with various incident angles. The vacuum chamber radius is either from 3.18 cm to 3.31 cm or from 3.68 cm to 3.81 cm. The incident beam angle at which protons strike the vacuum chamber with respect to the perfect beam orbit direction is either ±0.7 mrad, or zero (parallel incidence). The positive (negative) angle corresponds to a beam moving outward (inward) in the accelerator radius direction. The incident angle of ±0.7 mrad is roughly the maximum beam divergency angle after defocussing quadrupole magnets in the accelerator. The incident angle of 0 mrad corresponds to parallel beam particles along the vacuum chamber side wall. In the parallel case, when protons hit the edge of the vacuum chamber or plug, the probability that some of the protons are scattered out due to Coulomb scattering before nuclear interaction was crudely taken into account.

Figures S1 through S21 show energy density distributions in the Doubler magnet coils as functions of azimuthal angle and coil radius. Table I summarizes some of the intersting properties for all the cases.

The maximum energy deposition at the upstream end and in the shallow radial region of coils (3.81 cm to 4.4 cm) is very sensitive to the vacuum chamber radius. The maximum energy deposition is reduced by a factor of about 5 by changing the chamber inner radius from 3.68 cm to 3.18 cm in all the cases discussed here. The second peaks due to neutral pion production depend strongly upon beam conditions because the vacuum chamber material can absorb

photons from the neutral pion decay.

The enrgy deposition in the large radial region of coils (4.4 cm to 5.0 cm) is substantially smaller than that in the shallow region. This is due to shielding by the coil material itself.

The vacuum chamber plug suppresses the energy deposition level to 0.01 GeV/(cm^3 interacting proton) or less except for in the upstream end region.

TABLE I

	Vacuum Chamber Inner Radius (cm)	Beam Position on Chamber Radius	ϕ (rad)	θ_{Beam} (mrad)	Maximum Energy Deposition, GeV/(cm^3. Int. Protons) Coil Radius: 3.81-4.40 cm Upstream (ϕ)	3.81-4.40 cm 2nd peak*(ϕ)	4.40-5.00 cm Upstream (ϕ)	4.40-5.00 cm 2nd peak*(ϕ)
S1	3.18	Inside	0	0	0.38 (0)	0.12 (π)	0.19 (0)	0.05 (π)
S2	3.18	Inside	0	+0.7	0.56 (0)	0.03 (π)	0.24 (0)	0.01 (π)
S3	3.18	Middle	0	0	0.85 (0)	0.003 (π)	0.38 (0)	0.002 (π)
S4	3.18	Middle	0	+0.7	0.88 (0)	0.001 (π)	0.41 (0)	0.001 (π)
S5	3.18	Outside	0	0	0.67 (0)	0.01 (0)	0.28 (0)	0.003 (0)
S6	3.68	Inside	0	0	1.9 (0)	0.12 (π)	0.19 (0)	0.05 (π)
S7	3.68	Inside	0	+0.7	2.6 (0)	0.06 (π)	0.30 (0)	0.02 (π)
S8	3.68	Middle	0	+0.7	5.4 (0)	0.001 (π)	0.60 (0)	0.001 (π)
S9	3.18	Inside	π	0	0.30 (π)	0.015 (0)	0.19 (π)	0.01 (0)
S10	3.18	Inside	π	-0.7	0.52 (π)	0.006 (0)	0.25 (π)	0.004 (0)
S11	3.18	Middle	π	0	0.82 (π)	0.001 (0)	0.40 (π)	0.001 (0)
S12	3.18	Middle	π	-0.7	0.80 (π)	0.001 (π)	0.46 (π)	0.0005 (0)
S13	3.18	Outside	π	0	0.61 (π)	0.004 (π)	0.25 (π)	0.001(?)
S14	3.68	Inside	π	0	2.2 (π)	0.02 (0)	0.19 (π)	0.008 (0)
S15	3.68	Inside	π	-0.7	2.9 (π)	0.006 (0)	0.30 (π)	0.005 (0)
S16	3.68	Middle	π	-0.7	5.7 (π)	0.0005 (?)	0.62 (π)	0.0005 (0)
S17	3.68	Outside	π	-0.7	9.0 (π)	0.0005 (?)	0.62 (π)	0.0005 (?)
S18	Plug**	Inside	0	0	0.09 (0)	0.01 (π)	0.04 (?)	0.005 (π)
S19	Plug	Inside	0	+0.7	0.15 (0)	0.004 (π)	0.07 (?)	0.001 (?)
S20	Plug	Inside	π	0	0.10 (π)	0.005 (0)	0.05 (π)	0.002 (0)
S21	Plug	Inside	π	-0.7	0.12 (π)	0.002 (0)	0.06 (π)	0.001 (?)

* when no apparent second peak appears, the maximum energy deposition at about 10m from the upstream end of the Doubler magnet is quoted.

** the aperture of the vacuum chamber plug hole is 5cm (horizontal) x 3cm (vertical). The space between the coils and the plug aperture is filled with iron.

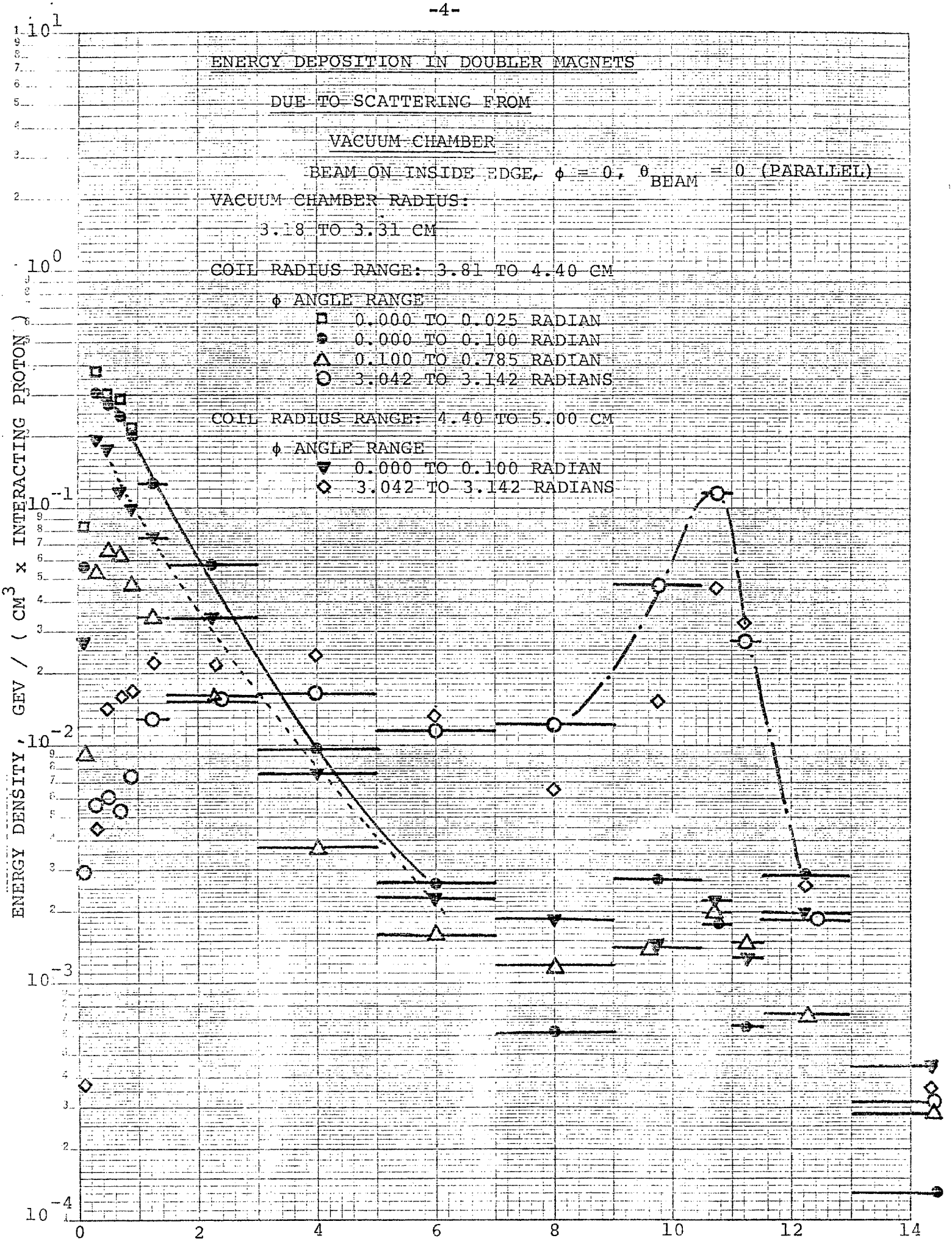
ENERGY DEPOSITION IN DOUBLER MAGNETS
DUE TO SCATTERING FROM
VACUUM CHAMBER
BEAM ON INSIDE EDGE, $\phi = 0$, $\theta_{BEAM} = 0$ (PARALLEL)
VACUUM CHAMBER RADIUS:
3.18 TO 3.31 CM
COIL RADIUS RANGE: 3.81 TO 4.40 CM
ϕ ANGLE RANGE
0.000 TO 0.025 RADIAN
0.000 TO 0.100 RADIAN
0.100 TO 0.785 RADIAN
3.042 TO 3.142 RADIANS
COIL RADIUS RANGE: 4.40 TO 5.00 CM
ϕ ANGLE RANGE
0.000 TO 0.100 RADIAN
3.042 TO 3.142 RADIANS
ENERGY DENSITY, GEV / (CM^3 x INTERACTING PROTON)
10^{1}
10^{0}
10^{-1}
10^{-2}
10^{-3}
10^{-4}
0
2
4
6
8
10
12
14
DISTANCE FROM UPSTREAM END OF MAGNET (M)

Figure S1.

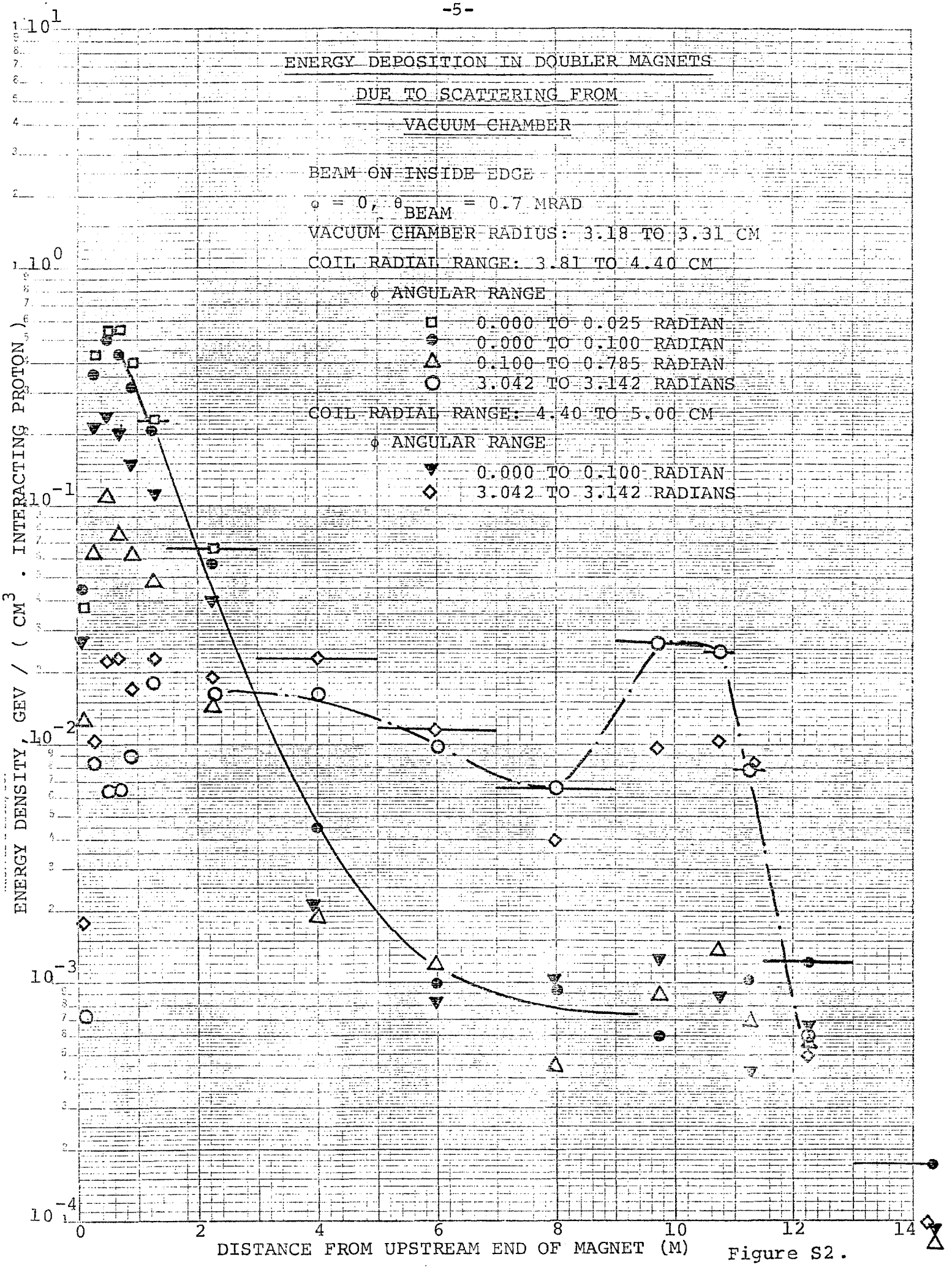
ENERGY DEPOSITION IN DOUBLER MAGNETS
DUE TO SCATTERING FROM
VACUUM CHAMBER
BEAM ON INSIDE EDGE
φ = 0, θ BEAM = 0.7 MRAD
VACUUM CHAMBER RADIUS: 3.18 TO 3.31 CM
COIL RADIAL RANGE: 3.81 TO 4.40 CM
φ ANGULAR RANGE
0.000 TO 0.025 RADIAN
0.000 TO 0.100 RADIAN
0.100 TO 0.785 RADIAN
3.042 TO 3.142 RADIANS
COIL RADIAL RANGE: 4.40 TO 5.00 CM
φ ANGULAR RANGE
0.000 TO 0.100 RADIAN
3.042 TO 3.142 RADIANS
ENERGY DENSITY, GEV / (CM3 . INTERACTING PROTON)
DISTANCE FROM UPSTREAM END OF MAGNET (M)

Figure S2.

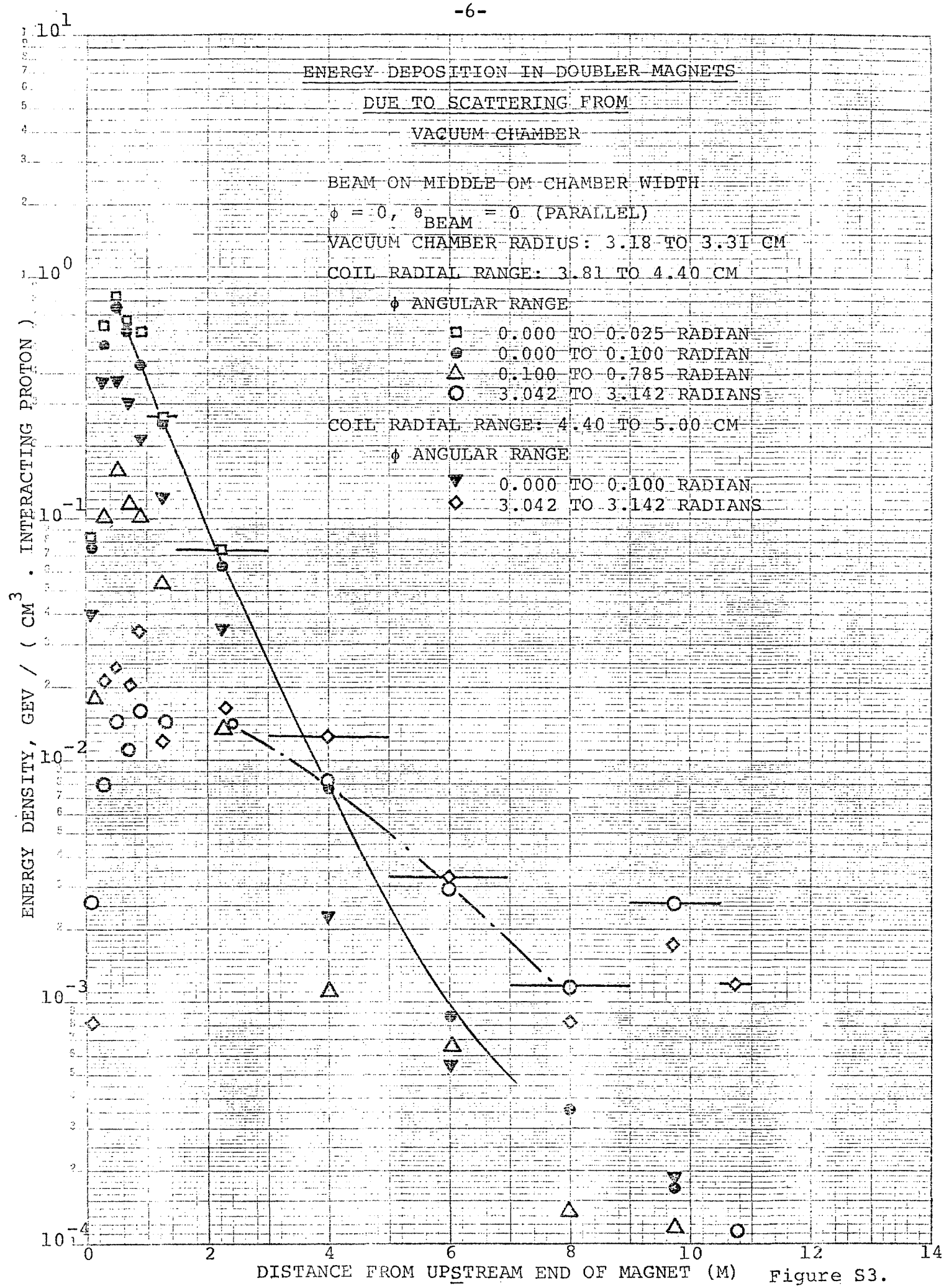
ENERGY DEPOSITION IN DOUBLER MAGNETS
DUE TO SCATTERING FROM
VACUUM CHAMBER
BEAM ON MIDDLE OM CHAMBER WIDTH
$\phi = 0$, $\theta_{BEAM} = 0$ (PARALLEL)
VACUUM CHAMBER RADIUS: 3.18 TO 3.31 CM
COIL RADIAL RANGE: 3.81 TO 4.40 CM
ϕ ANGULAR RANGE
0.000 TO 0.025 RADIAN
0.000 TO 0.100 RADIAN
0.100 TO 0.785 RADIAN
3.042 TO 3.142 RADIANS
COIL RADIAL RANGE: 4.40 TO 5.00 CM
ϕ ANGULAR RANGE
0.000 TO 0.100 RADIAN
3.042 TO 3.142 RADIANS
ENERGY DENSITY, GEV / (CM^3 . INTERACTING PROTON)
10^{1}
10^{0}
10^{-1}
10^{-2}
10^{-3}
10^{-4}
0
2
4
6
8
10
12
14
DISTANCE FROM UPSTREAM END OF MAGNET (M)

Figure S3.

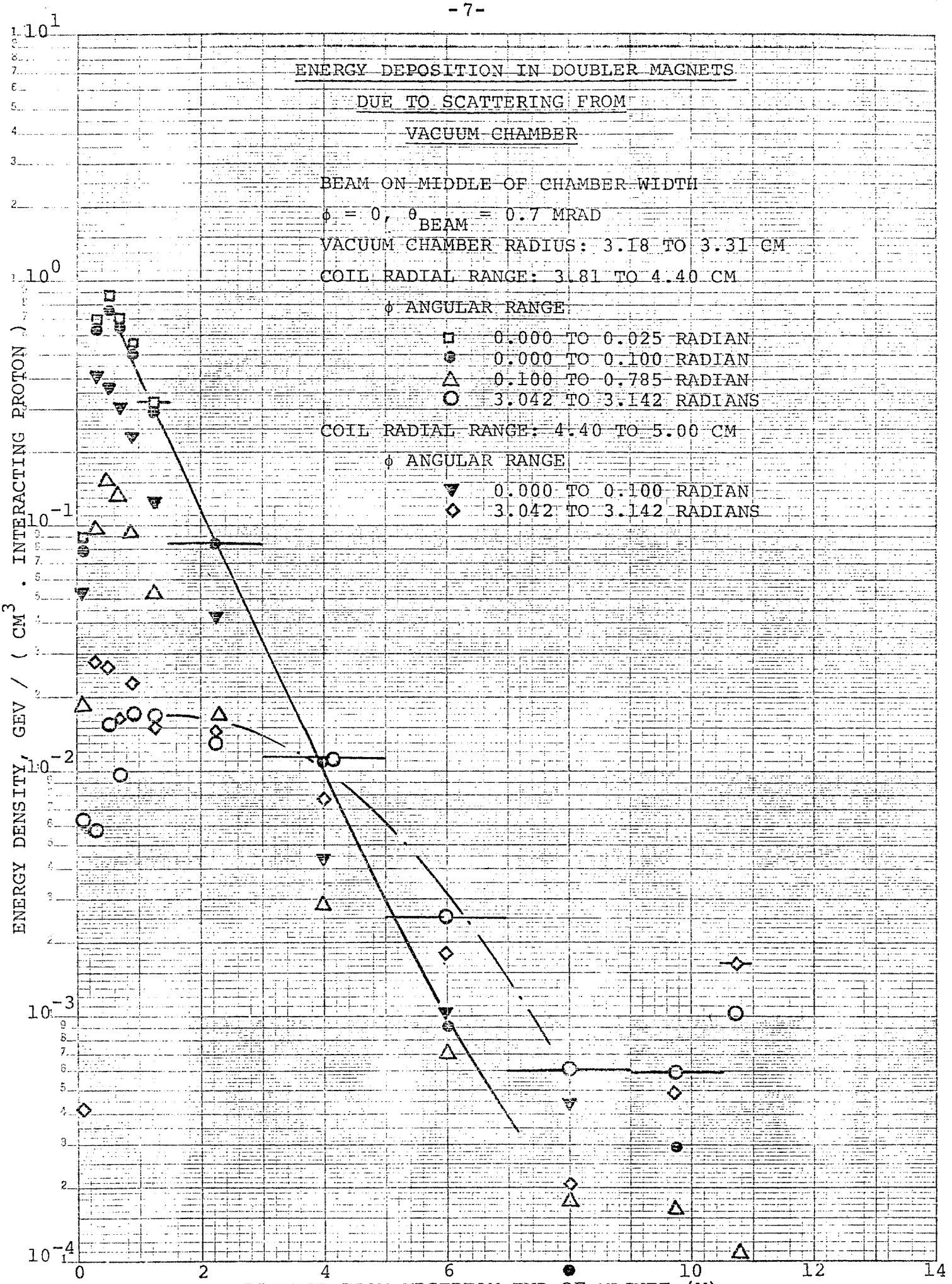
ENERGY DEPOSITION IN DOUBLER MAGNETS
DUE TO SCATTERING FROM
VACUUM CHAMBER
BEAM ON MIDDLE OF CHAMBER WIDTH
$\phi = 0$, $\theta_{BEAM} = 0.7$ MRAD
VACUUM CHAMBER RADIUS: 3.18 TO 3.31 CM
COIL RADIAL RANGE: 3.81 TO 4.40 CM
ϕ ANGULAR RANGE
0.000 TO 0.025 RADIAN
0.000 TO 0.100 RADIAN
0.100 TO 0.785 RADIAN
3.042 TO 3.142 RADIANS
COIL RADIAL RANGE: 4.40 TO 5.00 CM
ϕ ANGULAR RANGE
0.000 TO 0.100 RADIAN
3.042 TO 3.142 RADIANS
ENERGY DENSITY, GEV / (CM^3 . INTERACTING PROTON)
10^{1}
10^{0}
10^{-1}
10^{-2}
10^{-3}
10^{-4}
0
2
4
6
8
10
12
14
DISTANCE FROM UPSTREAM END OF MAGNET (M)

Figure S4.

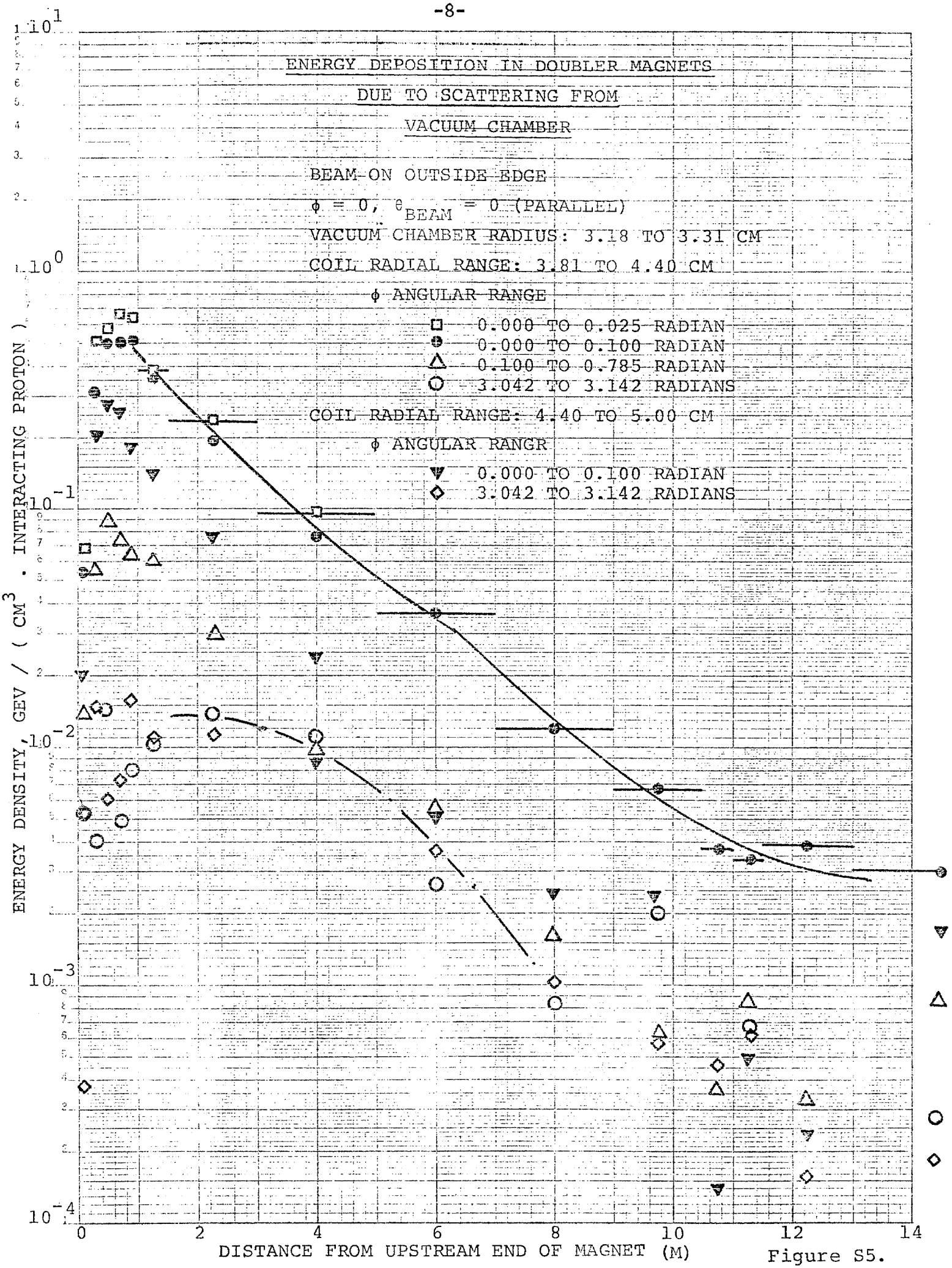
ENERGY DEPOSITION IN DOUBLER MAGNETS
DUE TO SCATTERING FROM
VACUUM CHAMBER
BEAM-ON OUTSIDE EDGE
$\phi = 0$, $\theta_{BEAM} = 0$ (PARALLEL)
VACUUM CHAMBER RADIUS: 3.18 TO 3.31 CM
COIL RADIAL RANGE: 3.81 TO 4.40 CM
ϕ ANGULAR RANGE
0.000 TO 0.025 RADIAN
0.000 TO 0.100 RADIAN
0.100 TO 0.785 RADIAN
3.042 TO 3.142 RADIANS
COIL RADIAL RANGE: 4.40 TO 5.00 CM
ϕ ANGULAR RANGR
0.000 TO 0.100 RADIAN
3.042 TO 3.142 RADIANS
ENERGY DENSITY, GEV / (CM^3 . INTERACTING PROTON)
10^{1}
10^{0}
10^{-1}
10^{-2}
10^{-3}
10^{-4}
0
2
4
6
8
10
12
14
DISTANCE FROM UPSTREAM END OF MAGNET (M)

Figure S5.

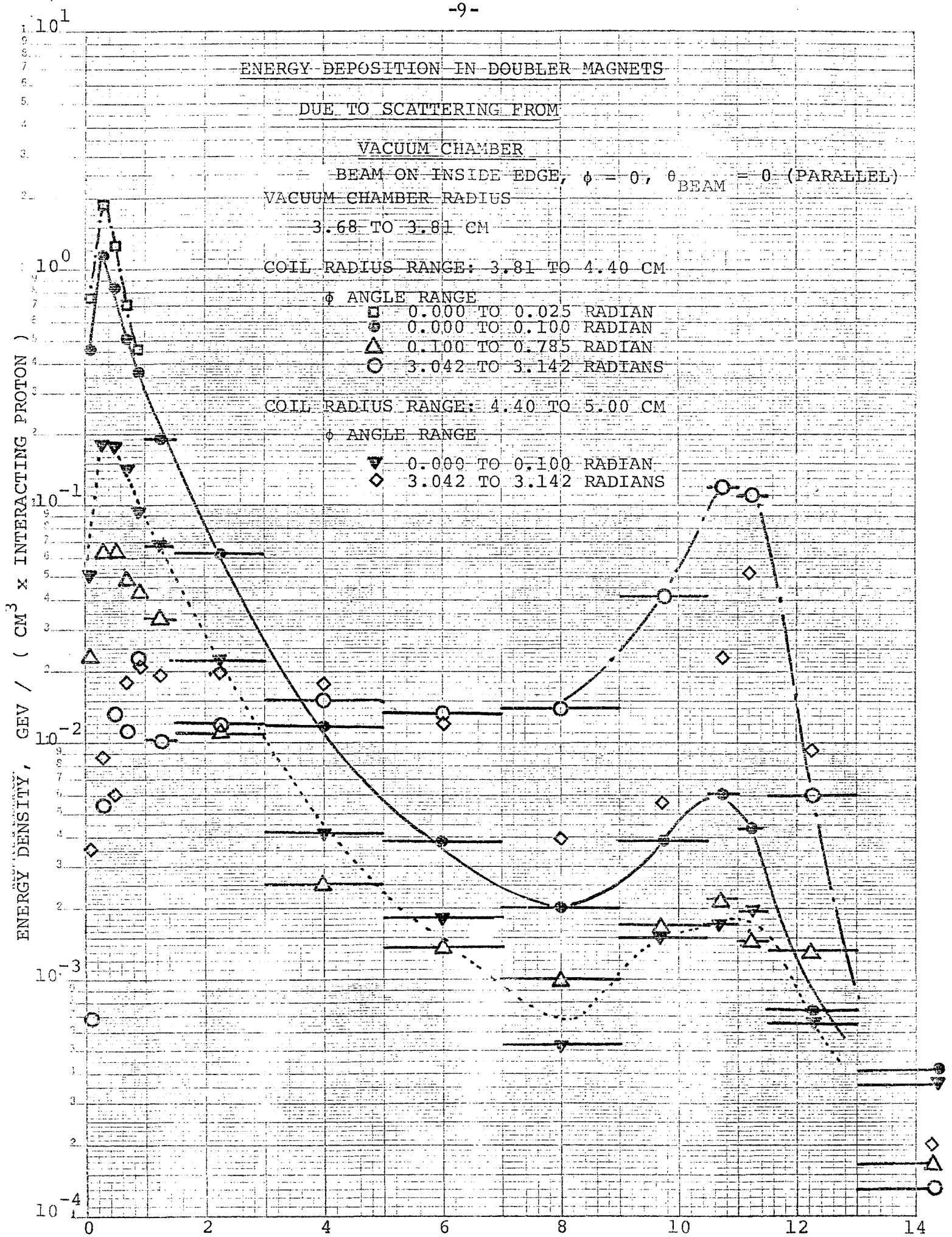
ENERGY DEPOSITION IN DOUBLER MAGNETS
DUE TO SCATTERING FROM
VACUUM CHAMBER
BEAM ON INSIDE EDGE, $\phi = 0$, $\theta_{BEAM} = 0$ (PARALLEL)
VACUUM CHAMBER RADIUS
3.68 TO 3.81 CM
COIL RADIUS RANGE: 3.81 TO 4.40 CM
ϕ ANGLE RANGE
0.000 TO 0.025 RADIAN
0.000 TO 0.100 RADIAN
0.100 TO 0.785 RADIAN
3.042 TO 3.142 RADIANS
COIL RADIUS RANGE: 4.40 TO 5.00 CM
ϕ ANGLE RANGE
0.000 TO 0.100 RADIAN
3.042 TO 3.142 RADIANS
ENERGY DENSITY, GEV / (CM^3 x INTERACTING PROTON)
10^{1}
10^{0}
10^{-1}
10^{-2}
10^{-3}
10^{-4}
0
2
4
6
8
10
12
14
DISTANCE FROM UPSTREAM END OF MAGNET (METERS)

Figure S6.

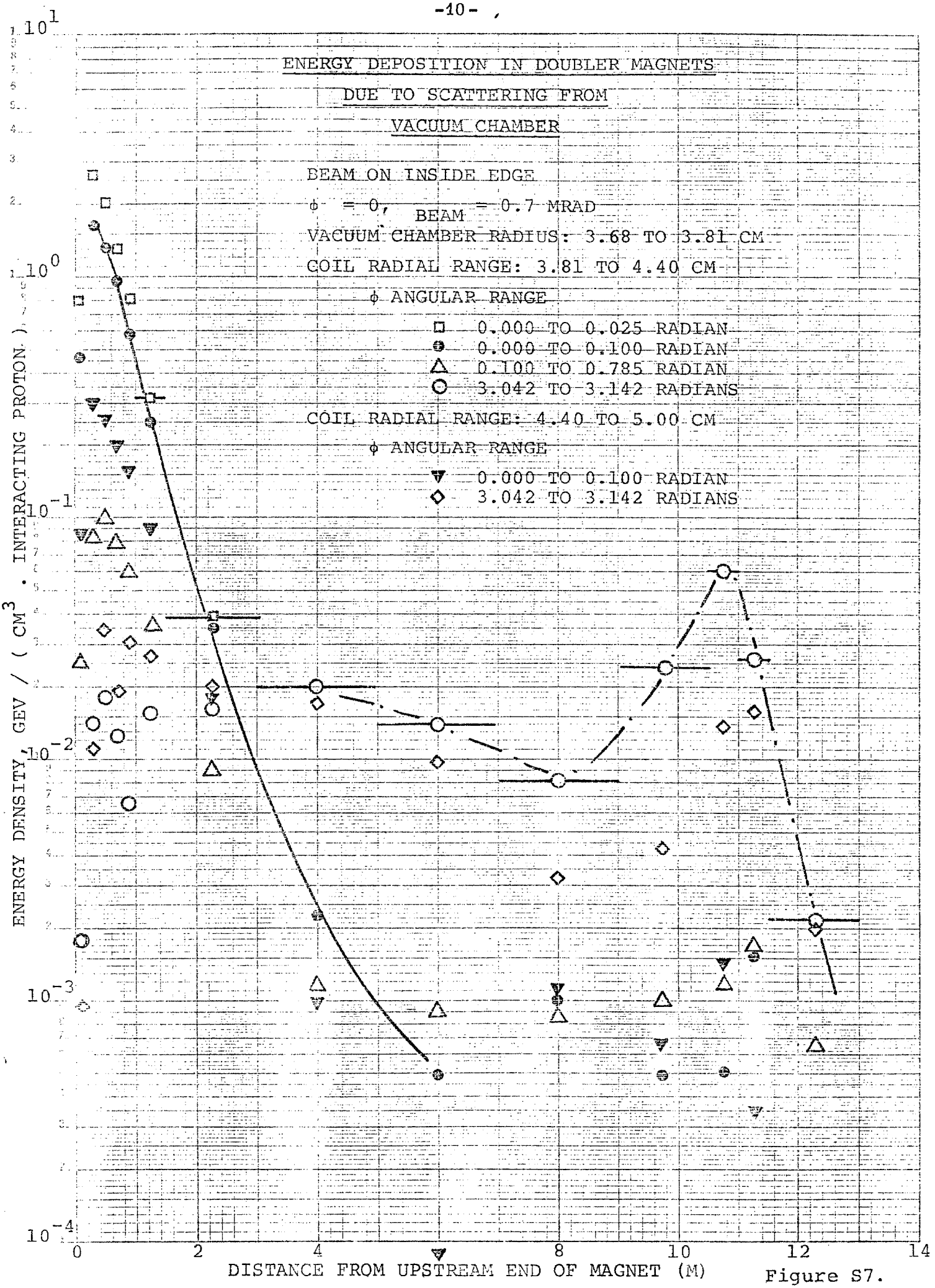
ENERGY DEPOSITION IN DOUBLER MAGNETS
DUE TO SCATTERING FROM
VACUUM CHAMBER
BEAM ON INSIDE EDGE
φ = 0, BEAM = 0.7 MRAD
VACUUM CHAMBER RADIUS: 3.68 TO 3.81 CM
COIL RADIAL RANGE: 3.81 TO 4.40 CM
φ ANGULAR RANGE
0.000 TO 0.025 RADIAN
0.000 TO 0.100 RADIAN
0.100 TO 0.785 RADIAN
3.042 TO 3.142 RADIANS
COIL RADIAL RANGE: 4.40 TO 5.00 CM
φ ANGULAR RANGE
0.000 TO 0.100 RADIAN
3.042 TO 3.142 RADIANS
ENERGY DENSITY, GEV / (CM3 . INTERACTING PROTON)
DISTANCE FROM UPSTREAM END OF MAGNET (M)

Figure S7.

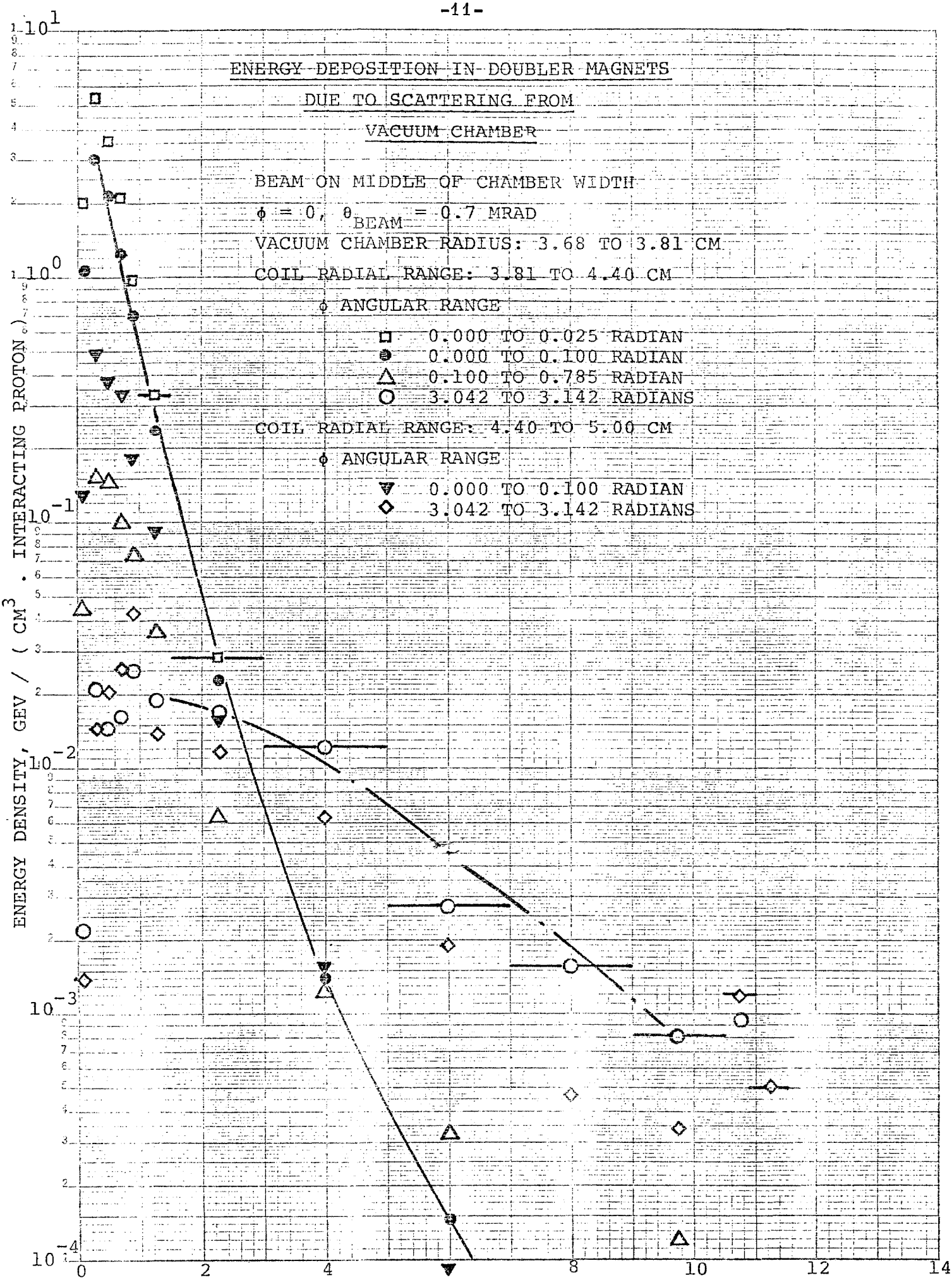
ENERGY DEPOSITION IN DOUBLER MAGNETS
DUE TO SCATTERING FROM
VACUUM CHAMBER
BEAM ON MIDDLE OF CHAMBER WIDTH
$\phi = 0$, $\theta_{BEAM} = 0.7$ MRAD
VACUUM CHAMBER RADIUS: 3.68 TO 3.81 CM
COIL RADIAL RANGE: 3.81 TO 4.40 CM
ϕ ANGULAR RANGE
0.000 TO 0.025 RADIAN
0.000 TO 0.100 RADIAN
0.100 TO 0.785 RADIAN
3.042 TO 3.142 RADIANS
COIL RADIAL RANGE: 4.40 TO 5.00 CM
ϕ ANGULAR RANGE
0.000 TO 0.100 RADIAN
3.042 TO 3.142 RADIANS
ENERGY DENSITY, GEV / (CM^3 . INTERACTING PROTON$_o$)
10^1
10^0
10^{-1}
10^{-2}
10^{-3}
10^{-4}
0
2
4
8
10
12
14
DISTANCE FROM UPSTREAM END OF MAGNET (M)

Figure S8.

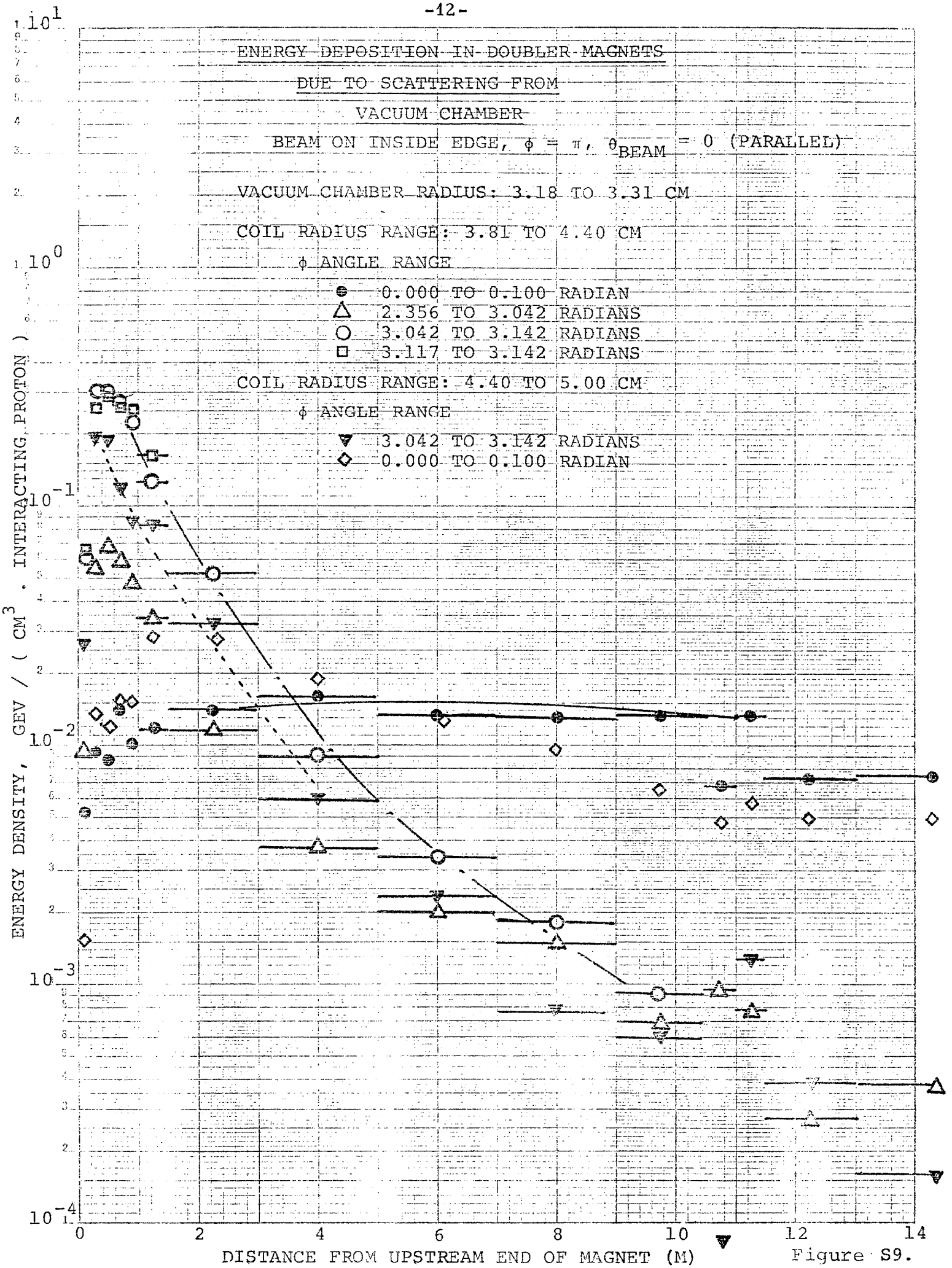
ENERGY DEPOSITION IN DOUBLER MAGNETS
DUE TO SCATTERING FROM
VACUUM CHAMBER
BEAM ON INSIDE EDGE, φ = π, θBEAM = 0 (PARALLEL)
VACUUM CHAMBER RADIUS: 3.18 TO 3.31 CM
COIL RADIUS RANGE: 3.81 TO 4.40 CM
φ ANGLE RANGE
0.000 TO 0.100 RADIAN
2.356 TO 3.042 RADIANS
3.042 TO 3.142 RADIANS
3.117 TO 3.142 RADIANS
COIL RADIUS RANGE: 4.40 TO 5.00 CM
φ ANGLE RANGE
3.042 TO 3.142 RADIANS
0.000 TO 0.100 RADIAN
ENERGY DENSITY, GEV / (CM3 . INTERACTING PROTON)
DISTANCE FROM UPSTREAM END OF MAGNET (M)

Figure S9.

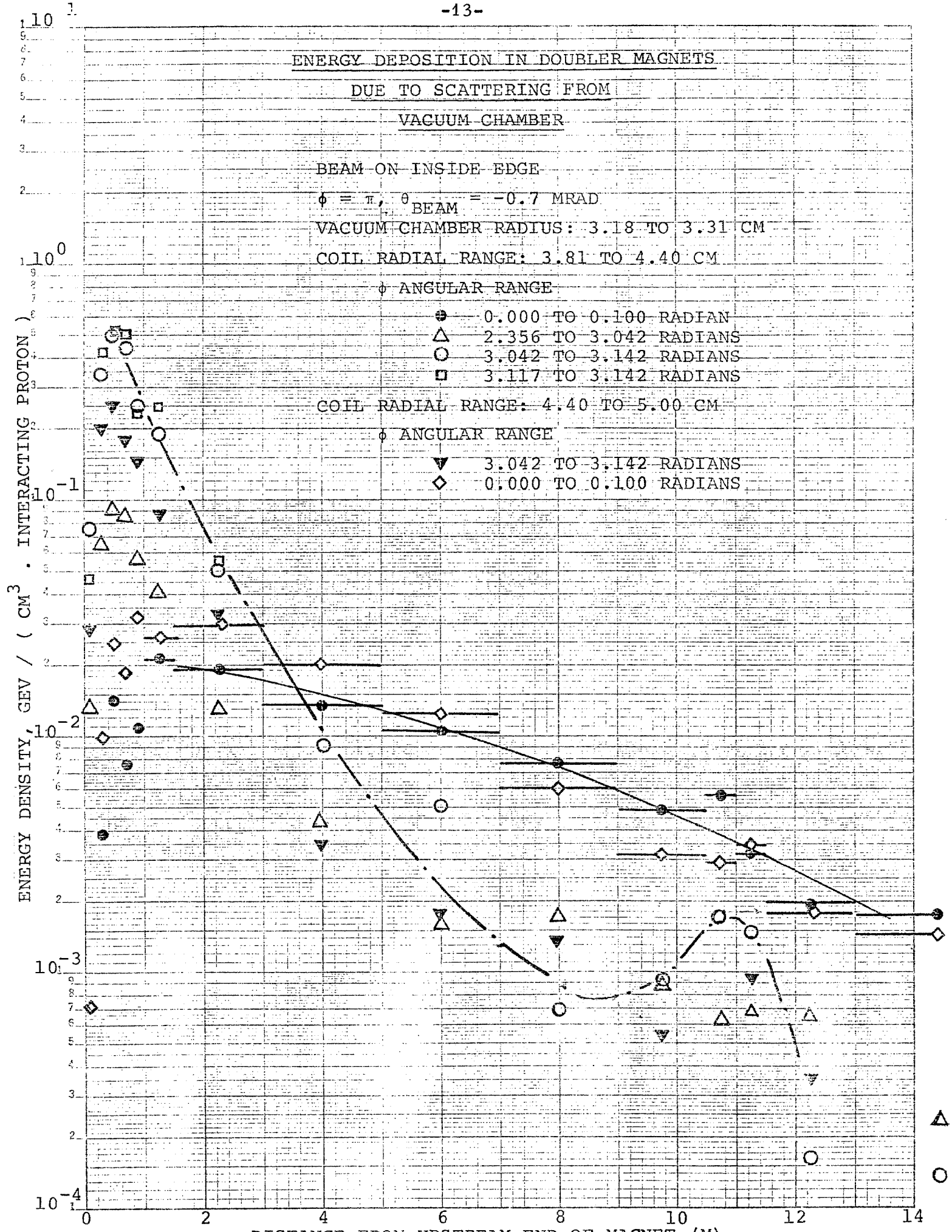
ENERGY DEPOSITION IN DOUBLER MAGNETS
DUE TO SCATTERING FROM
VACUUM CHAMBER
BEAM ON INSIDE EDGE
$\phi = \pi$, $\theta_{BEAM} = -0.7$ MRAD
VACUUM CHAMBER RADIUS: 3.18 TO 3.31 CM
COIL RADIAL RANGE: 3.81 TO 4.40 CM
ϕ ANGULAR RANGE
0.000 TO 0.100 RADIAN
2.356 TO 3.042 RADIANS
3.042 TO 3.142 RADIANS
3.117 TO 3.142 RADIANS
COIL RADIAL RANGE: 4.40 TO 5.00 CM
ϕ ANGULAR RANGE
3.042 TO 3.142 RADIANS
0.000 TO 0.100 RADIANS
ENERGY DENSITY, GEV / (CM^3 . INTERACTING PROTON)
DISTANCE FROM UPSTREAM END OF MAGNET (M)

Figure S10.

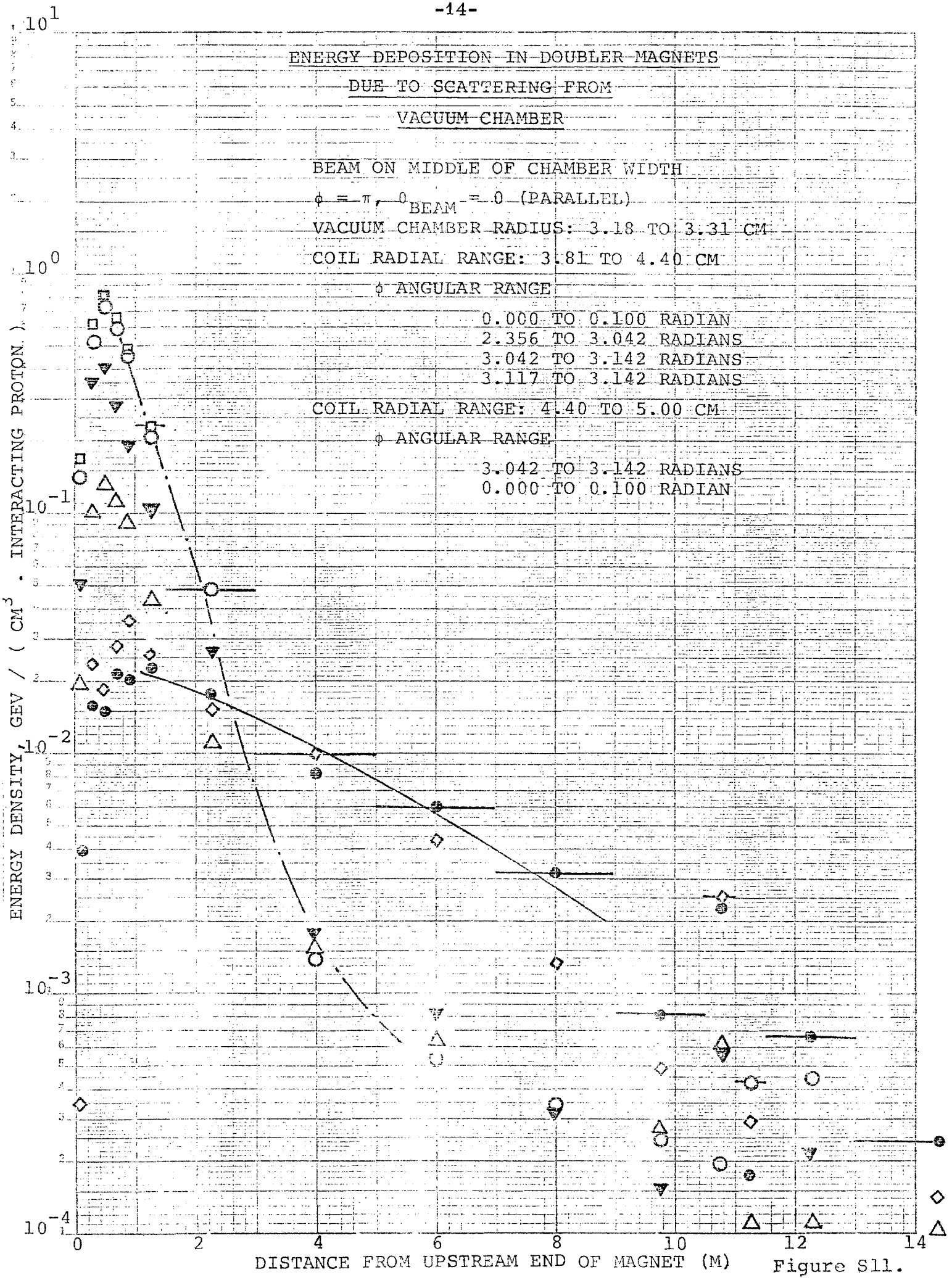
ENERGY DEPOSITION IN DOUBLER MAGNETS
DUE TO SCATTERING FROM
VACUUM CHAMBER
BEAM ON MIDDLE OF CHAMBER WIDTH
$\phi = \pi$, $\theta_{BEAM} = 0$ (PARALLEL)
VACUUM CHAMBER RADIUS: 3.18 TO 3.31 CM
COIL RADIAL RANGE: 3.81 TO 4.40 CM
ϕ ANGULAR RANGE
0.000 TO 0.100 RADIAN
2.356 TO 3.042 RADIANS
3.042 TO 3.142 RADIANS
3.117 TO 3.142 RADIANS
COIL RADIAL RANGE: 4.40 TO 5.00 CM
ϕ ANGULAR RANGE
3.042 TO 3.142 RADIANS
0.000 TO 0.100 RADIAN
ENERGY DENSITY, GEV / (CM^3 · INTERACTING PROTON)
DISTANCE FROM UPSTREAM END OF MAGNET (M)
10^1
10^0
10^{-1}
10^{-2}
10^{-3}
10^{-4}
0
2
4
6
8
10
12
14

Figure S11.

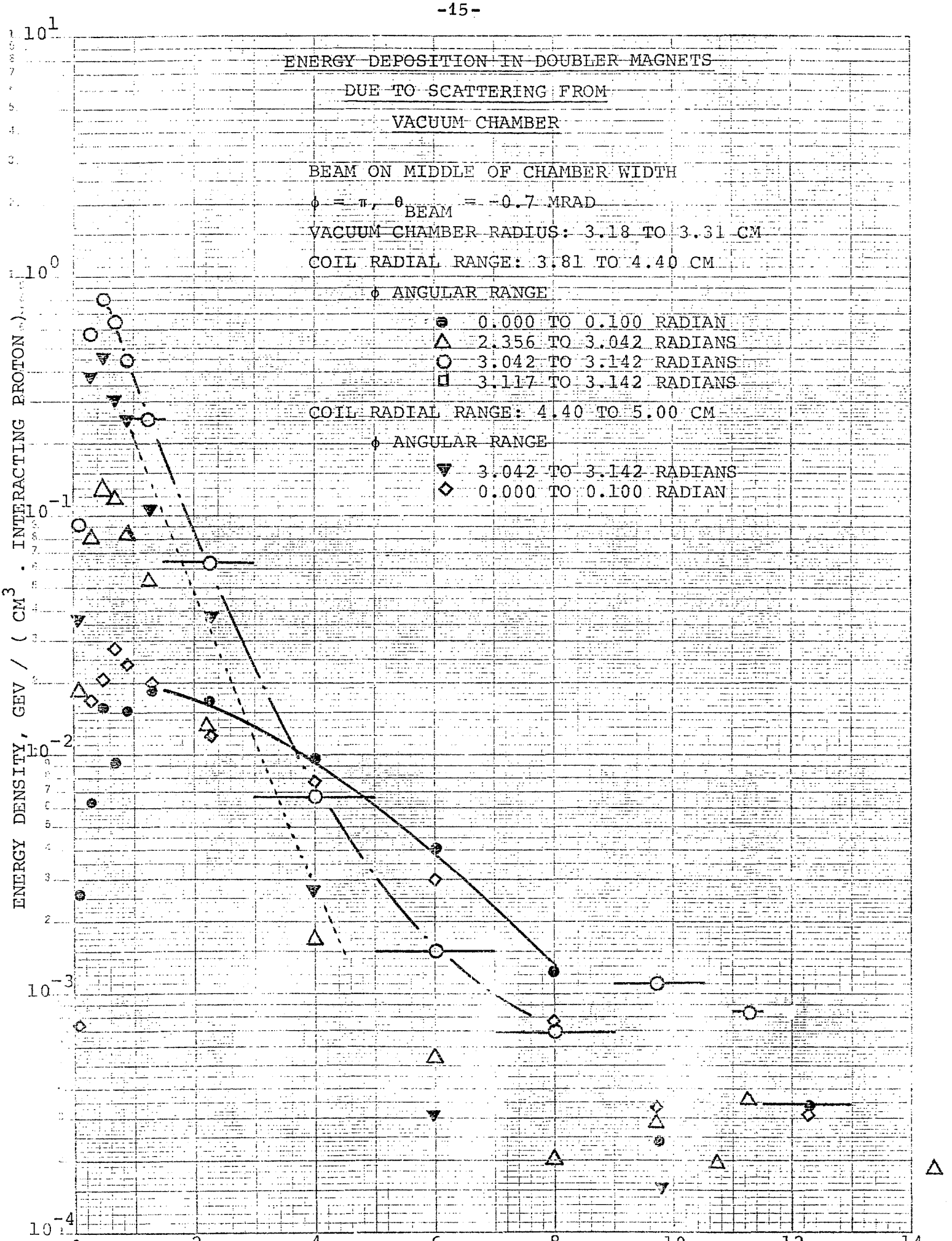
ENERGY DEPOSITION IN DOUBLER MAGNETS
DUE TO SCATTERING FROM
VACUUM CHAMBER
BEAM ON MIDDLE OF CHAMBER WIDTH
$\phi = \pi$, $\theta_{BEAM} = -0.7$ MRAD
VACUUM CHAMBER RADIUS: 3.18 TO 3.31 CM
COIL RADIAL RANGE: 3.81 TO 4.40 CM
ϕ ANGULAR RANGE
0.000 TO 0.100 RADIAN
2.356 TO 3.042 RADIANS
3.042 TO 3.142 RADIANS
3.117 TO 3.142 RADIANS
COIL RADIAL RANGE: 4.40 TO 5.00 CM
ϕ ANGULAR RANGE
3.042 TO 3.142 RADIANS
0.000 TO 0.100 RADIAN
ENERGY DENSITY, GEV / (CM^3 . INTERACTING PROTON)
10^1
10^0
10^{-1}
10^{-2}
10^{-3}
10^{-4}
0
2
4
6
8
10
12
14
DISTANCE FROM UPSTREAM END MAGNET (M)

Figure S12.

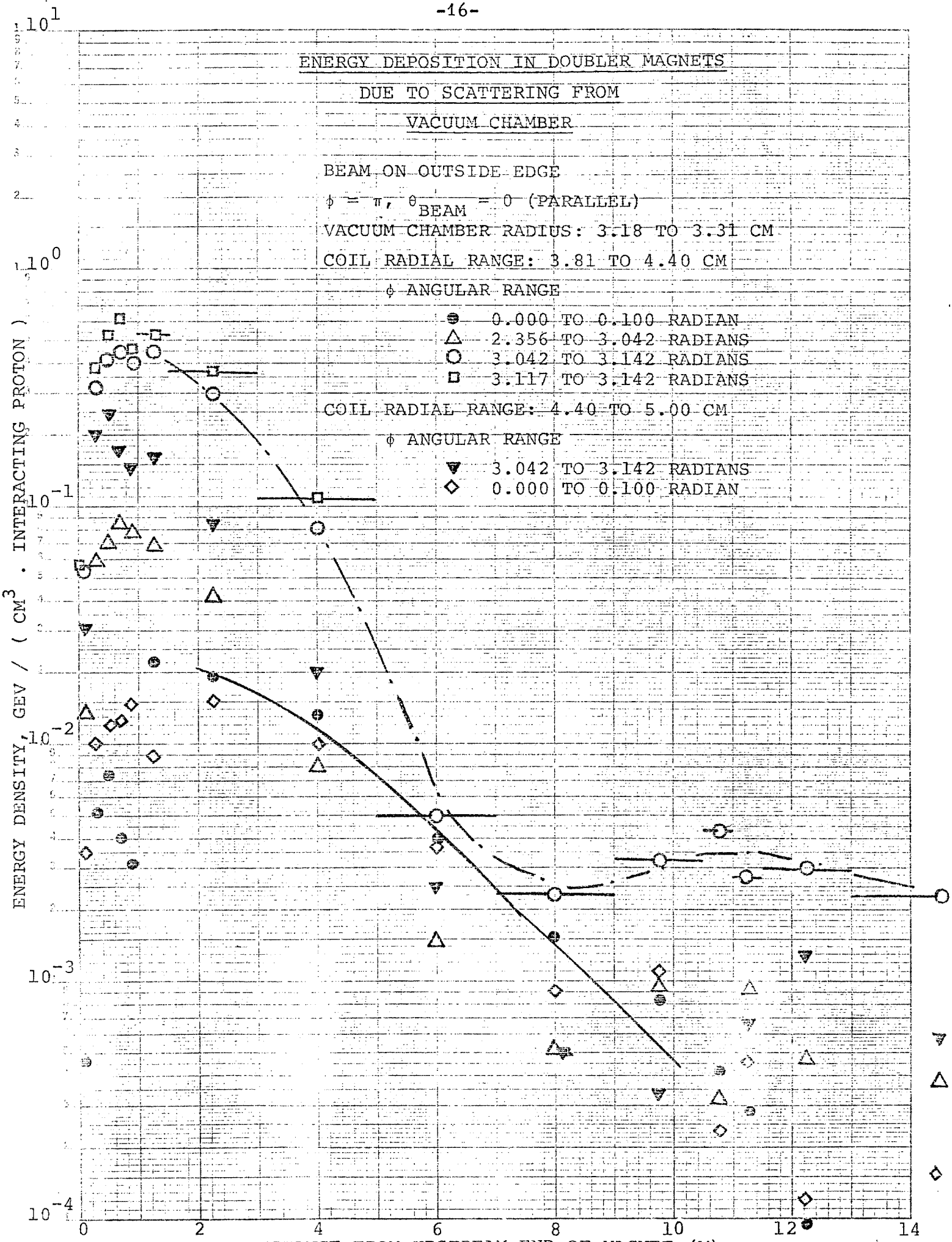
ENERGY DEPOSITION IN DOUBLER MAGNETS
DUE TO SCATTERING FROM
VACUUM CHAMBER
BEAM ON OUTSIDE EDGE
$\phi = \pi$, $\theta_{BEAM} = 0$ (PARALLEL)
VACUUM CHAMBER RADIUS: 3.18 TO 3.31 CM
COIL RADIAL RANGE: 3.81 TO 4.40 CM
ϕ ANGULAR RANGE
0.000 TO 0.100 RADIAN
2.356 TO 3.042 RADIANS
3.042 TO 3.142 RADIANS
3.117 TO 3.142 RADIANS
COIL RADIAL RANGE: 4.40 TO 5.00 CM
ϕ ANGULAR RANGE
3.042 TO 3.142 RADIANS
0.000 TO 0.100 RADIAN
ENERGY DENSITY, GEV / (CM^3 . INTERACTING PROTON)
10^1
10^0
10^{-1}
10^{-2}
10^{-3}
10^{-4}
0
2
4
6
8
10
12
14
DISTANCE FROM UPSTREAM END OF MAGNET (M)

Figure S13.

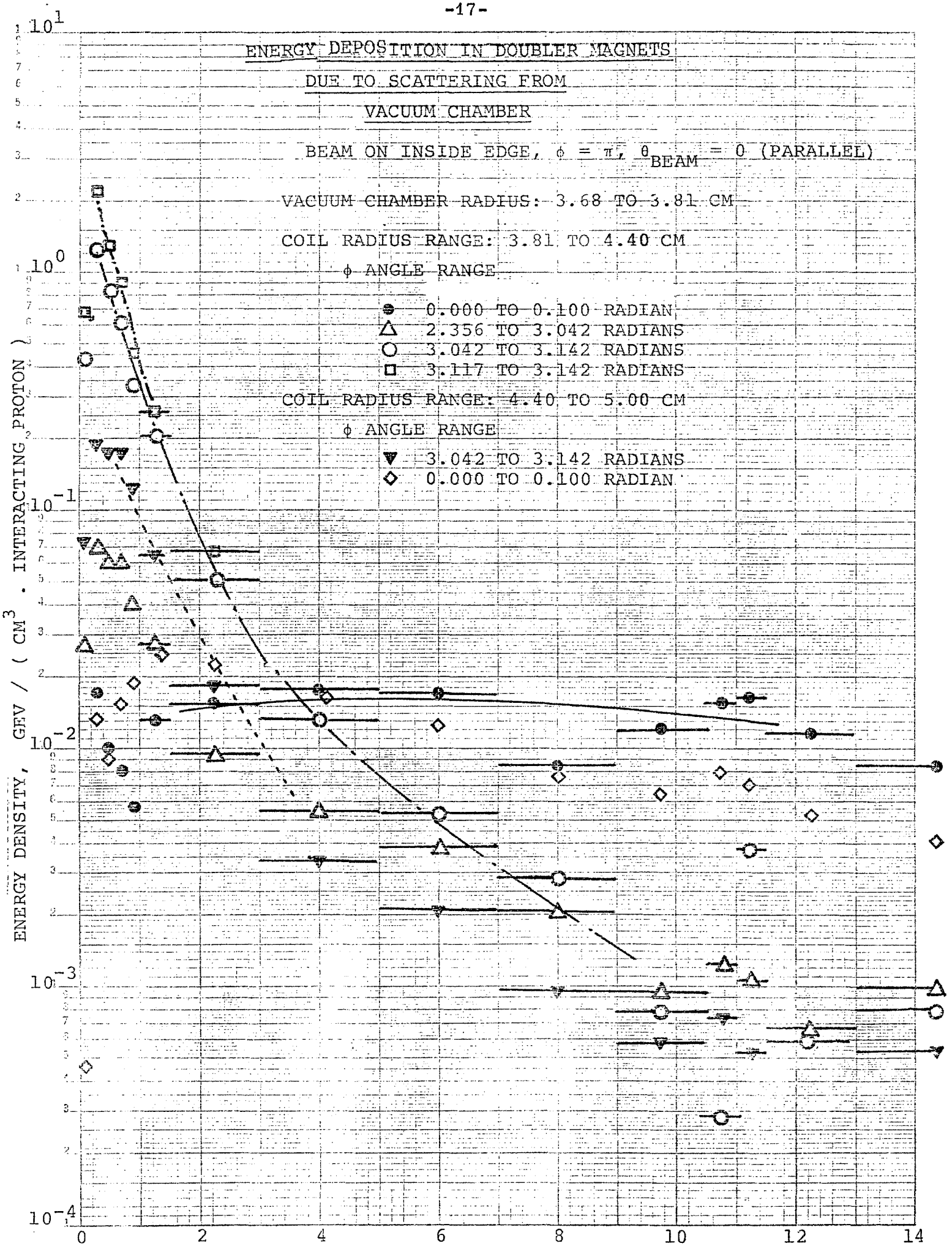
ENERGY DEPOSITION IN DOUBLER MAGNETS
DUE TO SCATTERING FROM
VACUUM CHAMBER
BEAM ON INSIDE EDGE, $\phi = \pi$, $\theta_{BEAM} = 0$ (PARALLEL)
VACUUM CHAMBER RADIUS: 3.68 TO 3.81 CM
COIL RADIUS RANGE: 3.81 TO 4.40 CM
ϕ ANGLE RANGE
0.000 TO 0.100 RADIAN
2.356 TO 3.042 RADIANS
3.042 TO 3.142 RADIANS
3.117 TO 3.142 RADIANS
COIL RADIUS RANGE: 4.40 TO 5.00 CM
ϕ ANGLE RANGE
3.042 TO 3.142 RADIANS
0.000 TO 0.100 RADIAN
ENERGY DENSITY, GEV / (CM^3 . INTERACTING PROTON)
10^{1}
10^{0}
10^{-1}
10^{-2}
10^{-3}
10^{-4}
0
2
4
6
8
10
12
14
DISTANCE FROM UPSTREAM END OF MAGNET (M)

Figure S14.

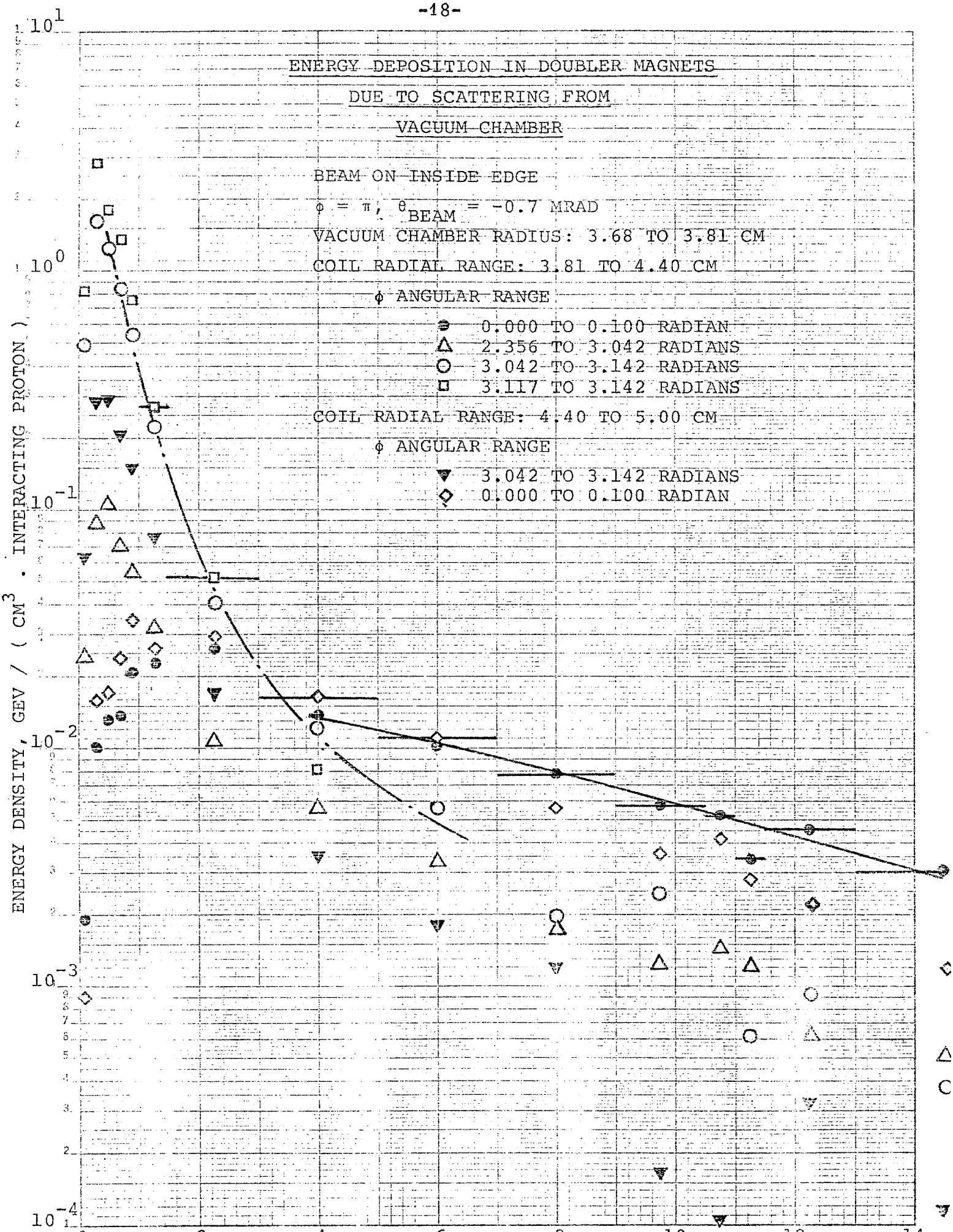
ENERGY DEPOSITION IN DOUBLER MAGNETS
DUE TO SCATTERING FROM
VACUUM CHAMBER
BEAM ON INSIDE EDGE
φ = π, θ BEAM = -0.7 MRAD
VACUUM CHAMBER RADIUS: 3.68 TO 3.81 CM
COIL RADIAL RANGE: 3.81 TO 4.40 CM
φ ANGULAR RANGE
0.000 TO 0.100 RADIAN
2.356 TO 3.042 RADIANS
3.042 TO 3.142 RADIANS
3.117 TO 3.142 RADIANS
COIL RADIAL RANGE: 4.40 TO 5.00 CM
φ ANGULAR RANGE
3.042 TO 3.142 RADIANS
0.000 TO 0.100 RADIAN
ENERGY DENSITY, GEV / (CM3 · INTERACTING PROTON)
DISTANCE FROM UPSTREAM END OF MAGNET (M)
10^1
10^0
10^-1
10^-2
10^-3
10^-4
0
2
4
6
8
10
12
14

Figure S15.

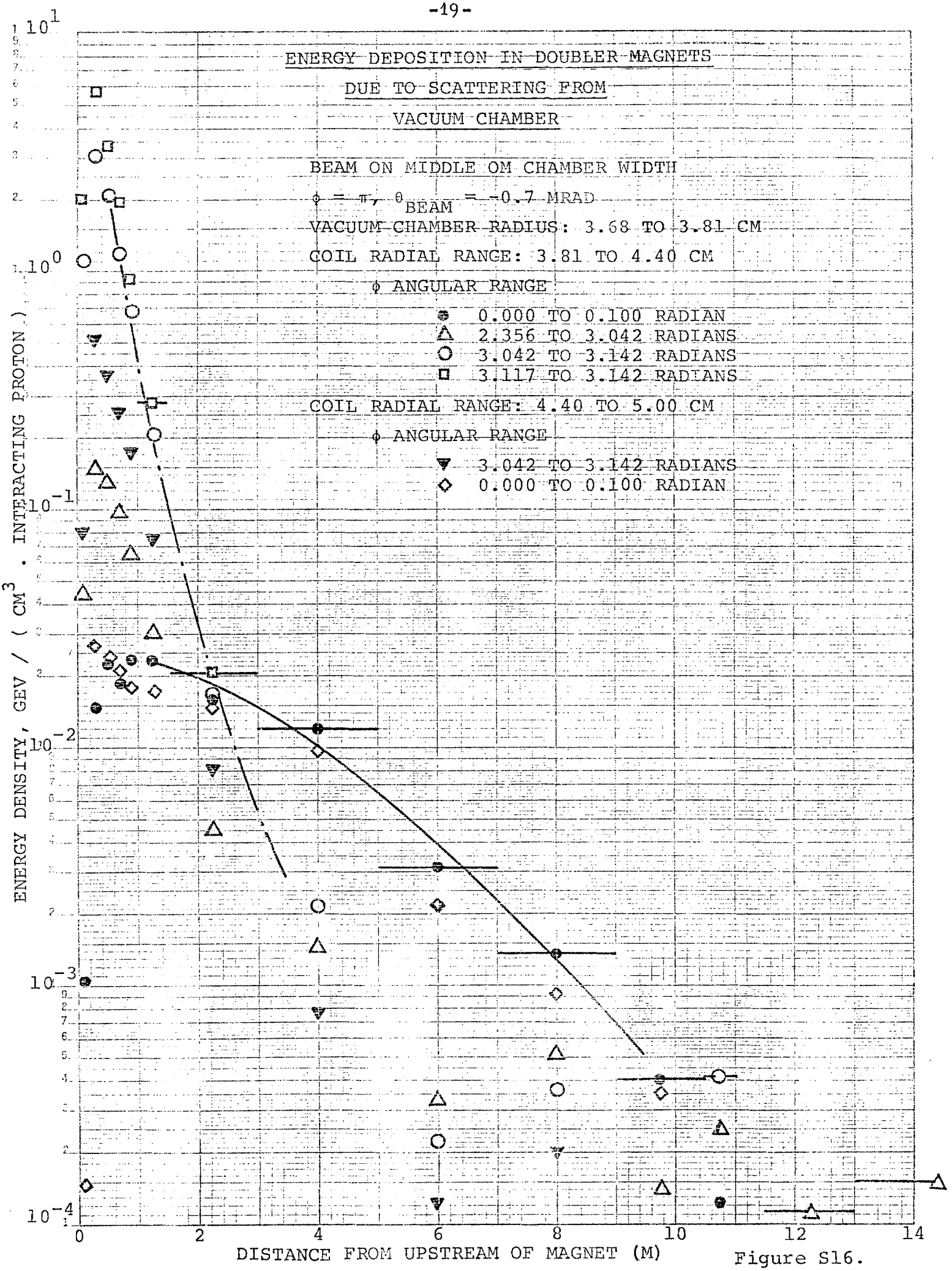
ENERGY DEPOSITION IN DOUBLER MAGNETS
DUE TO SCATTERING FROM
VACUUM CHAMBER
BEAM ON MIDDLE OM CHAMBER WIDTH
$\phi = \pi$, $\theta_{BEAM} = -0.7$ MRAD
VACUUM CHAMBER RADIUS: 3.68 TO 3.81 CM
COIL RADIAL RANGE: 3.81 TO 4.40 CM
ϕ ANGULAR RANGE
0.000 TO 0.100 RADIAN
2.356 TO 3.042 RADIANS
3.042 TO 3.142 RADIANS
3.117 TO 3.142 RADIANS
COIL RADIAL RANGE: 4.40 TO 5.00 CM
ϕ ANGULAR RANGE
3.042 TO 3.142 RADIANS
0.000 TO 0.100 RADIAN
ENERGY DENSITY, GEV / (CM^3 . INTERACTING PROTON)
DISTANCE FROM UPSTREAM OF MAGNET (M)

Figure S16.

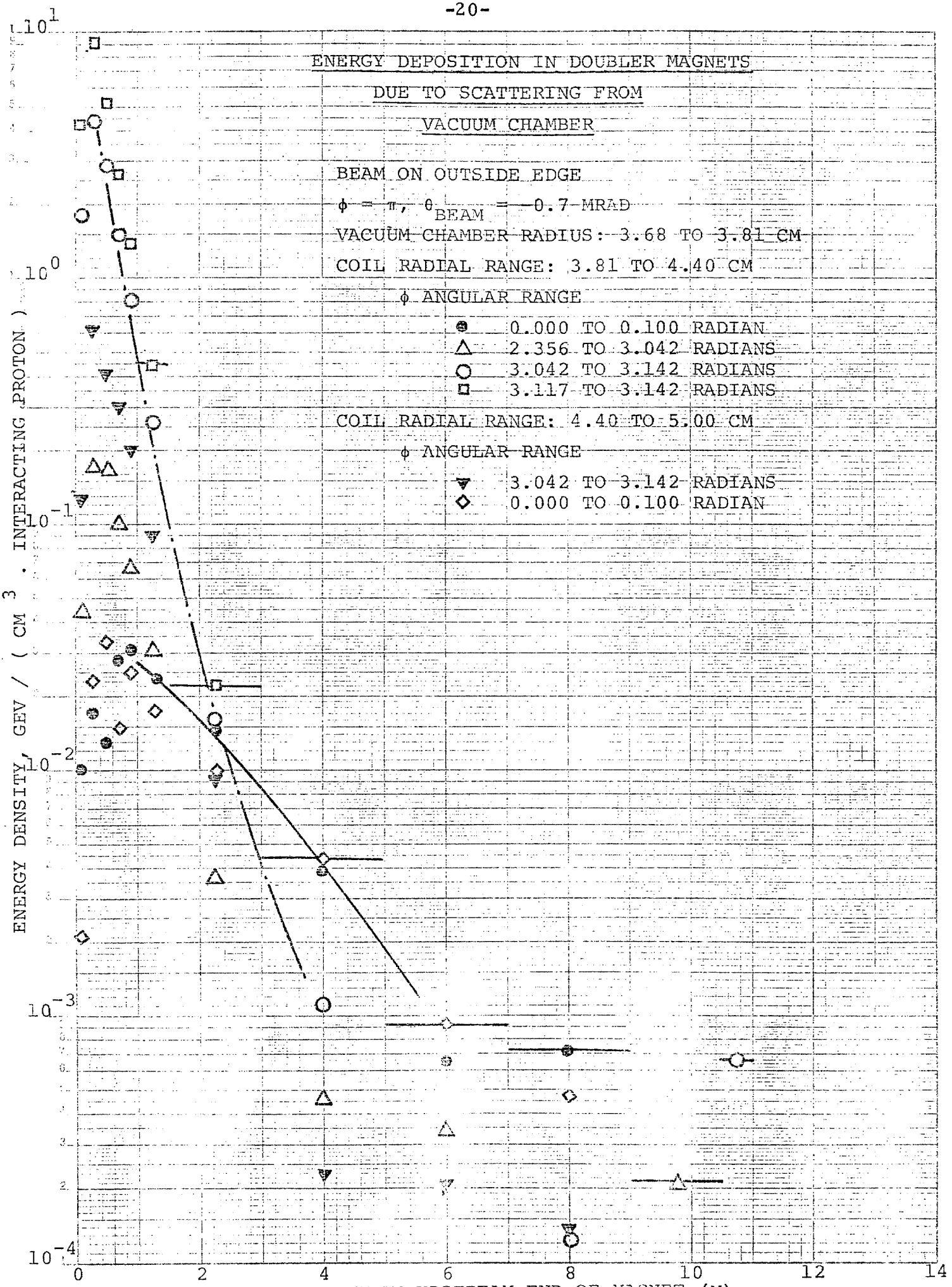
ENERGY DEPOSITION IN DOUBLER MAGNETS
DUE TO SCATTERING FROM
VACUUM CHAMBER
BEAM ON OUTSIDE EDGE
$\phi = \pi$, $\theta_{BEAM} = -0.7$ MRAD
VACUUM CHAMBER RADIUS: 3.68 TO 3.81 CM
COIL RADIAL RANGE: 3.81 TO 4.40 CM
ϕ ANGULAR RANGE
0.000 TO 0.100 RADIAN
2.356 TO 3.042 RADIANS
3.042 TO 3.142 RADIANS
3.117 TO 3.142 RADIANS
COIL RADIAL RANGE: 4.40 TO 5.00 CM
ϕ ANGULAR RANGE
3.042 TO 3.142 RADIANS
0.000 TO 0.100 RADIAN
ENERGY DENSITY, GEV / (CM 3 . INTERACTING PROTON)
10^{1}
10^{0}
10^{-1}
10^{-2}
10^{-3}
10^{-4}
0
2
4
6
8
10
12
14
DISTANCE FROM UPSTREAM END OF MAGNET (M)

Figure S17.

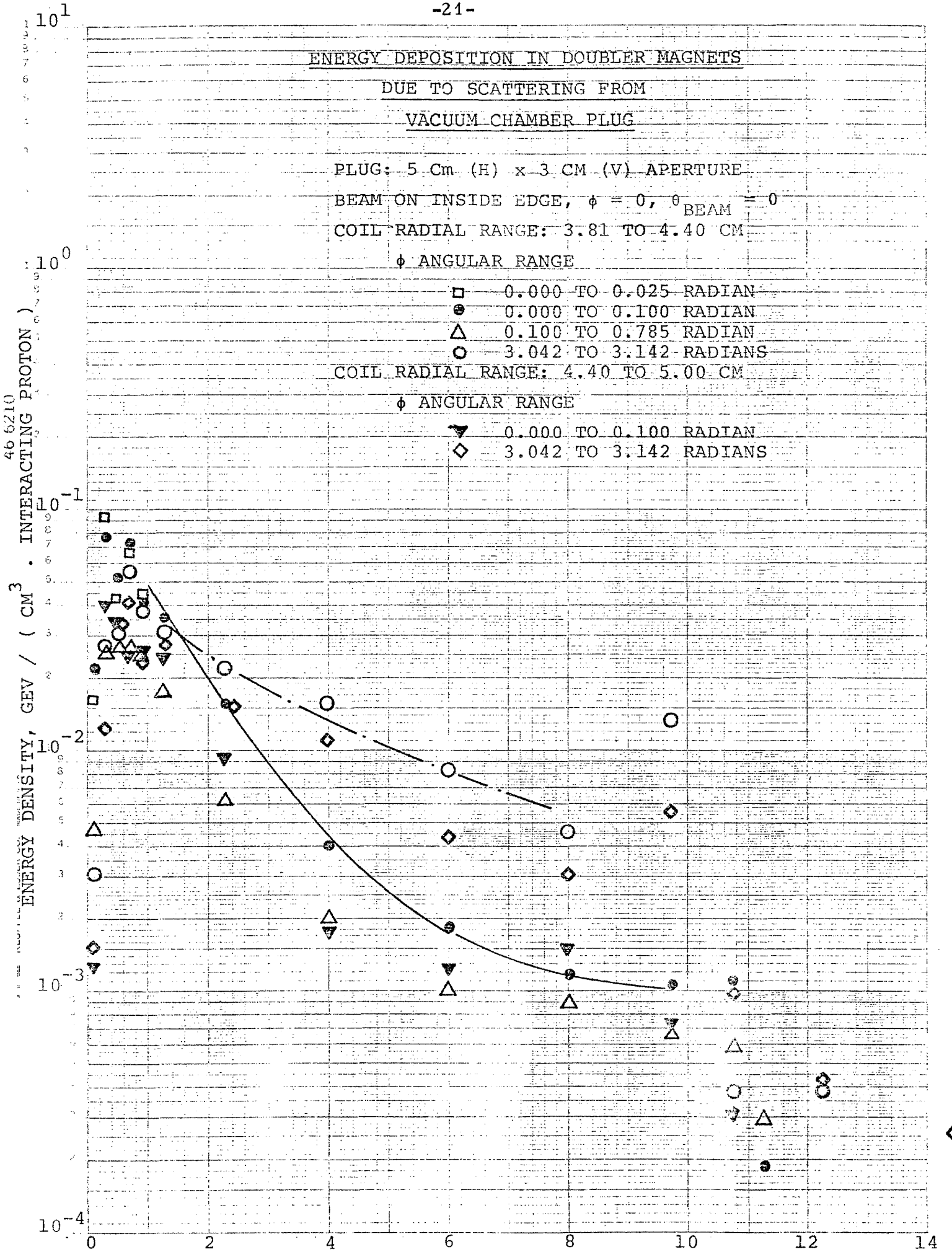
ENERGY DEPOSITION IN DOUBLER MAGNETS
DUE TO SCATTERING FROM
VACUUM CHAMBER PLUG
PLUG: 5 Cm (H) x 3 CM (V) APERTURE
BEAM ON INSIDE EDGE, φ = 0, θ BEAM = 0
COIL RADIAL RANGE: 3.81 TO 4.40 CM
φ ANGULAR RANGE
0.000 TO 0.025 RADIAN
0.000 TO 0.100 RADIAN
0.100 TO 0.785 RADIAN
3.042 TO 3.142 RADIANS
COIL RADIAL RANGE: 4.40 TO 5.00 CM
φ ANGULAR RANGE
0.000 TO 0.100 RADIAN
3.042 TO 3.142 RADIANS
ENERGY DENSITY, GEV / (CM3 . INTERACTING PROTON)
DISTANCE FROM UPSTREAM END OF MAGNET (M)
46 6210

Figure S18.

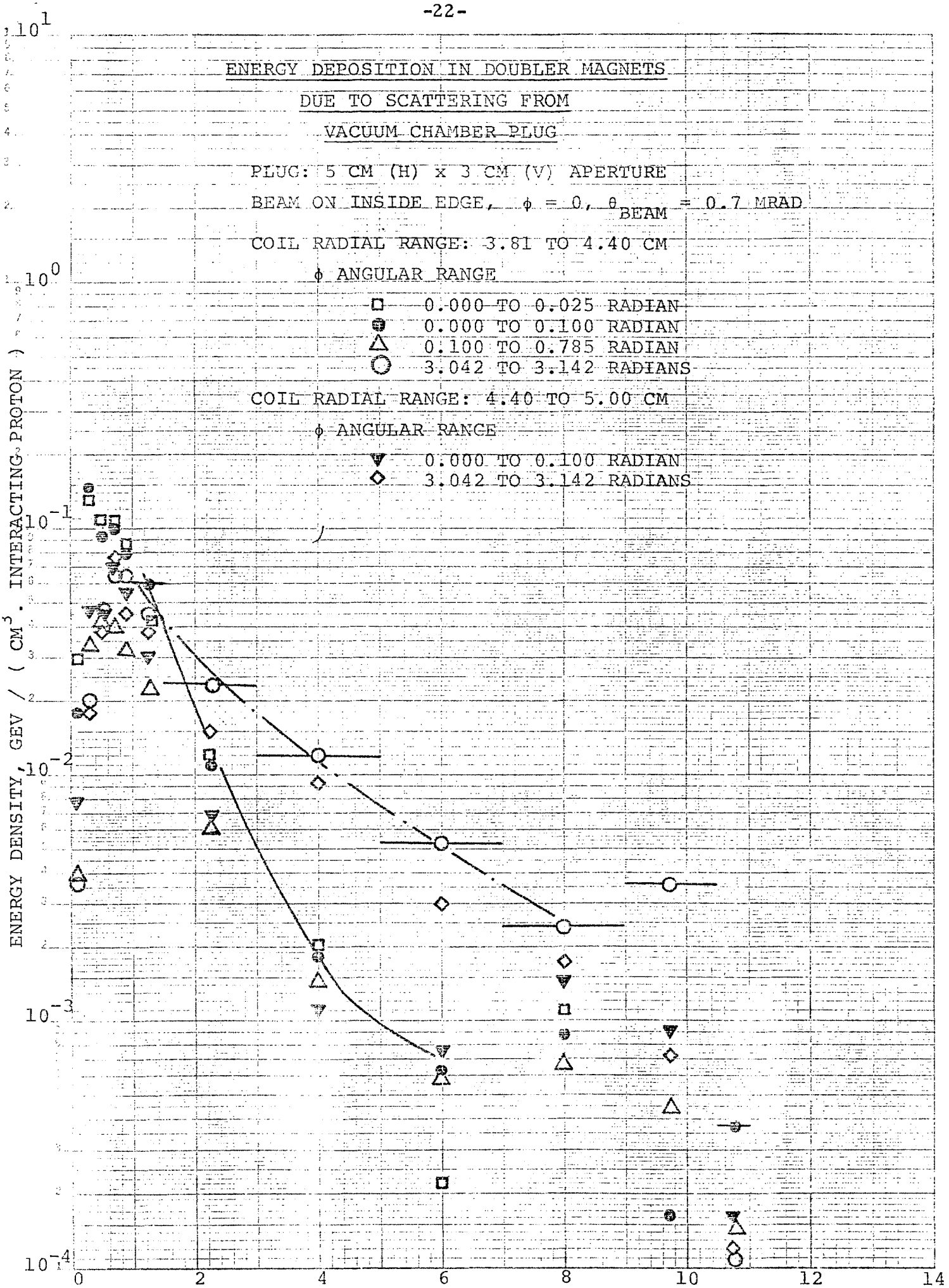
ENERGY DEPOSITION IN DOUBLER MAGNETS
DUE TO SCATTERING FROM
VACUUM CHAMBER PLUG
PLUG: 5 CM (H) x 3 CM (V) APERTURE
BEAM ON INSIDE EDGE, φ = 0, θBEAM = 0.7 MRAD
COIL RADIAL RANGE: 3.81 TO 4.40 CM
φ ANGULAR RANGE
0.000 TO 0.025 RADIAN
0.000 TO 0.100 RADIAN
0.100 TO 0.785 RADIAN
3.042 TO 3.142 RADIANS
COIL RADIAL RANGE: 4.40 TO 5.00 CM
φ ANGULAR RANGE
0.000 TO 0.100 RADIAN
3.042 TO 3.142 RADIANS
ENERGY DENSITY, GEV / (CM3. INTERACTING PROTON)
DISTANCE FROM UPSTREAM END OF MAGNET (M)
10^1
10^0
10^-1
10^-2
10^-3
10^-4
0
2
4
6
8
10
12
14

Figure S19.

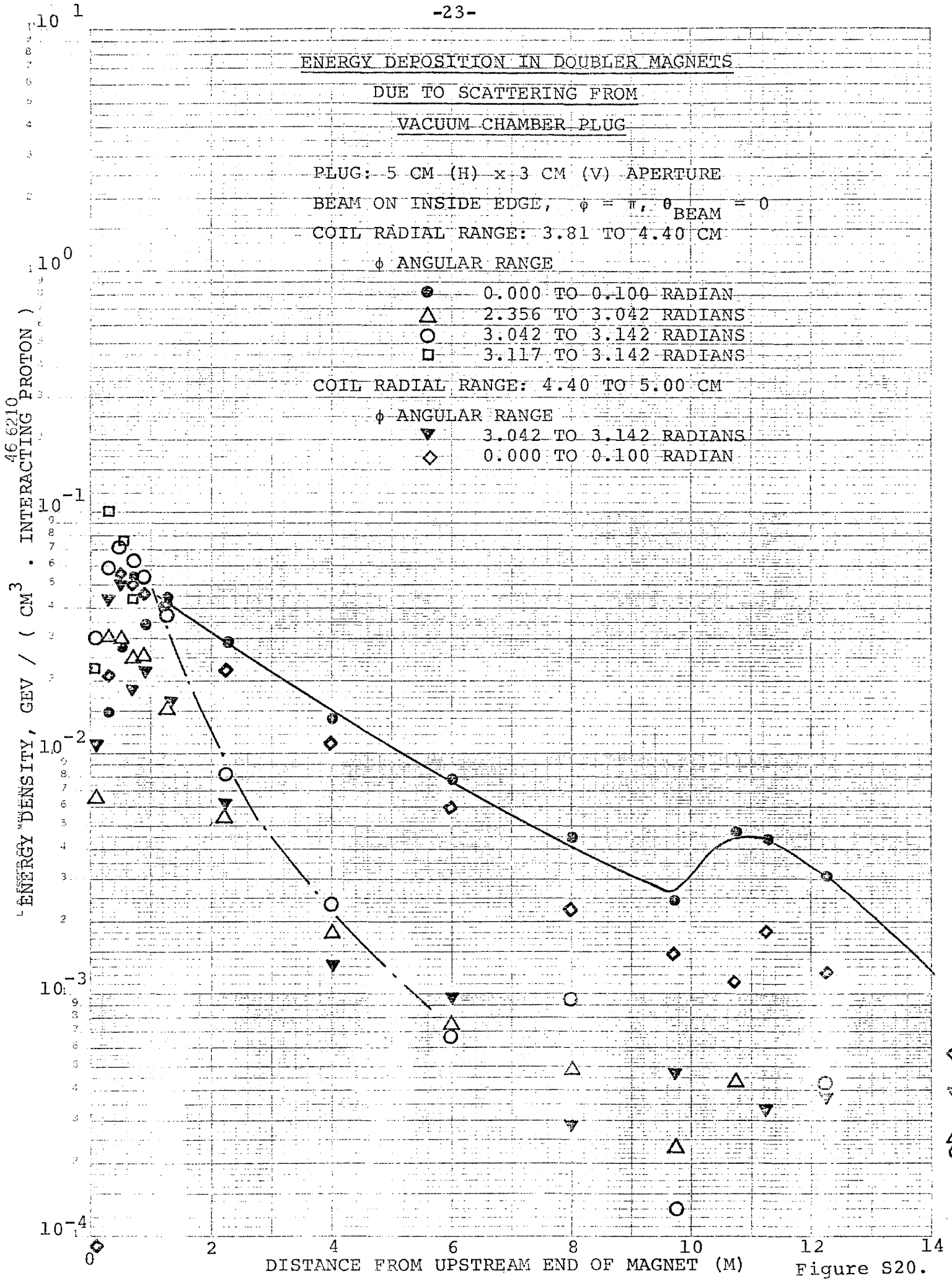
ENERGY DEPOSITION IN DOUBLER MAGNETS
DUE TO SCATTERING FROM
VACUUM CHAMBER PLUG
PLUG: 5 CM (H) x 3 CM (V) APERTURE
BEAM ON INSIDE EDGE, φ = π, θBEAM = 0
COIL RADIAL RANGE: 3.81 TO 4.40 CM
φ ANGULAR RANGE
0.000 TO 0.100 RADIAN
2.356 TO 3.042 RADIANS
3.042 TO 3.142 RADIANS
3.117 TO 3.142 RADIANS
COIL RADIAL RANGE: 4.40 TO 5.00 CM
φ ANGULAR RANGE
3.042 TO 3.142 RADIANS
0.000 TO 0.100 RADIAN
ENERGY DENSITY, GEV / (CM3 · INTERACTING PROTON)
46 6210
DISTANCE FROM UPSTREAM END OF MAGNET (M)
1
10^0
10^-1
10^-2
10^-3
10^-4
0
2
4
6
8
10
12
14

Figure S20.

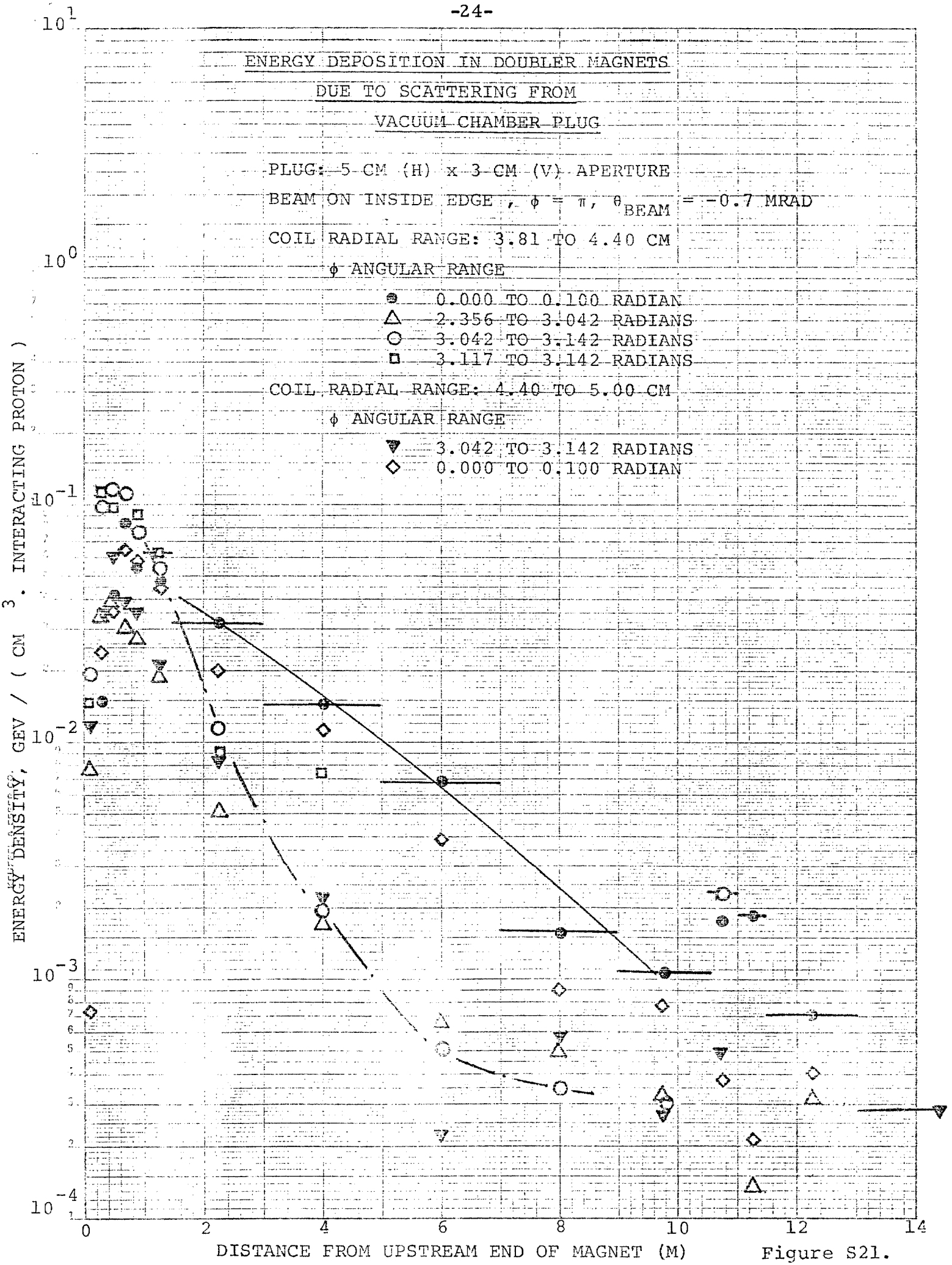
ENERGY DEPOSITION IN DOUBLER MAGNETS
DUE TO SCATTERING FROM
VACUUM CHAMBER PLUG
PLUG: 5 CM (H) x 3 CM (V) APERTURE
BEAM ON INSIDE EDGE , φ = π, θBEAM = -0.7 MRAD
COIL RADIAL RANGE: 3.81 TO 4.40 CM
φ ANGULAR RANGE
0.000 TO 0.100 RADIAN
2.356 TO 3.042 RADIANS
3.042 TO 3.142 RADIANS
3.117 TO 3.142 RADIANS
COIL RADIAL RANGE: 4.40 TO 5.00 CM
φ ANGULAR RANGE
3.042 TO 3.142 RADIANS
0.000 TO 0.100 RADIAN
ENERGY DENSITY, GEV / (CM 3 . INTERACTING PROTON)
DISTANCE FROM UPSTREAM END OF MAGNET (M)

Figure S21.

UPC No. 40 (Appendix)
S. Mori, H. Edwards, and
A. Van Ginneken

SUPPLEMENT TO UPC 40

Figures S22 through S25 show energy density distributions in the Doubler magnet coils due to scattering from a beam scraper at a medium straight section. The iron beam scraper with an aperture of 4.5 cm(horizontal) by 2 cm(vertical) and 2 m in length is placed 12 m upstream of the Doubler magnets. The incident proton energy is 1000 GeV. The beam strikes an inside edge of the scraper with an incident angle of 0 mrad. The ϕ angle is π in Figures S22, S23, and S24 and 0 in Figure S25. In Figure S22 beam collimator and vacuum chamber plug are not present. The vacuum chamber radius is 3.68 to 3.81 cm. The vacuum chamber plug with a 5 cm(H) by 3 cm(V) aperture is added in Figure S23. In Figures S24 and S25 a 2 m long iron collimator with a 5 cm(H) by 3 cm(V) aperture is placed immediately upstream of the Doubler magnets. The plug and collimator reduce the peak energy density to about 6×10^{-3} GeV/(cm^3.interacting proton) from 4×10^{-2} GeV/(cm^3.interacting proton).

Figures S26 through S33 show energy density distributions due to scattering from the extraction wire septum for various configurations of the beam bump arrangement at the long straight section. Four B-2 type bending magnets are used for the beam bump of 3 mrad as shown in Figure 6. The incident proton energy is 1000 GeV. A string of four quadrupole magnets which are to be placed upstream of the dipole string are omitted in the present study. Figure S26 is essentially the same as Figure 3 in which beam bump, vacuum chamber plug and collimator are not present. A small discrepancy at the upstream end is due to different

binnings in the two cases.

Table II summarizes the conditions and peak energy densities.

Table II. Peak energy densities due to scattering from the extraction electrostatic wire septum for various configurations shown in Figures S26 through S33.

Figure	Plug	Beam Bump	Collimator	Peak Energy Density GeV/(cm^3. incid.prot.)	
				First	Second
S26	No	No	No	4×10^{-3}	2×10^{-3}
S27	Yes	No	Yes	9×10^{-4}	6×10^{-4}
S28	No	4M, H-In	-	-	9×10^{-4}
S29	No	3M, H-In	-	-	4×10^{-4}
S30	Yes	3M, H-In	-	2×10^{-4}	5×10^{-5}
S31	Yes	3M, H-Out	-	2×10^{-4}	6×10^{-5}
S32	No	3M, V	-	-	8×10^{-5}
S33	Yes	3M, V	-	5×10^{-5}	4×10^{-5}

The 2 m long iron collimator with an aperture of 5 cm(H) by 3 cm(V) is used only in Figure S27. The vacuum chamber plug is made of iron and has an aperture of 5 cm(H) by 3 cm(V). The beam bumps, 4M and 3M correspond to the arrangements in which the electrostatic wire septum is placed upstream and downstream of the first bump magnet, respectively. The H-In and H-Out are the horizontal inward and outward bumps and the V is the vertical beam bump. The horizontal inward bump arrangement is slightly better than the horizontal outward bump when the vacuum chamber plug is not used, but

they are essentially the same when the plug is used. In general, the vertical bump gives much lower peak energy density in the Doubler magnet coils than the horizontal bump because the narrow vertical aperture of the bump magnets is more efficient to absorb off-momentum secondary particles scattered from septum wires.

The peak energy density of 5×10^{-5} GeV/(cm^3.incident proton) achieved by the vertical bump (Figure S33) gives the limits for extraction due to scattering from the electrostatic wire septum of 4.5×10^{14} protons/sec for slow extraction and 1.2×10^{14} protons/pulse of 1 msec. The extraction inefficiency was assumed to be 2.5 %, i.e. 2.5 % of protons strike septum wires.

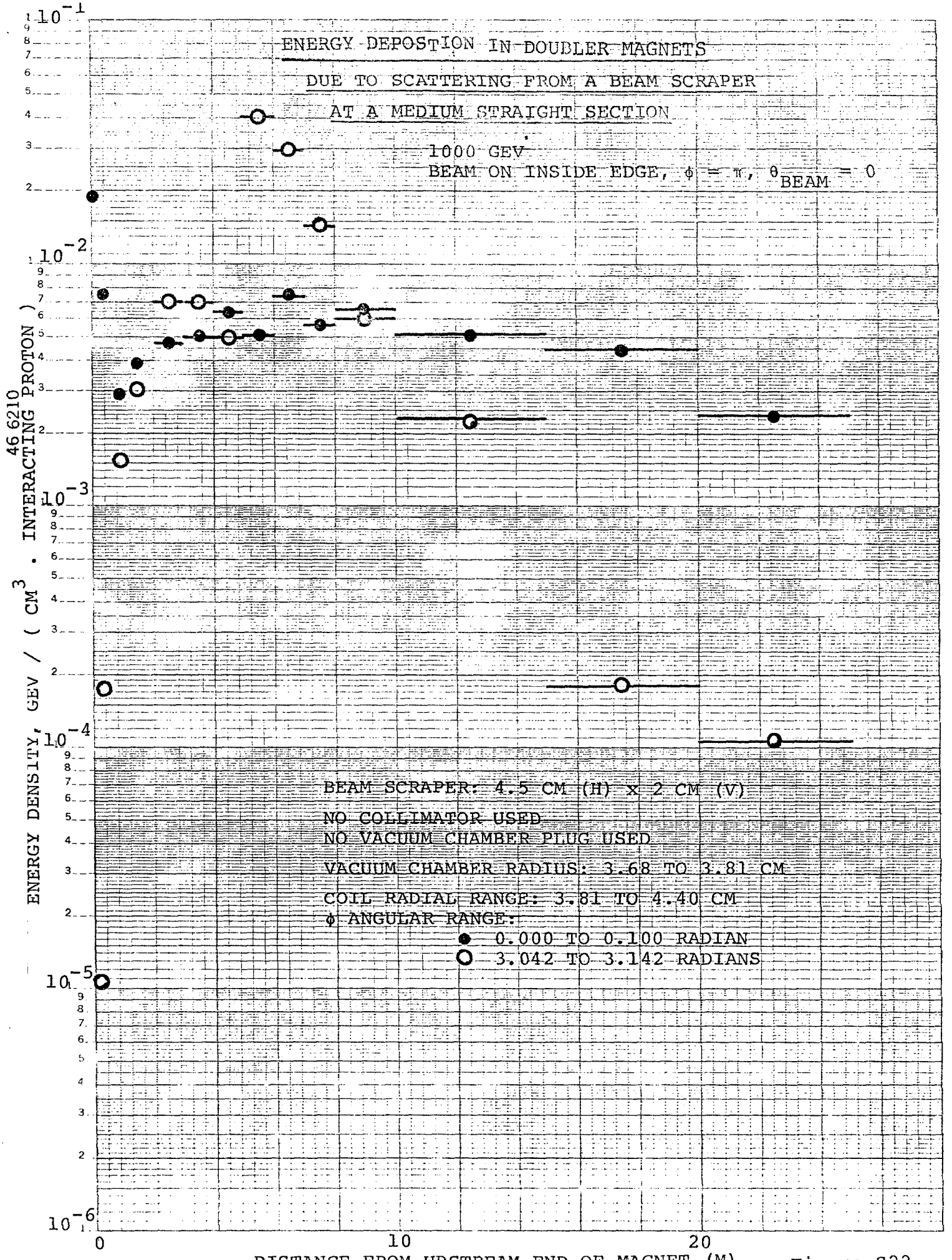
ENERGY DEPOSTION IN DOUBLER MAGNETS
DUE TO SCATTERING FROM A BEAM SCRAPER
AT A MEDIUM STRAIGHT SECTION
1000 GEV
BEAM ON INSIDE EDGE, $\phi = \pi$, $\theta_{BEAM} = 0$
ENERGY DENSITY, GEV / (CM^3 • INTERACTING PROTON) $\times 10^{46}$ 6210
10^{-1}
10^{-2}
10^{-3}
10^{-4}
10^{-5}
10^{-6}
BEAM SCRAPER: 4.5 CM (H) x 2 CM (V)
NO COLLIMATOR USED
NO VACUUM CHAMBER PLUG USED
VACUUM CHAMBER RADIUS: 3.68 TO 3.81 CM
COIL RADIAL RANGE: 3.81 TO 4.40 CM
ϕ ANGULAR RANGE:
● 0.000 TO 0.100 RADIAN
○ 3.042 TO 3.142 RADIANS
0
10
20
DISTANCE FROM UPSTREAM END OF MAGNET (M)

Figure S22.

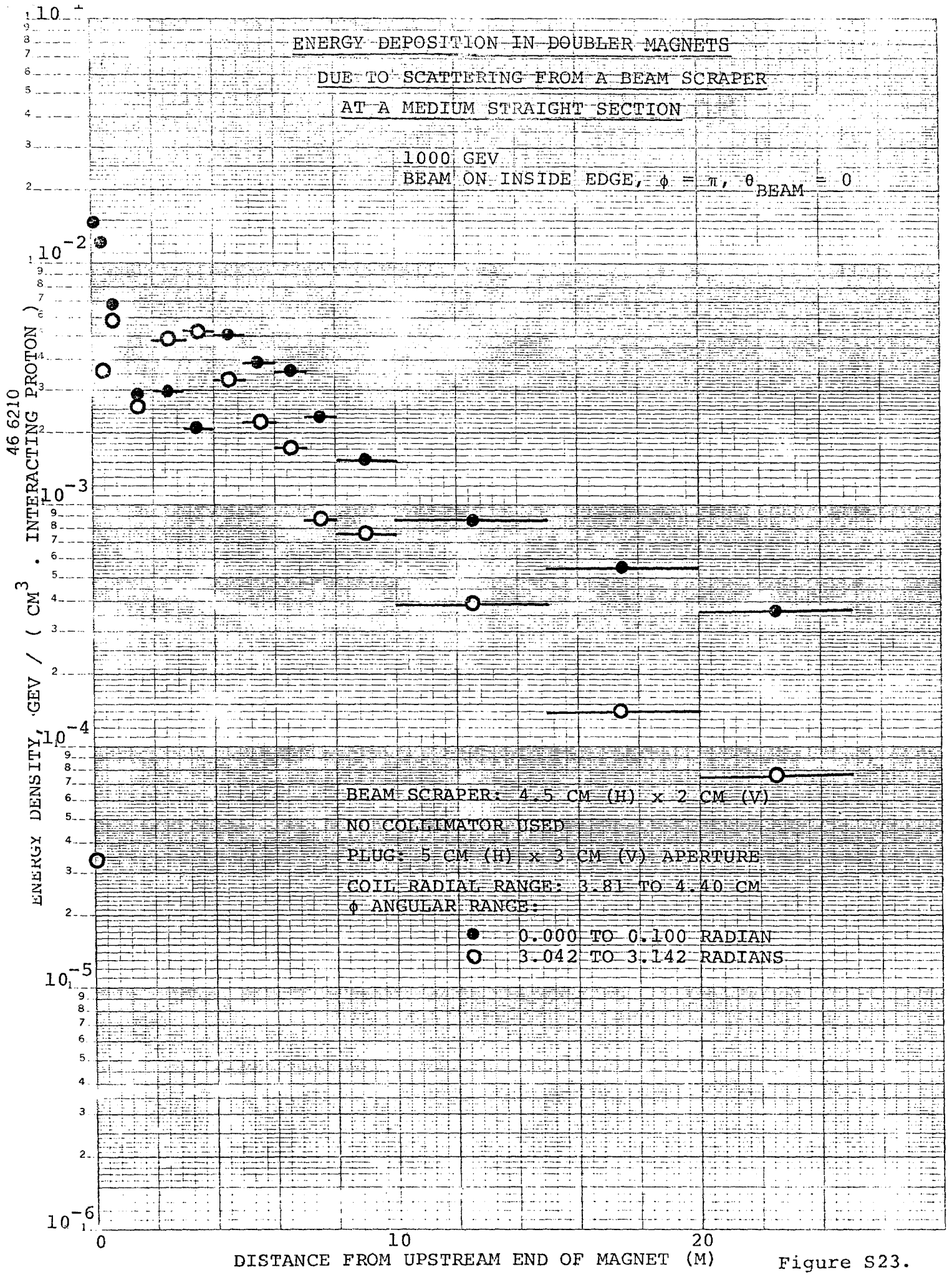
ENERGY DEPOSITION IN DOUBLER MAGNETS
DUE TO SCATTERING FROM A BEAM SCRAPER
AT A MEDIUM STRAIGHT SECTION
1000 GEV
BEAM ON INSIDE EDGE, $\phi = \pi$, $\theta_{BEAM} = 0$
ENERGY DENSITY, GEV / (CM^3 . INTERACTING PROTON)
46 6210
BEAM SCRAPER: 4.5 CM (H) x 2 CM (V)
NO COLLIMATOR USED
PLUG: 5 CM (H) x 3 CM (V) APERTURE
COIL RADIAL RANGE: 3.81 TO 4.40 CM
ϕ ANGULAR RANGE:
0.000 TO 0.100 RADIAN
3.042 TO 3.142 RADIANS
10^{-2}
10^{-3}
10^{-4}
10^{-5}
10^{-6}
0
10
20
DISTANCE FROM UPSTREAM END OF MAGNET (M)

Figure S23.

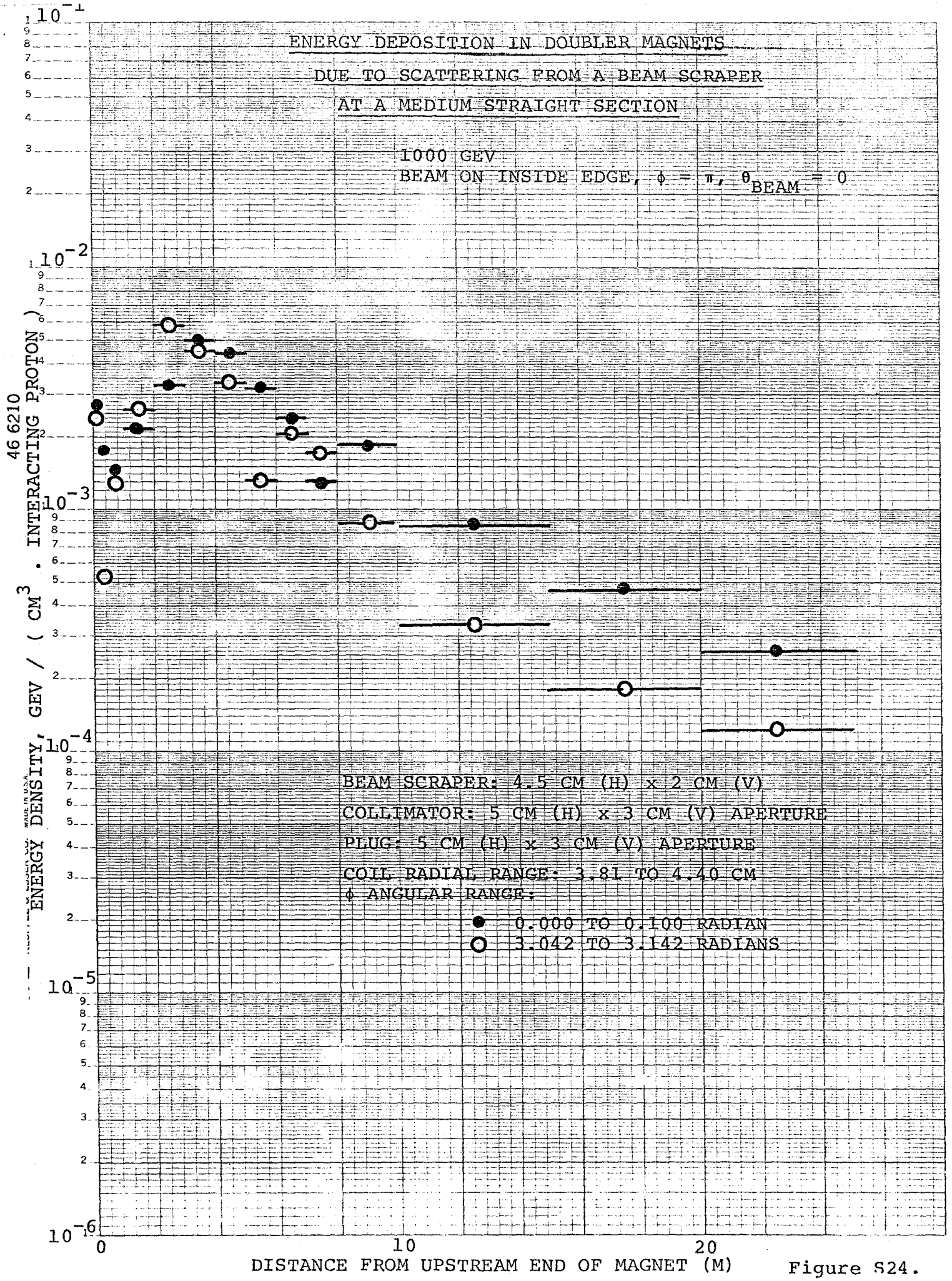
ENERGY DEPOSITION IN DOUBLER MAGNETS
DUE TO SCATTERING FROM A BEAM SCRAPER
AT A MEDIUM STRAIGHT SECTION
1000 GEV
BEAM ON INSIDE EDGE, $\phi = \pi$, $\theta_{BEAM} = 0$
ENERGY DENSITY, GEV / (CM^3 · INTERACTING PROTON)
DISTANCE FROM UPSTREAM END OF MAGNET (M)
BEAM SCRAPER: 4.5 CM (H) x 2 CM (V)
COLLIMATOR: 5 CM (H) x 3 CM (V) APERTURE
PLUG: 5 CM (H) x 3 CM (V) APERTURE
COIL RADIAL RANGE: 3.81 TO 4.40 CM
ϕ ANGULAR RANGE:
0.000 TO 0.100 RADIAN
3.042 TO 3.142 RADIANS
46 6210

Figure S24.

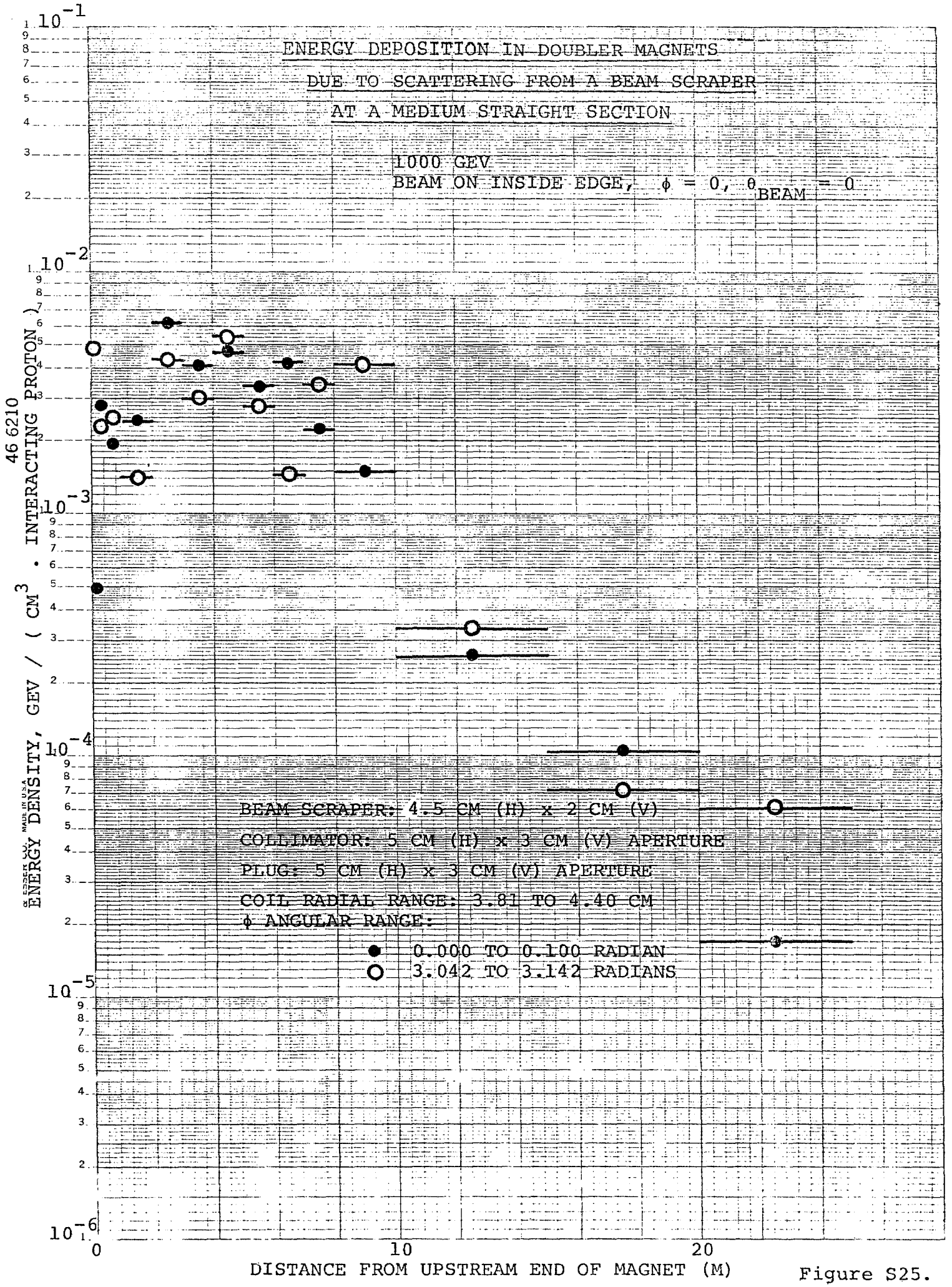
ENERGY DEPOSITION IN DOUBLER MAGNETS
DUE TO SCATTERING FROM A BEAM SCRAPER
AT A MEDIUM STRAIGHT SECTION
1000 GEV
BEAM ON INSIDE EDGE, ϕ = 0, θ_{BEAM} = 0
ENERGY DENSITY, GEV / (CM^3 • INTERACTING PROTON)
DISTANCE FROM UPSTREAM END OF MAGNET (M)
BEAM SCRAPER: 4.5 CM (H) x 2 CM (V)
COLLIMATOR: 5 CM (H) x 3 CM (V) APERTURE
PLUG: 5 CM (H) x 3 CM (V) APERTURE
COIL RADIAL RANGE: 3.81 TO 4.40 CM
ϕ ANGULAR RANGE:
0.000 TO 0.100 RADIAN
3.042 TO 3.142 RADIANS
46 6210

Figure S25.

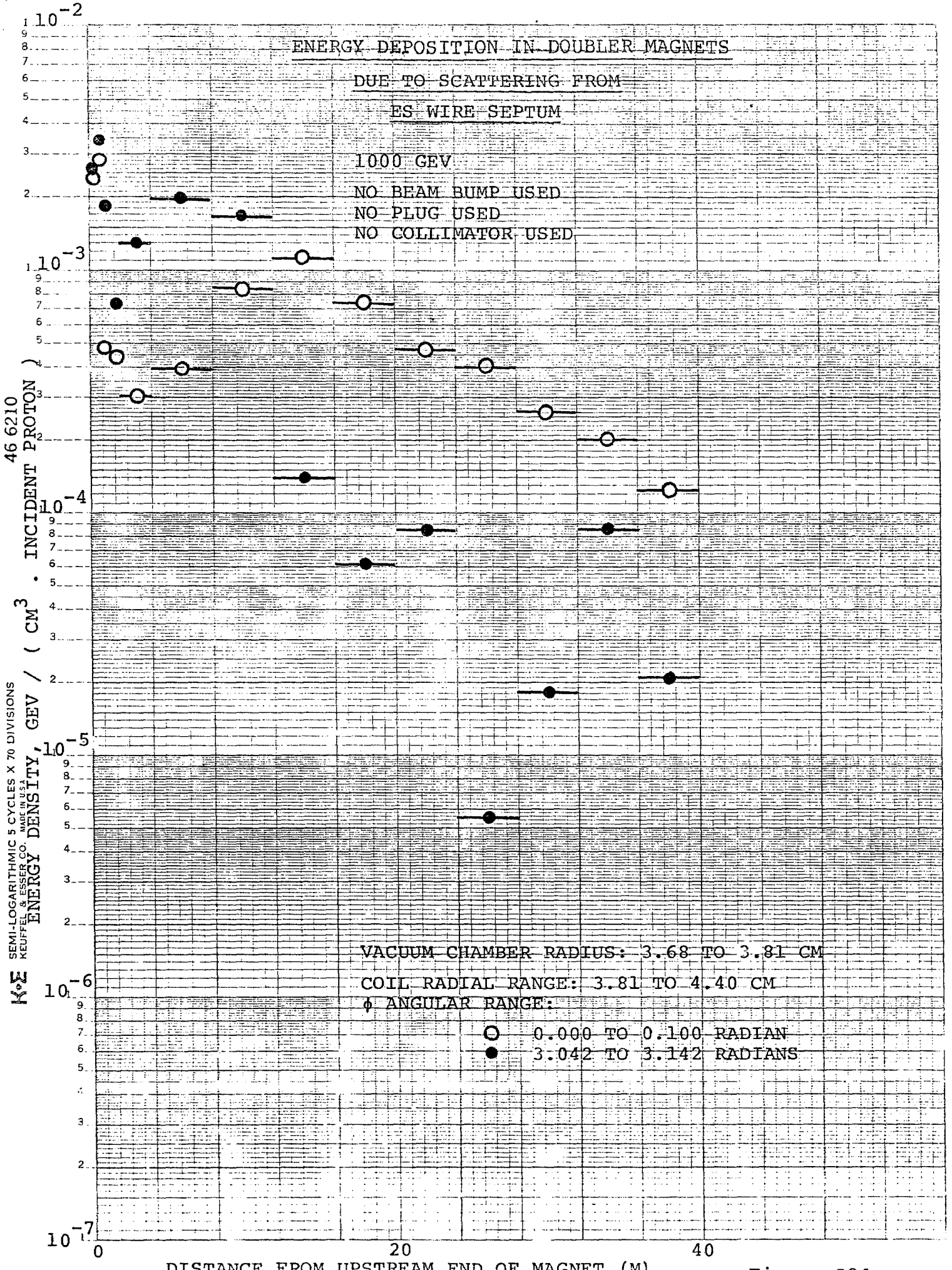
ENERGY DEPOSITION IN DOUBLER MAGNETS
DUE TO SCATTERING FROM
ES WIRE SEPTUM
1000 GEV
NO BEAM BUMP USED
NO PLUG USED
NO COLLIMATOR USED
VACUUM CHAMBER RADIUS: 3.68 TO 3.81 CM
COIL RADIAL RANGE: 3.81 TO 4.40 CM
φ ANGULAR RANGE:
0.000 TO 0.100 RADIAN
3.042 TO 3.142 RADIANS
ENERGY DENSITY, GEV / (CM3) . INCIDENT PROTON)
DISTANCE FROM UPSTREAM END OF MAGNET (M)
0
20
40
10-2
10-3
10-4
10-5
10-6
10-7
46 6210
K+E SEMI-LOGARITHMIC 5 CYCLES X 70 DIVISIONS
KEUFFEL & ESSER CO. MADE IN U.S.A.

Figure S26.

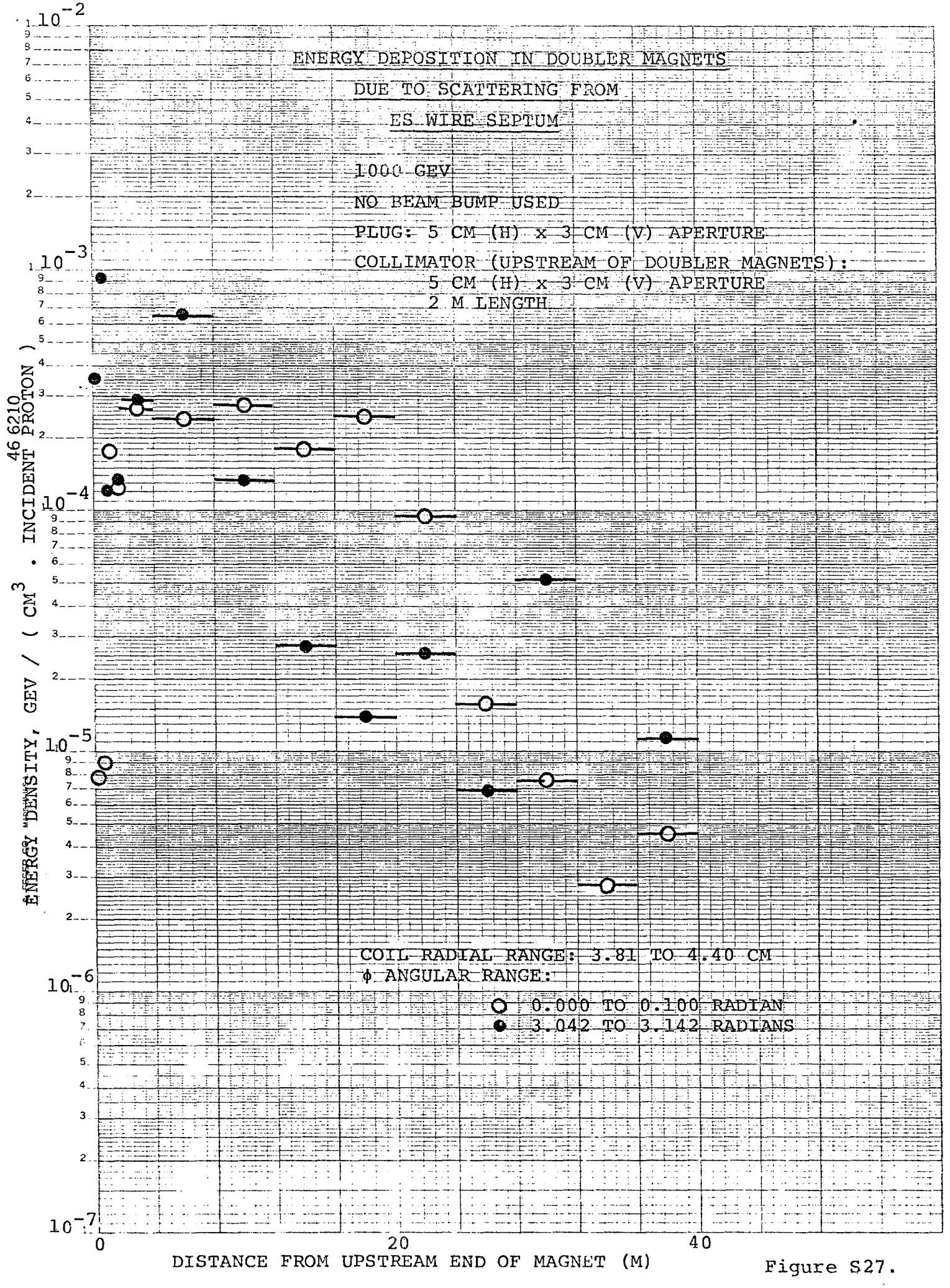
ENERGY DEPOSITION IN DOUBLER MAGNETS
DUE TO SCATTERING FROM
ES WIRE SEPTUM
1000 GEV
NO BEAM BUMP USED
PLUG: 5 CM (H) x 3 CM (V) APERTURE
COLLIMATOR (UPSTREAM OF DOUBLER MAGNETS):
5 CM (H) x 3 CM (V) APERTURE
2 M LENGTH
ENERGY DENSITY, GEV / (CM3 • INCIDENT PROTON)
46 6210
COIL RADIAL RANGE: 3.81 TO 4.40 CM
φ ANGULAR RANGE:
0.000 TO 0.100 RADIAN
3.042 TO 3.142 RADIANS
DISTANCE FROM UPSTREAM END OF MAGNET (M)

Figure S27.

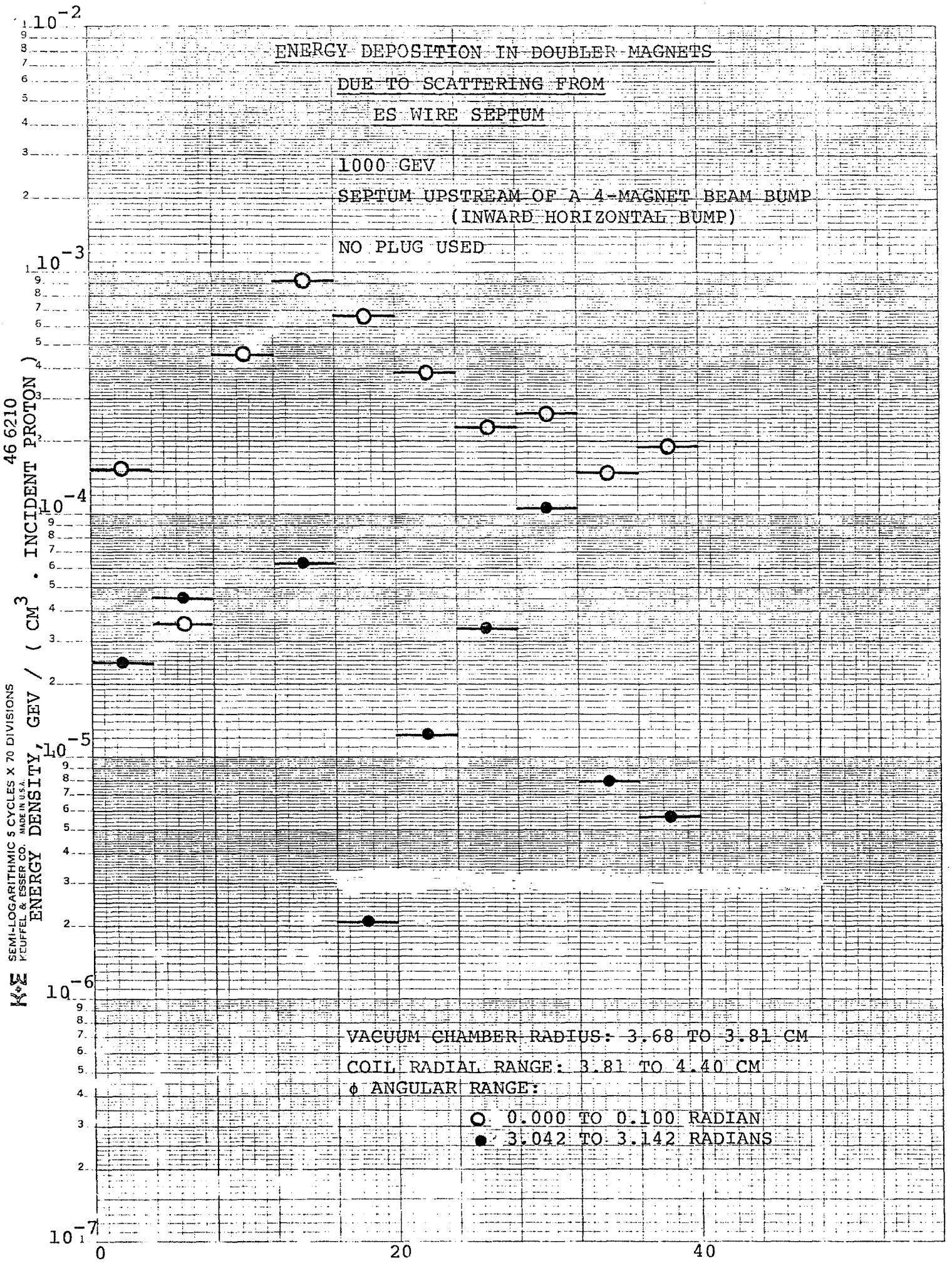
ENERGY DEPOSITION IN DOUBLER MAGNETS
DUE TO SCATTERING FROM
ES WIRE SEPTUM
1000 GEV
SEPTUM UPSTREAM OF A 4-MAGNET BEAM BUMP
(INWARD HORIZONTAL BUMP)
NO PLUG USED
ENERGY DENSITY, GEV / (CM3 . INCIDENT PROTON)
DISTANCE FROM UPSTREAM END OF MAGNET (M)
VACUUM CHAMBER RADIUS: 3.68 TO 3.81 CM
COIL RADIAL RANGE: 3.81 TO 4.40 CM
φ ANGULAR RANGE:
0.000 TO 0.100 RADIAN
3.042 TO 3.142 RADIANS
46 6210
SEMI-LOGARITHMIC 5 CYCLES X 70 DIVISIONS
KEUFFEL & ESSER CO. MADE IN U.S.A.

Figure S28.

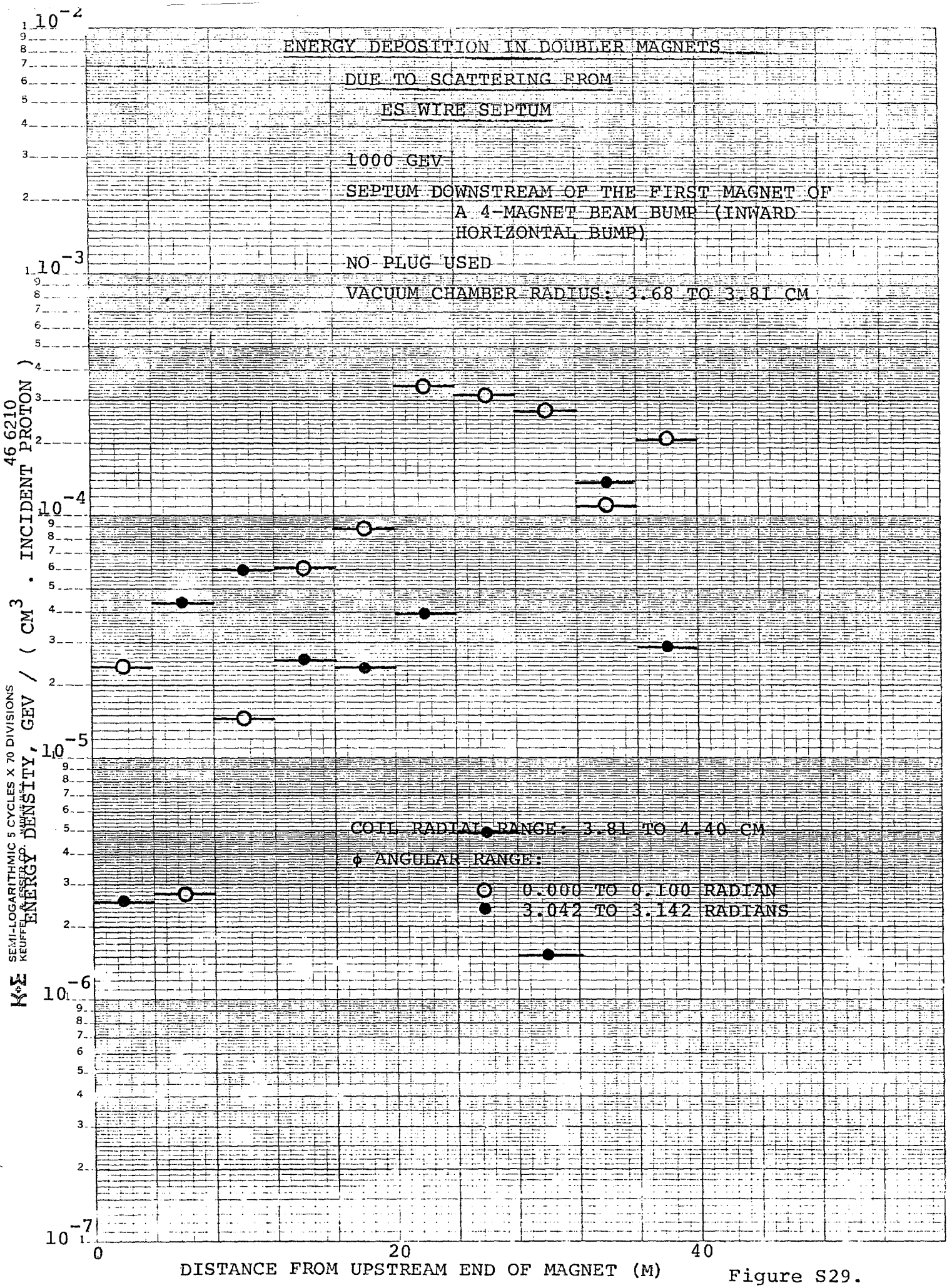
ENERGY DEPOSITION IN DOUBLER MAGNETS
DUE TO SCATTERING FROM
ES WIRE SEPTUM
1000 GEV
SEPTUM DOWNSTREAM OF THE FIRST MAGNET OF A 4-MAGNET BEAM BUMP (INWARD HORIZONTAL BUMP)
NO PLUG USED
VACUUM CHAMBER RADIUS: 3.68 TO 3.81 CM
COIL RADIAL RANGE: 3.81 TO 4.40 CM
φ ANGULAR RANGE:
0.000 TO 0.100 RADIAN
3.042 TO 3.142 RADIANS
ENERGY DENSITY, GEV / (CM3 . INCIDENT PROTON)
DISTANCE FROM UPSTREAM END OF MAGNET (M)
46 6210
SEMI-LOGARITHMIC 5 CYCLES X 70 DIVISIONS
KEUFFEL & ESSER CO.
K+E

Figure S29.

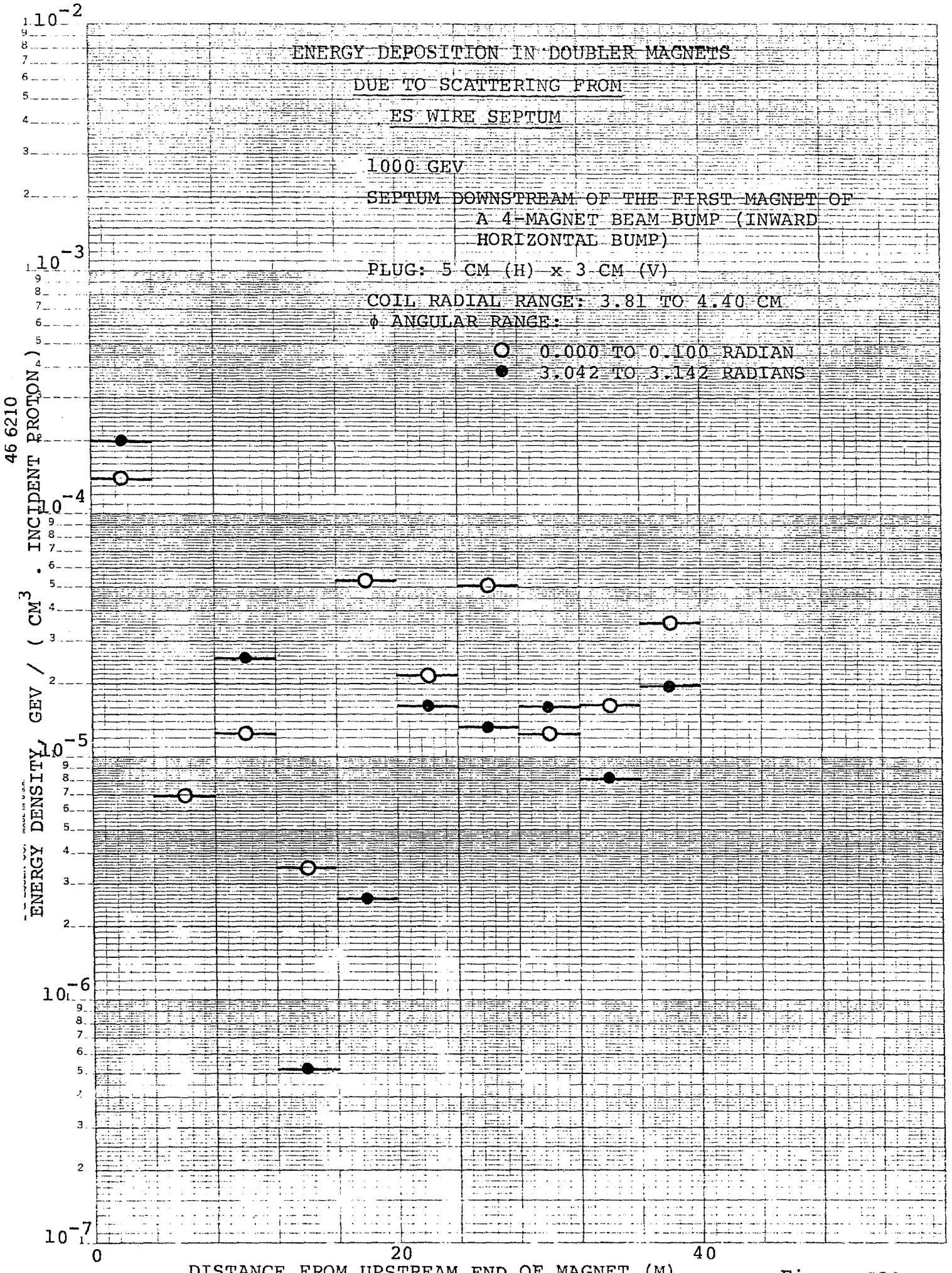
ENERGY DEPOSITION IN DOUBLER MAGNETS
DUE TO SCATTERING FROM
ES WIRE SEPTUM
1000 GEV
SEPTUM DOWNSTREAM OF THE FIRST MAGNET OF
A 4-MAGNET BEAM BUMP (INWARD
HORIZONTAL BUMP)
PLUG: 5 CM (H) x 3 CM (V)
COIL RADIAL RANGE: 3.81 TO 4.40 CM
φ ANGULAR RANGE:
0.000 TO 0.100 RADIAN
3.042 TO 3.142 RADIANS
46 6210
ENERGY DENSITY, GEV / (CM3 . INCIDENT PROTON)
DISTANCE FROM UPSTREAM END OF MAGNET (M)
0
20
40

Figure S30.

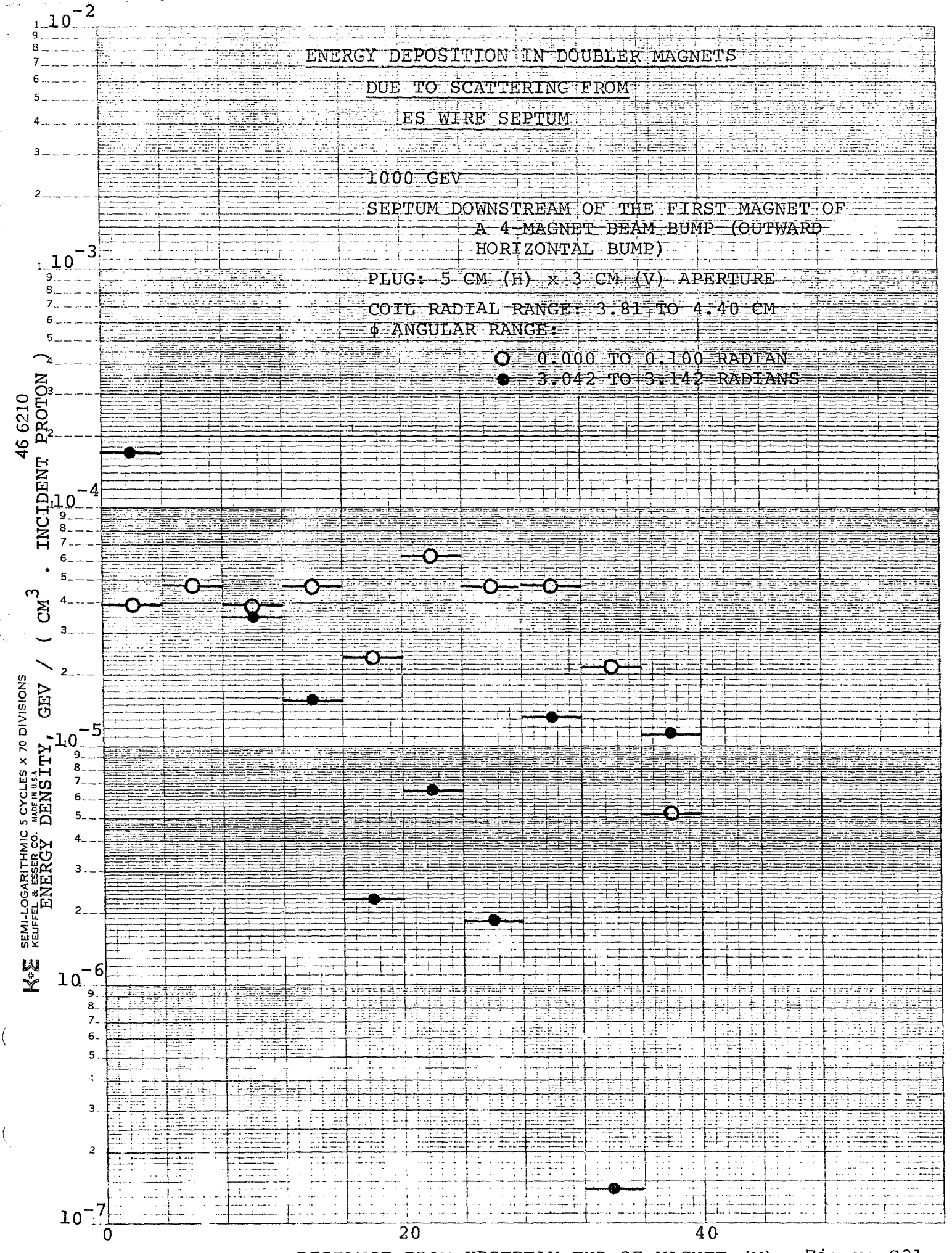
ENERGY DEPOSITION IN DOUBLER MAGNETS
DUE TO SCATTERING FROM
ES WIRE SEPTUM
1000 GEV
SEPTUM DOWNSTREAM OF THE FIRST MAGNET OF A 4-MAGNET BEAM BUMP (OUTWARD HORIZONTAL BUMP)
PLUG: 5 CM (H) x 3 CM (V) APERTURE
COIL RADIAL RANGE: 3.81 TO 4.40 CM
φ ANGULAR RANGE:
0.000 TO 0.100 RADIAN
3.042 TO 3.142 RADIANS
ENERGY DENSITY, GEV / (CM3 . INCIDENT PROTON)
DISTANCE FROM UPSTREAM END OF MAGNET (M)
0
20
40
10-2
10-3
10-4
10-5
10-6
10-7
46 6210
SEMI-LOGARITHMIC 5 CYCLES x 70 DIVISIONS
KEUFFEL & ESSER CO. MADE IN U.S.A.

Figure S31.

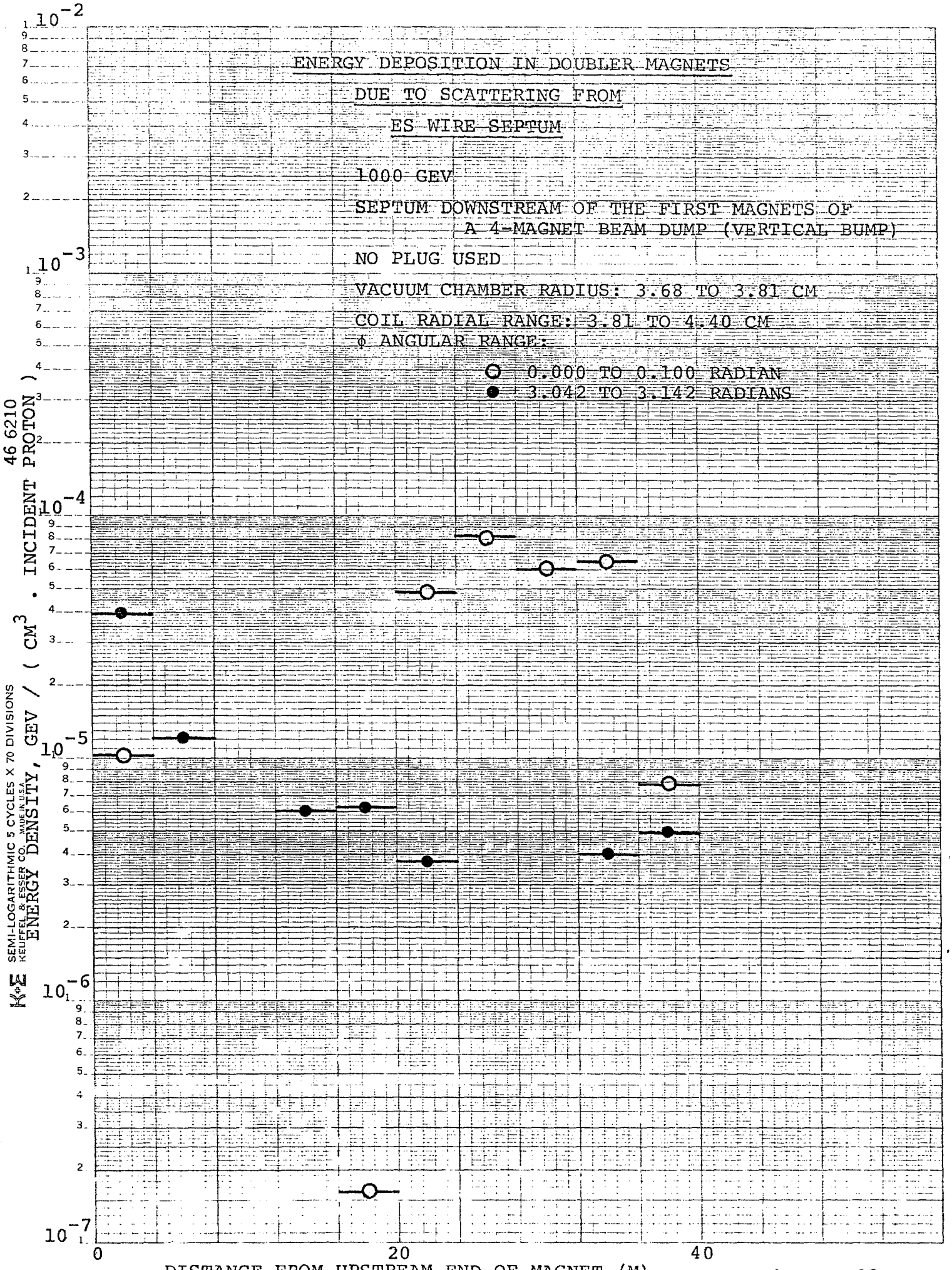
ENERGY DEPOSITION IN DOUBLER MAGNETS
DUE TO SCATTERING FROM
ES WIRE SEPTUM
1000 GEV
SEPTUM DOWNSTREAM OF THE FIRST MAGNETS OF
A 4-MAGNET BEAM DUMP (VERTICAL BUMP)
NO PLUG USED
VACUUM CHAMBER RADIUS: 3.68 TO 3.81 CM
COIL RADIAL RANGE: 3.81 TO 4.40 CM
φ ANGULAR RANGE:
0.000 TO 0.100 RADIAN
3.042 TO 3.142 RADIANS
ENERGY DENSITY, GEV / (CM3 . INCIDENT PROTON)
DISTANCE FROM UPSTREAM END OF MAGNET (M)
0
20
40
46 6210
SEMI-LOGARITHMIC 5 CYCLES X 70 DIVISIONS
KEUFFEL & ESSER CO. MADE IN U.S.A.

Figure S32.

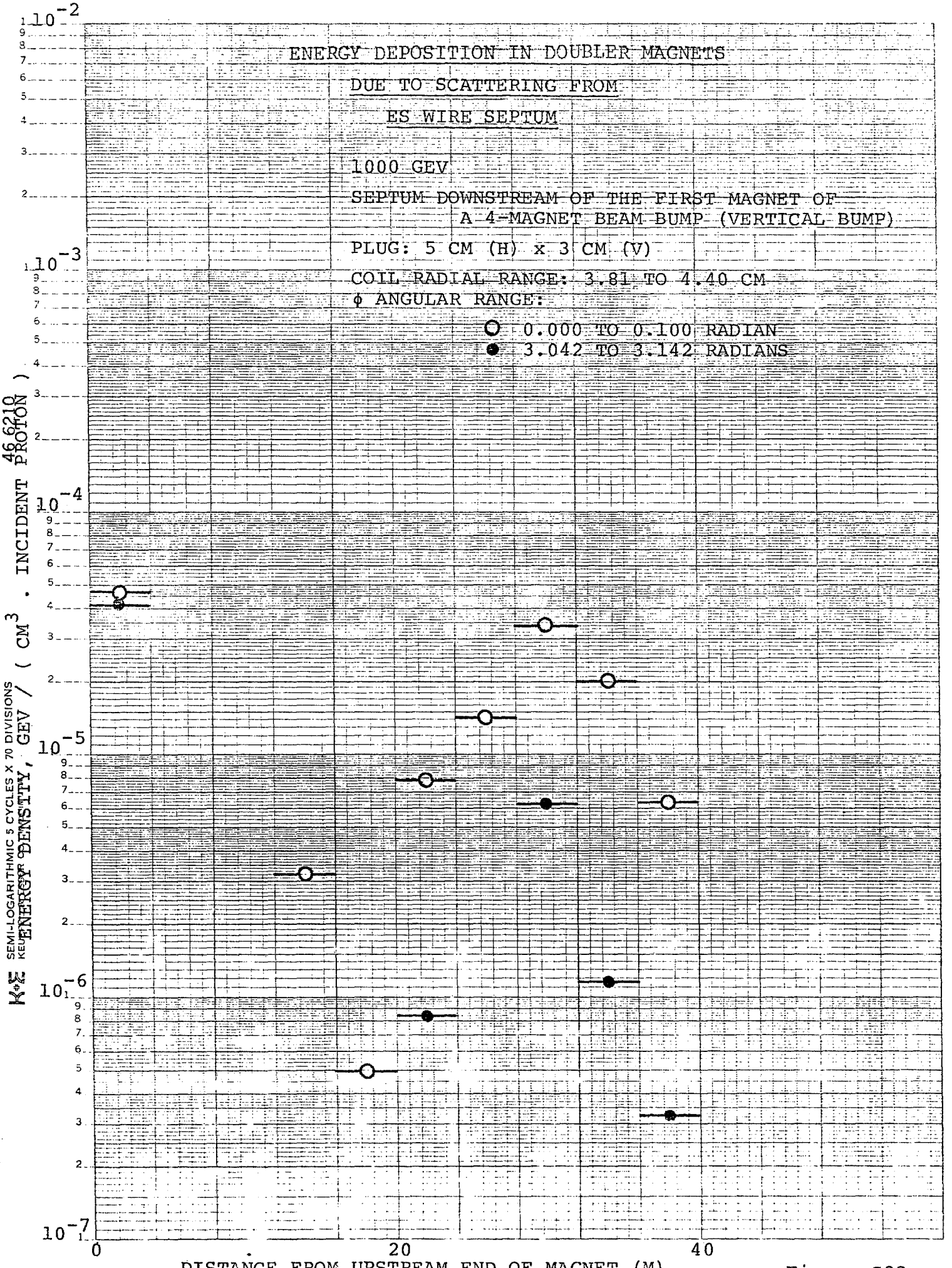
ENERGY DEPOSITION IN DOUBLER MAGNETS
DUE TO SCATTERING FROM
ES WIRE SEPTUM
1000 GEV
SEPTUM DOWNSTREAM OF THE FIRST MAGNET OF
A 4-MAGNET BEAM BUMP (VERTICAL BUMP)
PLUG: 5 CM (H) x 3 CM (V)
COIL RADIAL RANGE: 3.81 TO 4.40 CM
φ ANGULAR RANGE:
0.000 TO 0.100 RADIAN
3.042 TO 3.142 RADIANS
ENERGY DENSITY, GEV / (CM3 . INCIDENT PROTON)
46 6210
K+E SEMI-LOGARITHMIC 5 CYCLES X 70 DIVISIONS KEUFFEL & ESSER CO.
10-2
10-3
10-4
10-5
10-6
10-7
0
20
40
DISTANCE FROM UPSTREAM END OF MAGNET (M)

Figure S33.